ASTROPHYSICAL PROBES OF DARK MATTER

by

Travis J. Hurst

BS in Physics, University of Texas At Dallas, 2010

MS in Physics, University of Pittsburgh, 2012

Submitted to the Graduate Faculty of

the Kenneth P. Dietrich School of Arts and Sciences in partial

fulfillment

of the requirements for the degree of

Doctor of Philosophy

University of Pittsburgh

2016

UNIVERSITY OF PITTSBURGH

DIETRICH SCHOOL OF ARTS AND SCIENCES

This dissertation was presented

by

Travis J. Hurst

It was defended on

July 7, 2016

and approved by

Dr. Andrew Zentner, Physics & Astronomy, University of Pittsburgh

Dr. Arthur Kosowsky, Physics & Astronomy, University of Pittsburgh

Dr. Carles Badenes, Physics & Astronomy, University of Pittsburgh

Dr. Ayres Freitas, Physics & Astronomy, University of Pittsburgh

Dr. Hy Trac, Physics, Carnegie Mellon University

Dissertation Director: Dr. Andrew Zentner, Physics & Astronomy, University of Pittsburgh

ASTROPHYSICAL PROBES OF DARK MATTER

Travis J. Hurst, PhD

University of Pittsburgh, 2016

In the ΛCDM model, ≈ 26% of the matter-energy content of the Universe is in the form of an unidentified Cold Dark Matter. Observations indicate that the Dark Matter is a new exotic particle not accounted for in the Standard Model of particle physics. Identifying the Dark Matter particle is one of the most pressing problems in cosmology and particle physics. In this thesis we investigate several possible astrophysical signatures of Dark Matter: Dark Matter annihilations in cold White Dwarfs provide a source of luminosity that could halt their cooling. This effect can be used to constrain the Dark Matter density local to the White Dwarf. In the case of the coldest White Dwarf in a Globular Cluster, a constraint on the maximum Dark Matter content is derived. Globular Clusters do not appear to have Dark Matter halos today, but could have possessed them in the past. We investigate whether Globular Clusters could have lost their halos through multi-body gravitational interactions—we find that this scenario is unlikely. Finally, we explore the effects of Asymmetric Dark Matter on stellar evolution. Asymmetric Dark Matter can alter the transport of energy in the cores of stars. We show that this has potentially observable effects on low mass Main Sequence and post-Main Sequence stars. Our main conclusion is that astrophysical observations can potentially rule out some Dark Matter models. On the other hand, if the properties of the Dark Matter particle become known, then its astrophysical effects must be taken into account when evaluating observations.

TABLE OF CONTENTS

LIST OF TABLES

LIST OF FIGURES

1.0 INTRODUCTION

Modern cosmology is largely organized around a specific hot Big Bang model known as ΛCDM. According to this model, only $\approx 5\%$ of the energy content of the Universe is made up of ordinary baryonic matter, with the remainder being composed of $\approx 26\%$ Cold Dark Matter and $\approx 69\%$ Dark Energy [161]. Identifying the Dark Matter and Dark Energy are the two most outstanding problems in cosmology and two of the most significant problems in modern physics.

In this thesis we shall review the observational evidence for Dark Matter, the different methods for detecting and identifying the Dark Matter particle, and the current state of the field. We then present three astrophysical probes of Dark Matter physics.

1.1 OBSERVATIONAL EVIDENCE

There are several different lines of evidence in support of the ΛCDM model. Evidence for Dark Matter exists in the dynamics of galaxies and clusters of galaxies, the X-ray temperatures of galaxy clusters, both strong and weak gravitational lensing, the growth of structure, and the power spectrum of the Cosmic Microwave Background (CMB). Furthermore, observations indicate that the Dark Matter is not composed of astrophysical objects or the ordinary particles that appear in the Standard Model (SM) of particle physics, but is rather an exotic and hitherto undiscovered form of matter [17, 16, 194, 26, 85, 148].

Though it is not the focus of this thesis, Dark Energy is the dominant energy component of the Universe. The main lines of evidence in favor of Dark Energy are the Type Ia Supernovae (SN), the Baryon Acoustic Oscillations (BAO) and the CMB.

1.1.1 Cluster Dynamics

Evidence for Dark Matter dates back to at least the 1930s and the observation by Fritz Zwicky that the mass of the Coma cluster of galaxies as derived by the virial theorem is ∼160 times greater than what is inferred from the luminosity of the galaxies (a value that has since been revised) [204, 174].

For a relaxed, spherical distribution of galaxies, the virial theorem relates the total mass M of the cluster to the velocity dispersion σ_v as

$$M = \frac{5}{3}\frac{R\sigma_v^2}{\mathrm{G}}, \tag{1.1}$$

where R is the radius of the cluster and G is Newton's gravitational constant [204]. Zwicky observed that the galaxies in the Coma cluster were moving much too fast to remain gravitationally bound to the cluster if the only matter present was the luminous matter. Hence, he inferred that the majority of the matter is dark (i.e. non-luminous) and coined the term 'Cold Dark Matter' (Kalte Dunkle Materie in the original German). Modern observations of the kinematics of galaxies in the Coma cluster confirm that it is indeed Dark Matter dominated [126].

Figure 1.1 shows the enclosed mass within a given radius r (in units of $10^{15}\,\mathrm{M}_\odot$) as a function of r/r_{vir}. r_{vir} is the virial radius of the halo—the radius at which the density is 200 times the critical density of the Universe (a Universe with critical density is geometrically flat). Shown are the contributions of Dark Matter, galaxies, and gas to the total mass. Dark Matter contributes the vast majority of the mass at all scales.

Today we know that luminous stars make up only a small fraction of the mass in galaxy clusters, and that most of the baryonic matter is in the form of hot X-ray emitting gas—the Intra Cluster Medium (ICM). However, the ICM does not provide enough mass to explain the velocities of cluster galaxies and the temperature of the ICM is in fact further evidence for the presence of Dark Matter (see §1.1.3). Modern observations indicate that rich clusters contain about 85% Dark Matter, 14% ICM and only 1% stars [174, 51]. This approximate ratio is observed in clusters such as Coma (Figure 1.1) and the dynamically active cluster AC114. Figure 1.2 shows the contributions to the mass enclosed within a given projected radius of the various matter constituents in AC114.

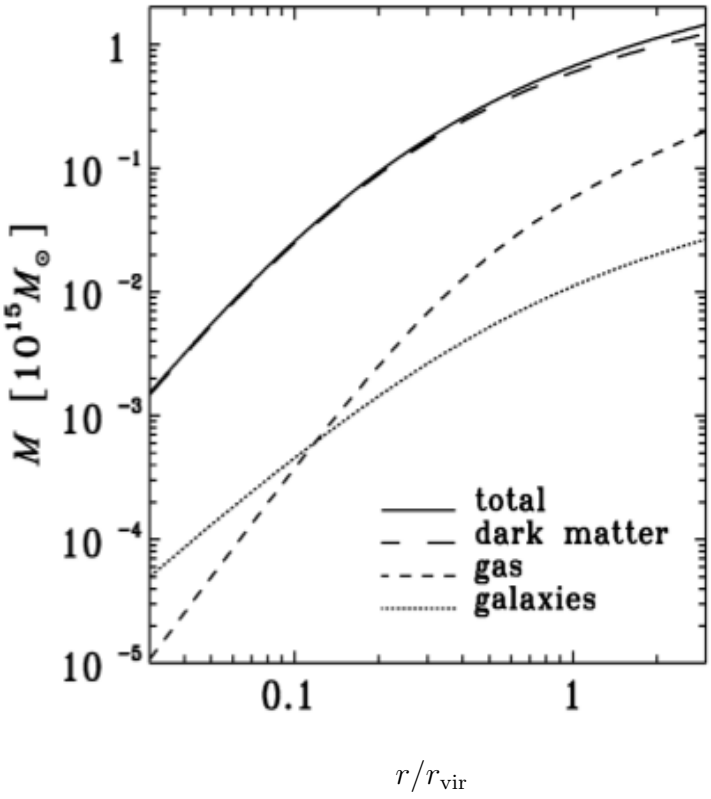

Figure 1.1: Mass fraction of various matter components in the Coma cluster. From Reference [126].

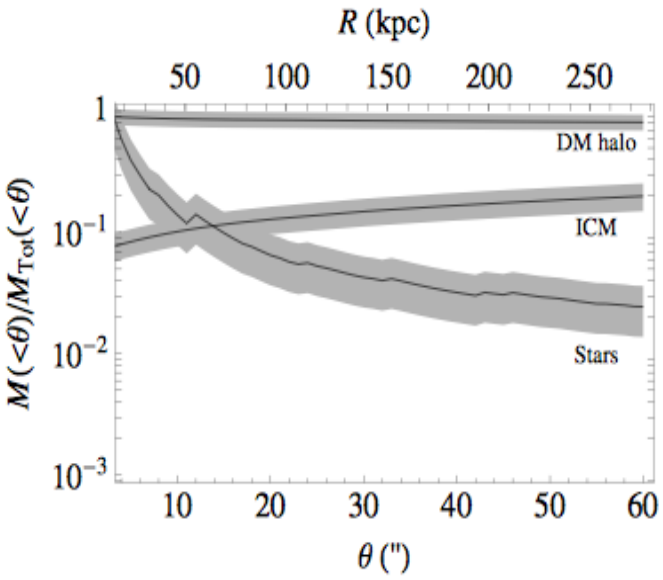

Figure 1.2: Mass fraction of various matter components in the galaxy cluster AC114. From Reference [182].

1.1.2 Galaxy Dynamics

Zwicky's work garnered little attention until more evidence of Dark Matter was discovered in the 1970s *via* the rotation curves of spiral galaxies. In 1970, Rubin & Ford published 21 cm observations of neutral hydrogen clouds in the Andromeda galaxy, which they used to determine the rotational velocity of the clouds [176].

For a test mass m on a circular orbit of radius r and velocity v, Newton's 2$^{\text{nd}}$ law reads

$$\frac{\mathrm{G}mM(r)}{r^2} = \frac{mv^2}{r}, \tag{1.2}$$

where $M(r)$ is the mass enclosed within radius r. The orbital velocity for a circular orbit is then

$$v_{\text{orb}} = \sqrt{\frac{\mathrm{G}M(r)}{r}}. \tag{1.3}$$

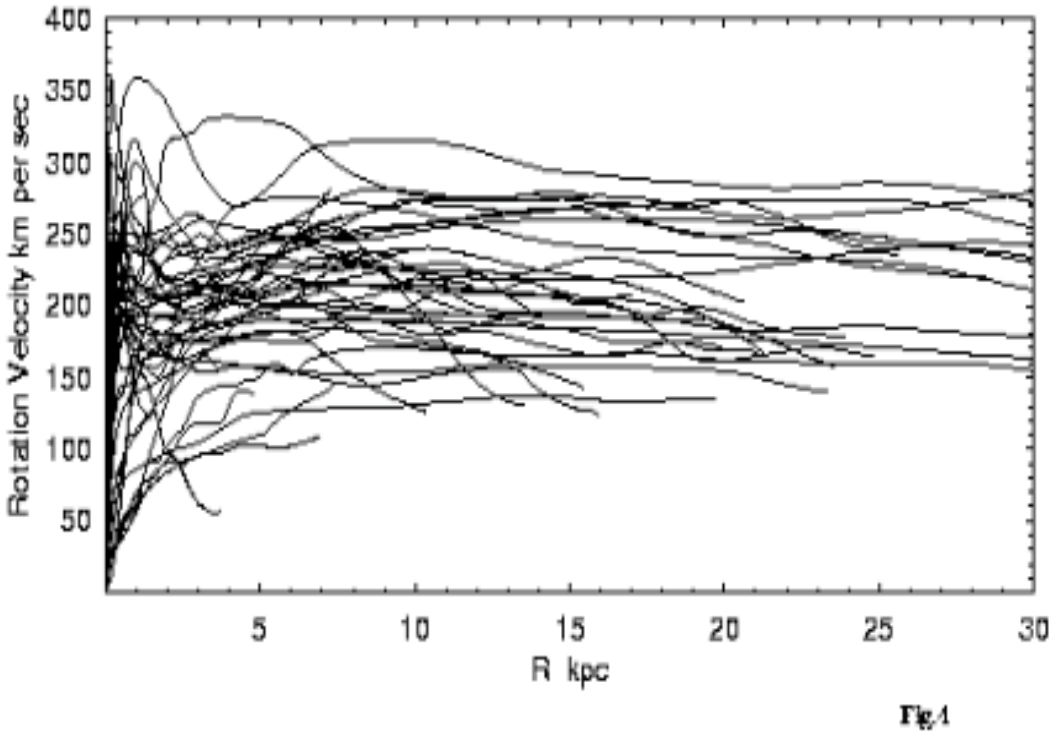

Figure 1.3: Rotation curves of many spiral galaxies. From Reference [185].

In the absence of Dark Matter, $v_{\rm orb}$ should decline as $\sqrt{1/r}$ beyond the visible extent of the galaxy where $M(r) = constant$. This relationship was first observed for planets orbiting the Sun by Johannes Kepler.

What Rubin & Ford observed was that rotational velocities do not fall off in the expected Keplerian or Newtonian manner. Rather, the rotational velocities of gas clouds far beyond the visible extent of the galaxy actually stayed roughly constant. As can be seen in Figure 1.3, further observations of other spiral galaxies indicated that this phenomenon is not unique to Andromeda, but is characteristic of all spiral galaxies [178, 177, 185]. The constant nature of the rotation curve at high radius indicates that there is more mass present than suggested by the luminous matter [177].

A simple solution to this problem is that $M(r) \propto r$. Then as can be readily seen from Equation (1.3), $v_{\rm orb} = constant$. Therefore, a spherical Dark Matter halo of density $\rho(r) \propto 1/r^2$ naturally explains the data. This observation launched the modern interest in Dark Matter.

1.1.3 Cluster X-ray Temperatures

As mentioned in §1.1.1, the majority of the baryonic mass present in galaxy clusters is in the ICM. X-ray observations measure the gas density and temperature profiles of the ICM. Adding the gas mass to the observed luminous matter, the total amount of baryonic matter $M_{\rm b}$ can be estimated [174, 55, 131]. Under the assumptions that the ICM is supported by its own thermal pressure and is in hydrostatic equilibrium in the cluster gravitational well, the temperature of the ICM at a given radius will be directly related to the total mass enclosed within that radius [131].

Figure 1.4 shows the X-ray temperature profile of the relaxed galaxy clusters A496 and Coma. The thick line is the prediction for a Relaxed Spherical Isothermal (RIS) Dark Matter profile, while the thin line is the profile of Nevarro-Frenk-&White (NFW) [144]. Note that the Dark Matter prediction fits the data well except at the smallest scale. This is an example of the well known 'core/cusp' problem in ΛCDM—the centers of Dark Matter halos are predicted to be more dense than observed [54].

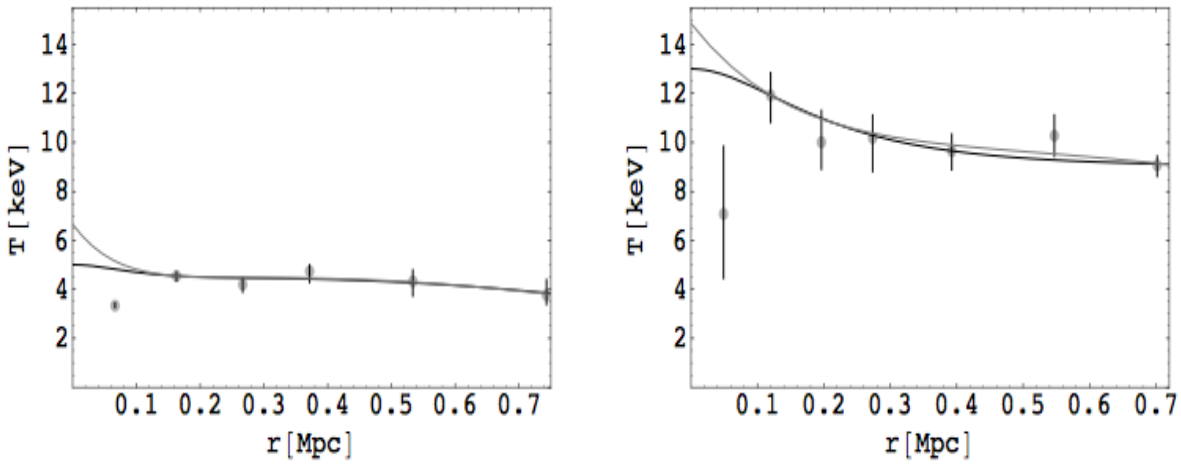

Figure 1.4: X-ray temperature profiles of A496 (*left*) and Coma (*right*). From Reference [55].

The top panel of Figure 1.5 shows the mass profiles (in units of $10^{14}\,M_{\odot}$) inferred from the X-ray temperature profiles for the RIS and NFW profiles in A496 and Coma. The thick short-dashed line is the mass associated with the ICM, the thick long-dashed-line (RIS model) and the thin long-dashed line (NFW) are the mass associated with the dark matter, and the thick solid line (RIS model) and the thin solid line (NFW) are the total mass profile. Dark Matter is the dominant mass constituent at all scales. The bottom panel shows the fraction of gas in each cluster and for each Dark Matter profile (line thicknesses are the same as in the top panels).

Observations of several small X-ray emitting groups of galaxies indicate that $M/M_{\rm b} \gtrsim 3$, demonstrating the presence of a significant Dark Matter halo [174]. An accurate measurement of M requires that Dark Energy (§1.1.8) is also taken into account as it reduces the strength of the gravitational potential [174]. Another source of error is the erroneous identification of cluster members. If galaxies are assigned to the cluster which are not actually physical members, the increase in velocity scatter can lead to an overestimate of the virial mass [174].

On larger scales such as the Coma cluster it is observed that $\approx 85\%$ of the total mass is in the form of Dark Matter (see §1.1.1).

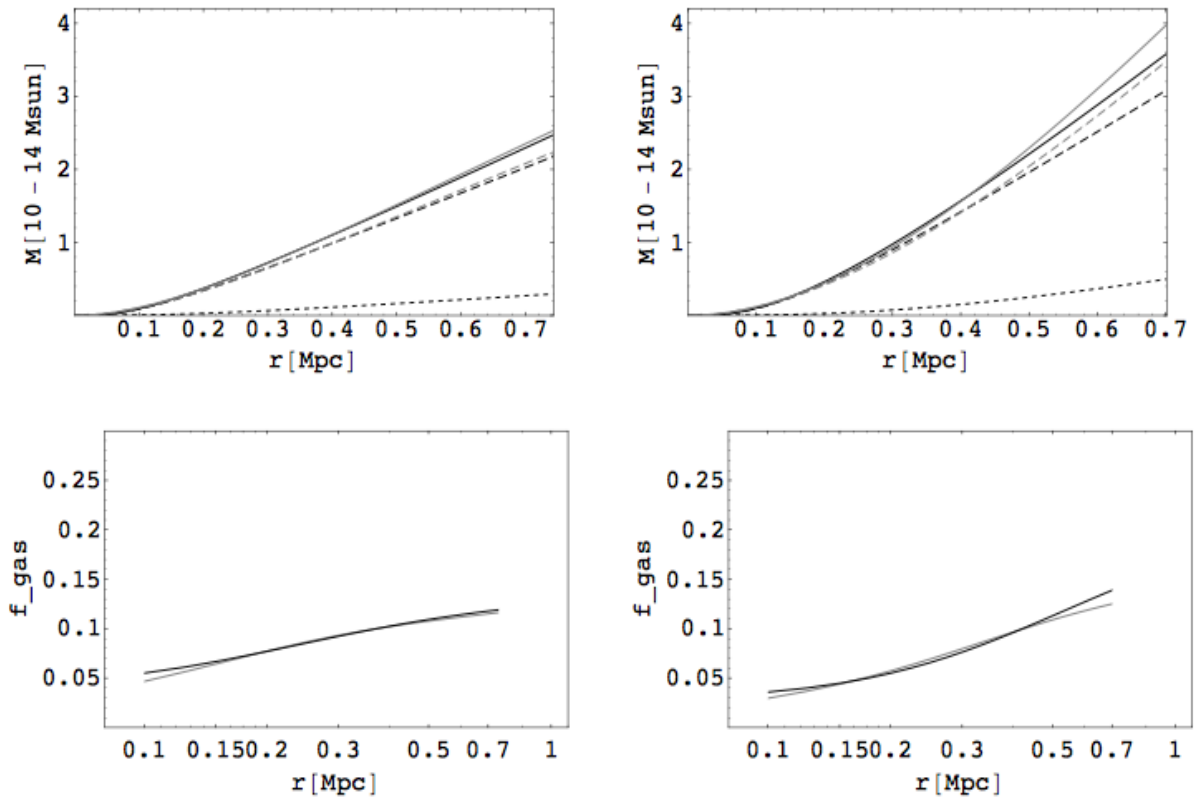

Figure 1.5: (*Top*) Mass profiles for A496 (*left*) and Coma (*right*). (*Bottom*) Gas fraction for A496 (*left*) and Coma (*right*). From Reference [55].

1.1.4 Gravitational Lensing by Clusters

Galaxy clusters provide further evidence for the presence of Dark Matter in the form of strong and weak gravitational lensing. In General Relativity (GR) the presence of matter causes space-time curvature and the 'force' of gravity is actually just the result of encountering this curvature. According to the Strong Equivalence Principal, light is also affected by gravity, therefore as a photon traverses the Universe, its path will be deflected whenever it encounters curved space-time. Hence, light is bent when it passes near a massive object (whether the mass is baryonic or Dark Matter) in a phenomenon known as gravitational lensing.

1.1.4.1 Strong Lensing For a sufficiently massive lens in favorable alignment with a background source, the deflection angle with regard to the line of site of the observer can be large, and multiple images of a background source can be formed. A phenomenon known as strong gravitational lensing. The multiple images are stretched out into long arcs or arclets (the case of a single image stretched into an arclet is sometimes referred to as intermediate gravitational lensing). The number of images and the amount of stretch depends on the geometry of the source-lens-observer system and the mass of the lens.

The top panel of Figure 1.6 shows strong gravitational lensing in a Hubble Space Telescope (HST) image of the cluster Abell 370. The lensing effect is readily observed as the long arc in the bottom center of the image. Within this arc are multiple images of several background galaxies. These systems are highlighted with colored ellipses in the bottom left panel. The different colors denote different galaxies which have been multiply imaged. In the bottom right panel is a reconstruction of the source galaxy labeled 2.1 [170].

1.1.4.2 Weak Lensing When the deflection angles are small the effect of space-time curvature on light is referred to as weak gravitational lensing. In the case of weak lensing multiple images are not formed. Rather, one image of the source is observed to be slightly stretched in the direction tangential to the lens (by slightly stretched we mean that no arclet is formed) and slightly compressed along the direction perpendicular to the lens. Thus, in the case of a spherical lens, a spherical background galaxy will appear to have ellipticity.

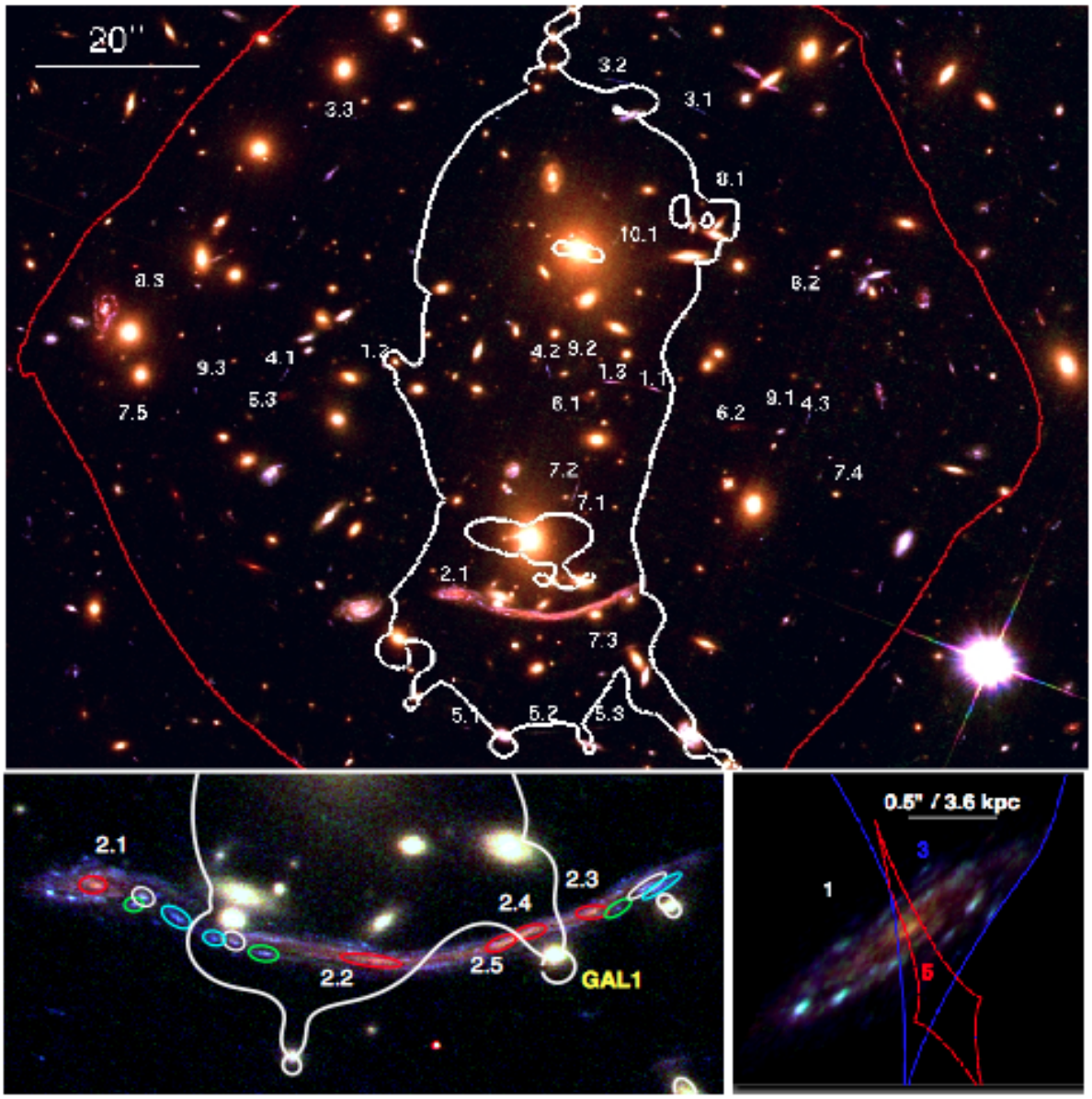

Figure 1.6: HST image of the cluster Abell 370 and reconstruction of the source system 2.1. From Reference [170].

This slight distortion of the image is called 'shear'.

In principle, one could measure the weak lensing of individual galaxies, but in practice galaxies have 'shape'—they are intrinsically elliptical rather than spherical. Therefore, weak lensing studies are done statistically with large samples of galaxies, in order to account for this 'shape noise'.

The effect of weak lensing is illustrated in Figure 1.7 where it has been greatly exaggerated for the purpose of visualization. The top panels show the effect of a single spherical lens at the center of the image on a collection of background galaxies in the absence of shape—if all of the galaxies were spherical. The bottom panels show the same effect but with shape noise included.

Observations of clusters such as Coma [146, 115] and Abell 370 [97] indicate that there is more lensing than would be expected from the luminous matter alone. Figure 1.8 shows the mass profile of Abell 370 as reconstructed from the weak lensing signal. The background shows the HST image of Abell 370. Overlaid are contours showing the distribution of galaxies (green), gas (red), and total mass (dark blue). Note that the total mass is dominated by Dark Matter (light blue).

A particularly striking example of cluster lensing is the Bullet Cluster. This is a system of 2 clusters of galaxies which recently, in a cosmological sense, passed through one another. Measurements of the gravitational lensing signal of this cluster indicate that the majority of the lensing is not coming from the baryonic matter.

In the left panel of Figure 1.9 is a color image from the Magellan images of the Bullet Cluster with the white bar indicating 200 kpc at the distance of the cluster. The blue +s show the location of the centers used to measure the masses of the plasma clouds. In the right panel is a 500 ks Chandra image of the cluster. Shown in green contours in both panels are the weak lensing reconstruction [48]. The majority of the baryonic matter of the cluster is in the form of the hot X-ray emitting gas shown in the right panel. Note that the X-ray emitting gas has a high collisional cross-section while the galaxies have effectively zero cross-section. Thus, the X-ray emitting gas has been separated from the stellar component by the collision of these 2 clusters. The contours show the strength of the lensing signal which is clearly aligned with the dissipationless stellar component and not the X-ray emitting plasma.

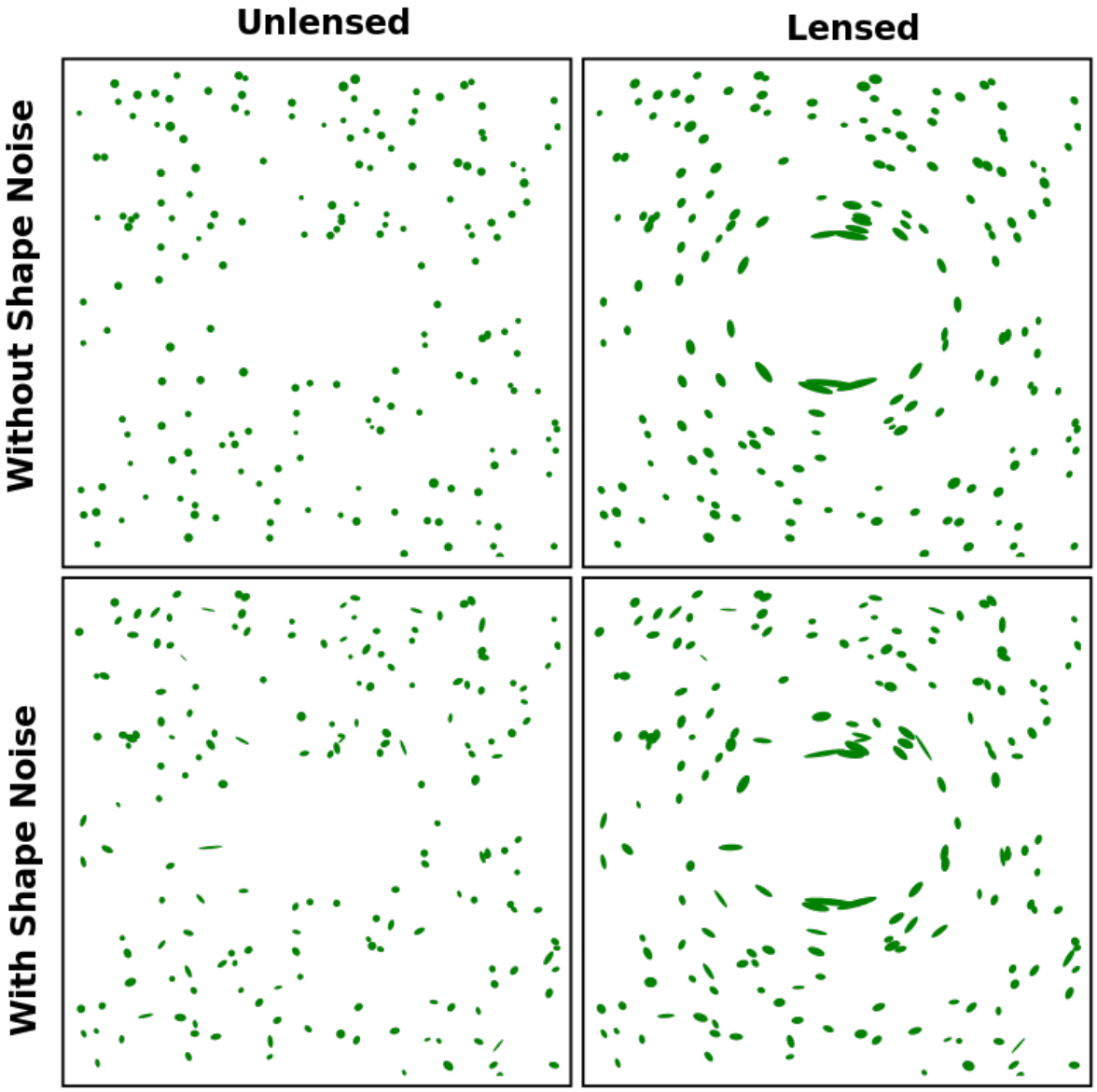

Figure 1.7: Simulation of lensing by an object at the center of the image with and without shape noise. Image distributed under a CC BY-SA 3.0 license.

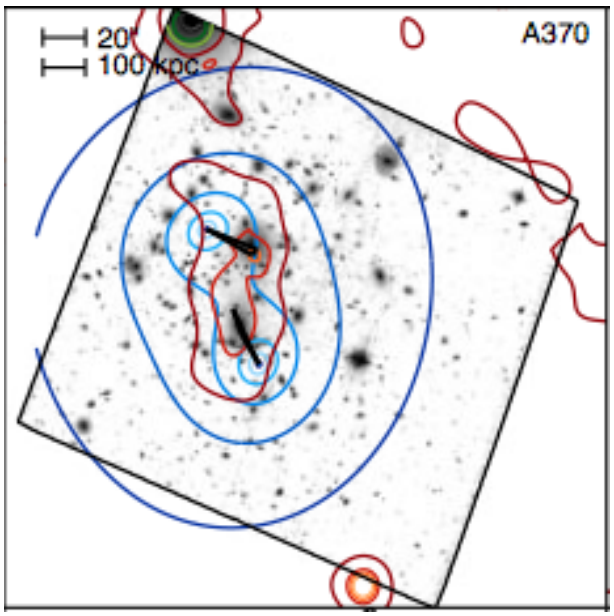

Figure 1.8: Contours of mass constituents (gas, galaxies, Dark Matter) overlaid on the HST image of Abell 370. From Reference [97].

As the stars make up only a small fraction of the baryonic matter present, the majority of the mass in the cluster must be Dark Matter.

Comparison of the distribution of galaxies and Dark Matter in the Bullet cluster gives a powerful constraint on the self-interaction cross-section of Dark Matter particles—meaning the cross-section for Dark Matter-Dark Matter particle scattering. The fact that the Dark Matter is roughly aligned with the galaxies indicates that the Dark Matter is collisionless (or nearly so). If the Dark Matter is not completely collisionless, it will lag behind the galaxies. Observations of this lag in e.g. the Bullet Cluster can then be used to constrain the Dark Matter self-interaction cross-section. The cross-section for non-gravitational interactions between SM particles and Dark Matter is known experimentally to be exceedingly small (e.g. [127, 13]). As an example the LUX collaboration has found that the Dark Matter-nucleon scattering cross-section $\sigma_{\chi p} \lesssim 10^{-44}\,\mathrm{cm}^2$ for $m_\chi \gtrsim 10\,\mathrm{GeV}/c^2$ [127]. Therefore, if Dark Matter is not completely collisionless, it must be due to self-interactions. Observations of the Bullet Cluster indicate that $\sigma/m_\chi \lesssim 1.25\,\mathrm{cm}^2\mathrm{g}^{-1}$ where σ is the Dark Matter self-

interaction cross-section and m_χ is the Dark Matter particle mass [167]. For context, models of mirror and hidden sector dark matter predict $\sigma/m_\chi \approx 0.6\,\mathrm{cm}^2\mathrm{g}^{-1}$, comparable to nuclear cross-sections in the standard model [97].

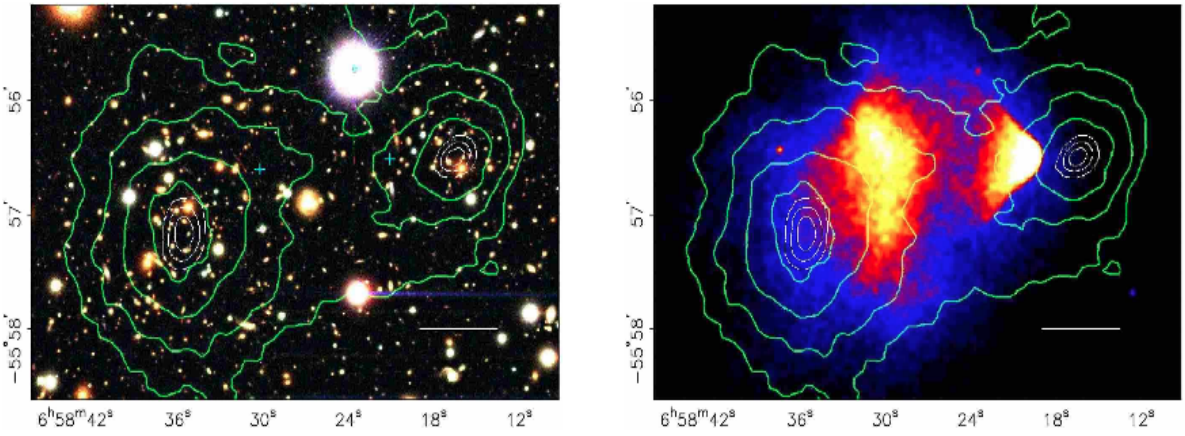

Figure 1.9: (*Left*) Color image of the Bullet Cluster. (*Right*) X-ray image of the Bullet Cluster. Green contours show the weak lensing signal. From Reference [48].

1.1.5 CMB Anisotropies

First predicted in 1948 by Alpher & Herman [18], the CMB was not observed until 1965 when it was accidentally discovered by Penzias & Wilson—it constituted an unexplained source of noise in a radio antenna they were testing [156]. This noise had a blackbody spectrum corresponding to 3.5 K, was isotropic, unpolarized, and displayed no seasonal variation [156]. The explanation for this 'noise' was given by Dicke, Peebles, Roll & Wilkinson in a paper published along with the measurements of Penzias & Wilson [61]. Penzias & Wilson were awarded the 1978 Nobel prize in physics for their discovery.

In the early Universe, the temperature was much too hot and dense for neutral hydrogen to form

$$p^+ + e^- \rightleftharpoons H + \gamma. \tag{1.4}$$

During this epoch the photons were effectively coupled to the matter in a hot plasma through

Thomson scattering

$$e^- + \gamma \rightarrow e^- + \gamma. \tag{1.5}$$

Eventually the Universe expanded and cooled to the point that the reverse reaction in Equation (1.4) no longer occurred and neutral hydrogen formed, a process called Recombination. As the free electron density decreased a related phenomenon of photon decoupling occurred. After decoupling the photons were free to propagate throughout the Universe and reach us today as the CMB, having been redshifted to a temperature of 2.7 K (redshift $z \approx 1100$) [161].

Figure 1.10 shows a map of the CMB as observed by the *Planck* satellite. The color coding represents variation in the temperature. Deviations from the average, known as CMB anisotropies, are of order 1 part in 10^5 [161]. At scales $\lesssim 1^o$ these slight temperature fluctuations correspond to density fluctuations in the early Universe, while at larger scales the Sachs-Wolfe effect dominates. Density fluctuations are encoded in the CMB by acoustic oscillations, which also induce line-of-site velocities. Therefore, the Doppler effect also contributes to the CMB power spectrum at small scales.

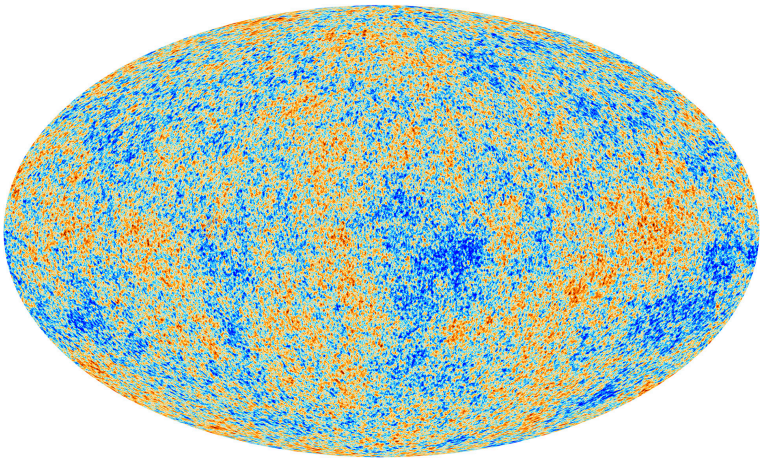

Figure 1.10: The CMB. Image credit: Planck Collaboration, ESA.

Overdense regions of the Universe tend to collapse and attract more matter *via* the force of gravity. Prior to decoupling, the photons were dragged into the overdensities along with matter, heating the plasma and causing it to expand. Thus prior to decoupling, the plasma

oscillated between compression and rarefaction. The hottest spots observed on the CMB today correspond to overdensities which were of the right size to be maximally compressed at the time of decoupling. The coldest spots correspond to underdensities which were at maximum rarefaction at the time of decoupling. Further anisotropies correspond to overdensities that had time to collapse, expand, and then collapse back to maximal compression again, underdensities which reach maximum rarefaction a second time, and so on.

The top panel of Figure 1.11 shows the power spectrum of the CMB versus multipole. Note that large multipole numbers correspond to small scales and *vice versa*. At least 7 peaks in the spectrum can be identified by eye. The peaks correspond to the hot and cold spots observed in the CMB, while the depts of the troughs are determined by the plasma velocity. The solid red line is the best fit ΛCDM model. The bottom panel shows the residual once the best fit ΛCDM model has been subtracted.

Comparison between the predicted acoustic peak scale and its angular extent provides a measurement of the angular diameter distance to recombination. The angular diameter distance in turn depends on the spatial curvature and expansion history of the universe [106]. Sensitivity to the expansion of the Universe is due to the radial distance travelled by a photon

$$D^* = \int_0^{z_*} \frac{dz}{H(z)}, \tag{1.6}$$

where the Hubble parameter $H(z)$ parametrizes the expansion history of the Universe. With the matter and radiation energy densities measured, the remaining contributor to the expansion rate $H(z)$ is the Dark Energy (§1.1.8) [106]. Sensitivity to the curvature arises because in a curved Universe the angular diameter distance is different from the radial distance. (This is because in a curved Universe, parallel lines can converge or diverge. Therefore, the angle subtended by an object of a given size is different in a curved Universe than in a flat one.) The first acoustic peak in the CMB indicates that the Universe is nearly spatially flat [106]. The second peak represents rarefaction of the acoustic wave in a gravitational potential and hence is suppressed in amplitude by the baryon inertia [106]. Measurement of the second peak then determines the baryon density. The third peak begins to show the effects of the matter-radiation ratio on the overall amplitude of the acoustic peaks. Furthermore, decay in the gravitational potential during radiation domination would change the

peak height ratios of the second and third peaks [106]. Measurement of the third peak then determines the total matter density. Therefore, comparison of the second and third peaks yields the Dark Matter density. Using the temperature data (combined with lensing data, see §1.1.7) the *Planck* collaboration finds $\Omega_\Lambda = 0.692 \pm 0.012$ and $\Omega_\mathrm{m} = 0.308 \pm 0.012$, with $\Omega_\mathrm{dm}h^2 = 0.1186 \pm 0.0020$ and $\Omega_\mathrm{b}h^2 = 0.02226 \pm 0.00023$, where $h = H_0/100$ [161].

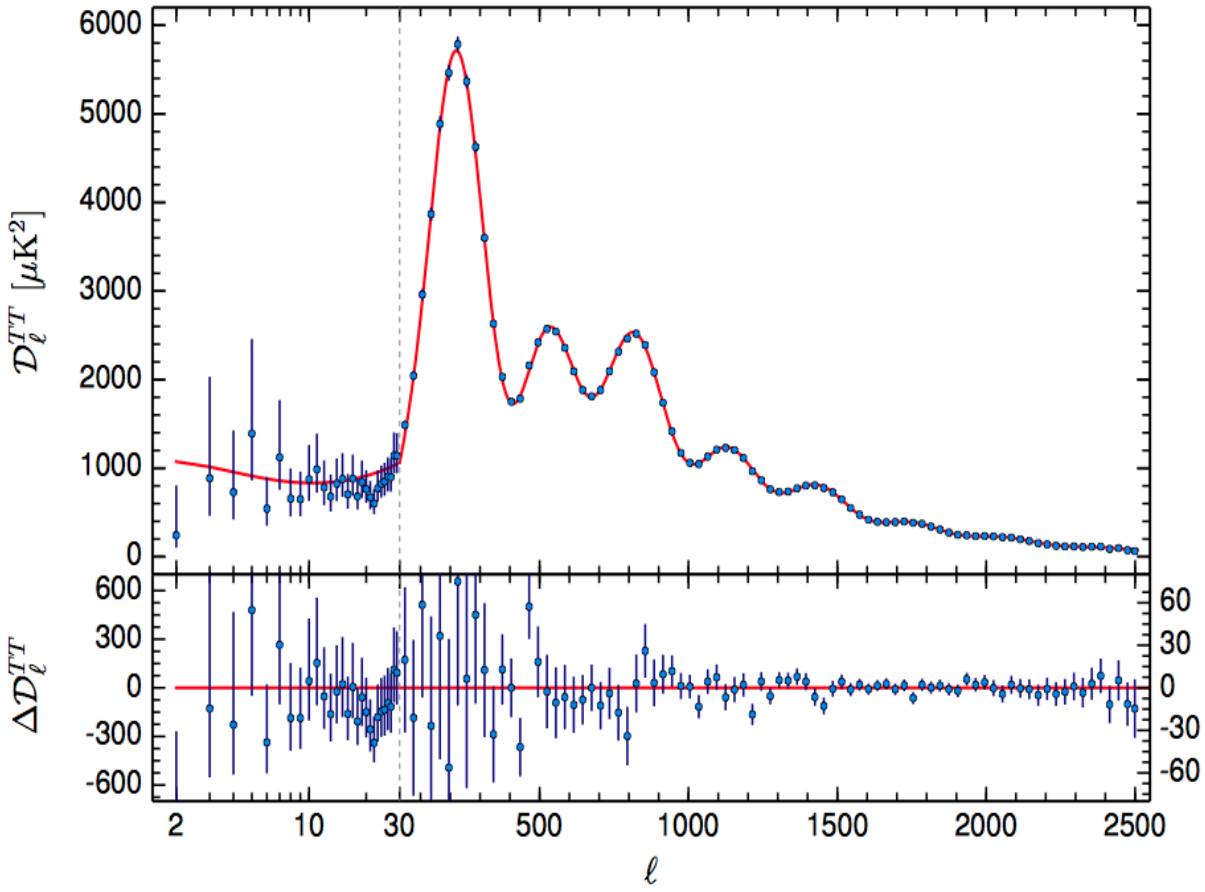

Figure 1.11: The power spectrum of the CMB as observed by *Planck*. From Reference [161].

1.1.6 Growth of Structure

As discussed in §1.1.5 the anisotropies observed in the CMB correspond to density fluctuations in the early Universe ($\approx 375,000$ years after the Big Bang [162]). One can then ask the question: Could galaxies have grown within these overdensities? If the only matter present

were baryonic, then the amplitude of the primordial density fluctuations would have to be quite large, leading to CMB anisotropies with amplitudes much larger than what is observed. Hence, this scenario is ruled out [174].

On the other hand, Dark Matter is collisionless and does not interact electromagnetically. Therefore, Dark Matter simply collapses, while baryonic matter is pressure supported. Thus, Dark Matter fluctuations could collapse earlier than baryons, and the additional gravitating mass explains how galaxies could form in a manner consistent with the CMB observations.

It should also be noted that cosmological simulations with Dark Matter produce structure that is consistent with that observed in the Universe on large scales. So-called N-body simulations model the Universe as being made of collisionless Dark Matter particles and allow the Universe to evolve over time through Newtonian gravity. In these simulations Dark Matter particles are seen to form roughly spherical Dark Matter halos—galaxy scale Dark Matter overdensities. Dark Matter halos are then the structures within which galaxies form. In fact, structure formation is the reason the Dark Matter must be cold—meaning the Dark Matter particle was not relativistic during 'freeze out' (the point at which the annihilation rate of Dark Matter dropped below the expansion rate, leaving the relic abundance). Hot Dark Matter predicts 'top-down' structure formation; the largest structures form first and then dissipate. However, what is observed is that structure formation is 'bottom-up'; the smallest structures form first and merge to form larger and larger structures, consistent with Cold Dark Matter.

Figure 1.12 shows a visualization of a slice of the Millennium Simulation at z = 0 [35, 2]. This simulation follows $N = 2160^3$ Dark Matter particles from redshift $z = 127$ to $z = 0$ in a cubic box of side $500h^{-1}$ Mpc where h is the Hubble constant in units of 100 km/s/Mpc [2]. Figure 1.13 shows a slice of the real Universe as observed by the Sloan Digital Sky Survey (SDSS) [200]. Comparing the simulation with the data we see that N-body simulations do indeed recover the filamentary structure of the Universe—galaxies and clusters mostly lie within filaments, which surround voids. However, it is worth mentioning that N-body simulations, and ΛCDM generally, suffer from several problems on smaller scales. Notably the 'core/cusp' problem on the scales of clusters and smaller structures [54] and the 'missing satellites' [134, 119, 139], 'too big to fail' [34], and 'satellite alignment' [150] problems on the

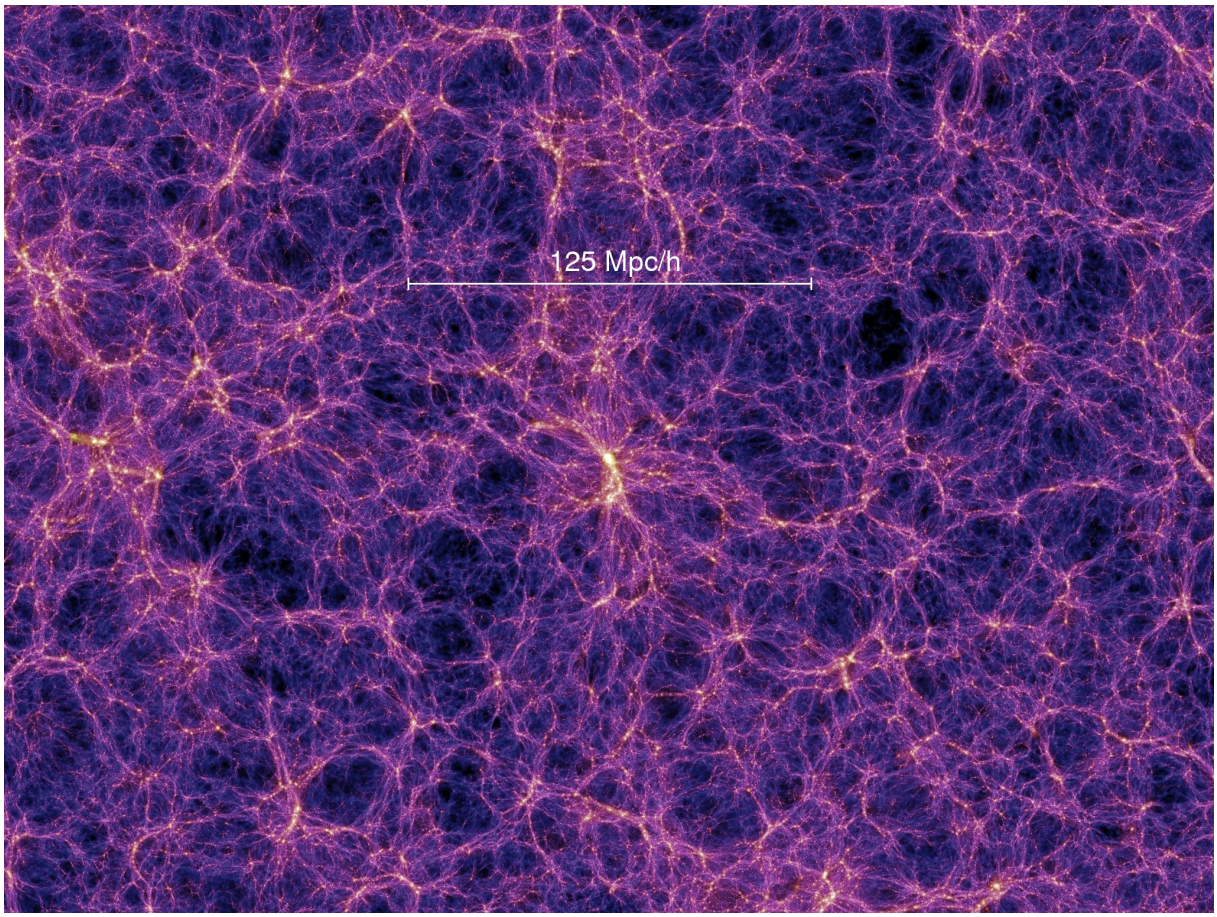

Figure 1.12: Visualization of the Millennium Simulation. From Reference [2].

scale of the dwarf satellite galaxies in the Local Group.

The missing satellite problem refers to the fact that N-body simulations predict that a MW-like halo should have more dwarf satellite galaxies than are observed. Additionally, the observed dwarfs are less concentrated than many of the simulated sub-halos. The simulated sub-halos are more massive at a given size and should be able to form stars. Hence, they are too big to fail. Finally, the alignment problem refers to the fact that the MW dwarf satellites lie in roughly the same plane and all orbit in the same direction. This observation could be explained by e.g. self-interacting Dark Matter. In such a model, in addition to a spherical halo a dark disk can be formed. It is then natural that the MW satellites lie in this dark disk (e.g. [68]).

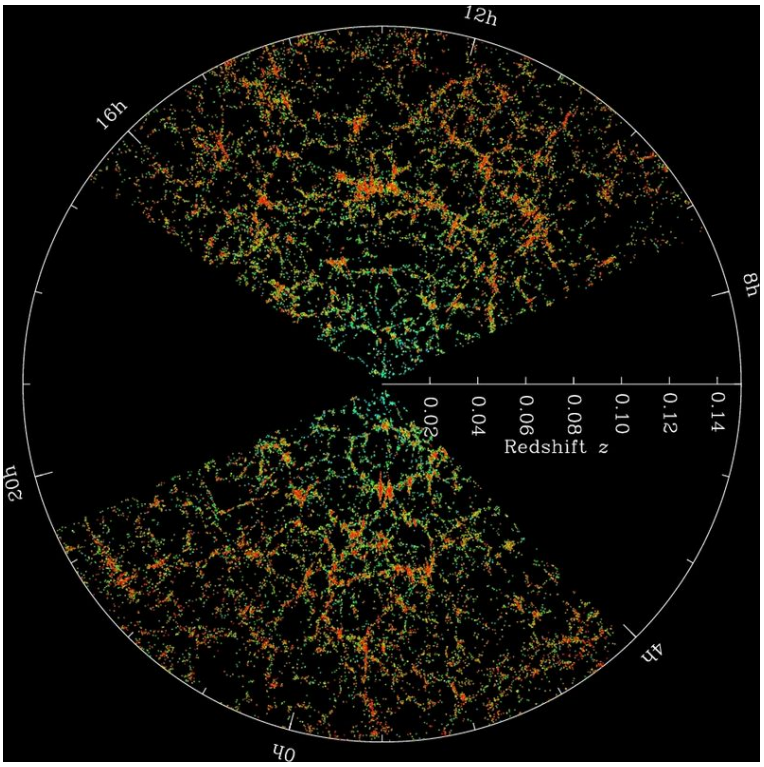

Figure 1.13: A slice of the Universe as observed by SDSS. Image credit: M. Blanton and SDSS.

1.1.7 Cosmic Shear & CMB Lensing

As a photon traverses the Universe it is likely to encounter not one structure, but many galaxies, clusters, and the filaments in which they reside (i.e. the Large Scale Structure (LSS) of the Universe). Thus the path of a photon undergoes many tiny deflections when it travels cosmological distances. The cumulative effect of these weak lensing events from LSS is known as Cosmic Shear and probes the amount of LSS, and hence matter, in the Universe [74, 191].

Figure 1.14 shows a simulation of Cosmic Shear. In the left panel is a side view of a simulation and the theoretical paths photons would take as they traversed this simulated Universe. The right panel shows the front view of the same slice. As can be clearly seen, the photons undergo numerous weak lensing events as they travel across the cosmos. The result of Cosmic Shear is that the galaxy images have been stretched and aligned preferentially along filaments.

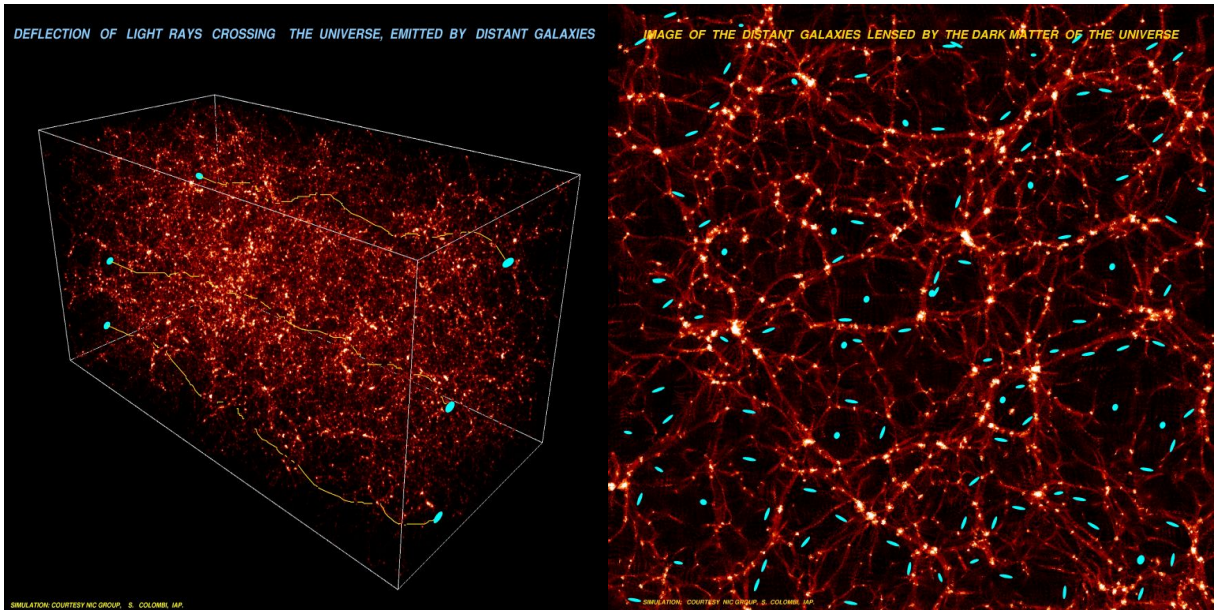

Figure 1.14: Simulation of Cosmic Shear. Image Credit: S. Colombi and the NIC group, IAP.

Similar to Cosmic Shear, photons from the CMB experience weak lensing from LSS. This

slightly perturbs the CMB anisotropies. The effect is subtle but can be measured statistically with high angular resolution, low-noise observations of the CMB, such as those provided by *Planck* [162].

Figure 1.15 shows the CMB lensing potential power spectrum as a function of multipole. Measurements include those by the Atacama Cosmology Telescope (ACT) [52], the South Pole Telescope (SPT) [195], and *Planck* 2013 [160] & 2015 [162]. The solid line is a fiducial ΛCDM model described in Reference [162], which is an excellent fit to the data.

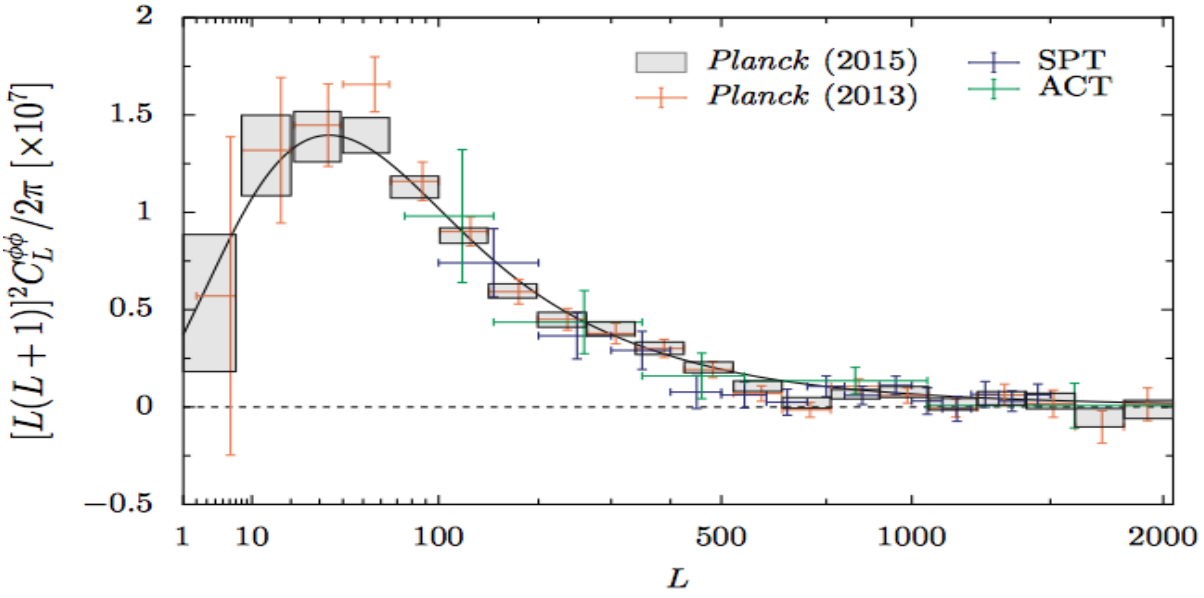

Figure 1.15: The CMB lensing potential power spectrum and best fit ΛCDM model. From Reference [162].

1.1.8 Dark Energy

In addition to Dark Matter, the ΛCDM model has a second mysterious energy density constituent: Dark Energy. Naively one might expect that in a flat Universe containing matter, the expansion of the Universe should be slowed by the force of gravity. This expectation arises from the fact that gravity is an attractive force. However, what is inferred from observations of Type Ia SuperNovae (SN) is that the expansion rate of the Universe is actually increasing.

Type Ia SN are believed to arise from the explosion of either 1 or 2 White Dwarfs (WD). A WD is the compact relic core of a dead star. These objects are completely supported against gravity by electron degeneracy pressure. A WD cannot exceed the Chandrasekhar mass ($\approx 1.4\,M_\odot$) without collapsing, as the force of gravity will overcome the degeneracy pressure [43]. A WD which approaches the Chandrasekhar limit will begin to collapse triggering a Type Ia SN.

There are 2 scenarios discussed in the literature whereby a WD in a binary system can gain enough mass to approach the Chandrasekhar limit. In the Single Degenerate scenario, one member of the binary is a WD and the other member is a Red Giant. The Red Giant overflows its Roche lobe and loses matter, which accretes onto the WD. In the Double Degenerate scenario both members of the binary are WDs. The eventual merger of the WDs leads to the SN.

Type Ia SN are what astronomers refer to as standard candles—meaning they all have the same peak luminosity. (Really they are standardizable candles.) Figure 1.16 shows the light curves of several 'nearby' Type Ia SN. The y-axes are a measure of the absolute brightness and the x-axes are the days since the peak brightness was reached. As can be seen in the top panel, the brightest SN also have the widest peaks. By adjusting for this so-called stretch factor the Type Ia SN can be standardized [173, 159]. The bottom panel shows the result of this correction, which fits the data well until over 45 restframe days past peak luminosity [157].

Standard candles are useful in astronomy and cosmology because they can be used to calculate distances. The observed flux of an object decreases as $1/4\pi r^2$, because as distance increases, the luminosity is spread over a sphere of increasing radius r. Therefore the apparent brightness of an object is related to its absolute brightness or luminosity as

$$b = \frac{L}{4\pi r^2}. \tag{1.7}$$

Standard candles have a known intrinsic luminosity, so observations of their apparent brightness can be used to calculate the distance to the candle.

Observations of high redshift SN, indicate that their host galaxies are further away than would be expected in a decelerating Universe. Furthermore, the data indicate that the

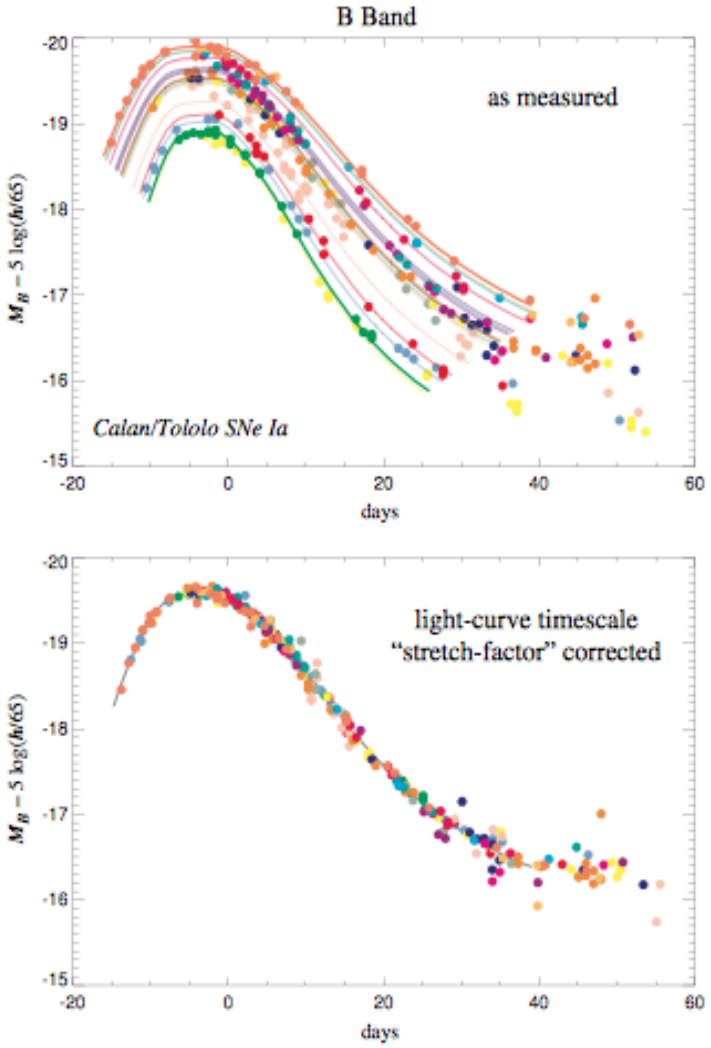

Figure 1.16: Uncorrected and stretch corrected light curves of 'nearby' SN. From Reference [73].

expansion has been accelerating for the past 5 Gyr [157, 172]. These results provide evidence for $\Omega_\Lambda > 0$ at greater than 99% confidence [73]. The top panel of Figure 1.17 shows the distance modulus (apparent magnitude minus absolute magnitude) of the Type Ia SN versus redshift z. The lines represent the Einstein-de Sitter matter dominated Universe ($\Omega_\mathrm{m} = 1.0, \Omega_\Lambda = 0$), an open universe without Dark Energy ($\Omega_\mathrm{m} = 0.3, \Omega_\Lambda = 0$), and a ΛCDM universe ($\Omega_\mathrm{m} = 0.3, \Omega_\Lambda = 0.7$). The bottom panel shows the residual after subtracting the open universe model. ΛCDM is clearly preferred by the data.

An accelerating expansion can be understood in the standard cosmology as being due to a vacuum energy density with negative equation of state

$$w = \frac{P}{\rho}, \tag{1.8}$$

with P and ρ the pressure and density of the vacuum energy respectively. In the standard cosmology, this vacuum energy is parametrized by Einstein's cosmological constant Λ. This so called Dark Energy is the dominant energy component of the Universe today ($\Omega_\Lambda \approx 0.61$ [161]). In the standard cosmology $w = -1$, but more generally the equation of state can be a function of redshift, or alternatively scale factor a. Frequently the equation of state is parametrized as $w(a) = w_0 + w_\mathrm{a} a$, a cosmology sometimes called wCDM. Such dynamical Dark Energy could be the result of e.g. a scalar field [73]. Some models of scalar field Dark Energy can solve the so-called "cosmic coincidence" or "why now?" problem. This problem asks why we happen to live at a time in the Universe that Dark Energy is becoming dominant, given that the Universe was either matter or radiation dominated for most of its history. It certainly could be simply a product of the scalings of matter, radiation and Dark energy density. A perhaps more satisfying explanation is provided by "freezing" scalar field models. In these models, the scalar field energy density tracks that of the dominant component at early times and then dominates at late times, providing a dynamical origin for the coincidence [73].

Dark Energy was discovered by 2 groups in the late 1990s [157, 172]. Leaders of the groups were awarded the Nobel Prize in physics in 2011. Since its discovery *via* type Ia SN, further evidence in favor of Dark Energy has been observed. As discussed in §1.1.5 the anisotropies in the CMB are the result of acoustic oscillations prior to Recombination.

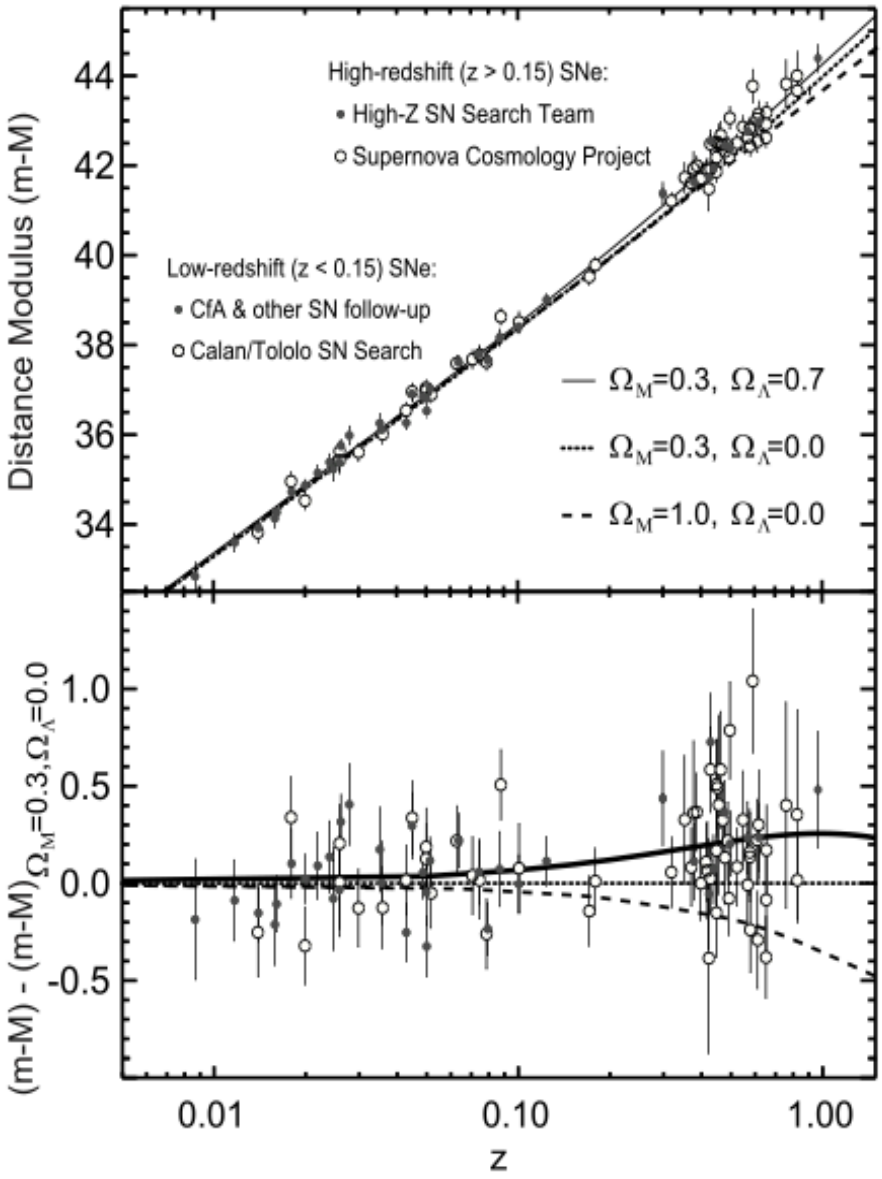

Figure 1.17: *(Top)* Type Ia SN distance modulus versus redshift. (*Bottom*) Residual compared to the open universe model. From Reference [73].

The first peak in the CMB power spectrum provides evidence for Dark Energy through its role in the expansion history of the Universe. Furthermore, the scale of the acoustic oscillations is the sound horizon at the time of Recombination, which provides a standard ruler. After photon decoupling, the effective sound speed of the baryons plummets due to loss of photon pressure. The acoustic oscillations remain imprinted in the baryon distribution, and through gravitational interactions, in the Dark Matter distribution [73]. Combined with the standard ruler calibrated by the CMB, the Baryon Acoustic Oscillation (BAO) scale in the galaxy distribution yields a geometric probe of the expansion history, and therefore Dark Energy. The BAO is observed in the galaxy power spectrum, where it induces oscillations with amplitude of order 10%. The BAO amplitude is small compared to that of the CMB anisotropies because the baryons have only a small impact on the far larger Dark Matter component [73].

1.1.9 Fits From Multiple Probes

By combining cosmological probes it is possible to derive tight constraints on Dark Energy and Dark Matter in the parameter space of Ω_Λ-Ω_m, where Ω_Λ & Ω_m are the energy densities of Dark Energy and matter respectively, in units of the critical density of the Universe. Figure 1.18 shows several different observational probes in this parameter space. Since many of the constraints are orthogonal to one another, it is possible to derive constraints which are tighter than for any of the individual probes. Note that baryons cannot account for more than a small fraction of Ω_m.

1.2 ALTERNATIVES TO DARK MATTER

It is worth mentioning that the Dark Matter hypothesis is not the only possible explanation for the missing mass problem. It could be the case that our understanding of physics is incorrect. Either our understanding of the laws of gravity themselves or the response of matter to gravity could be flawed.

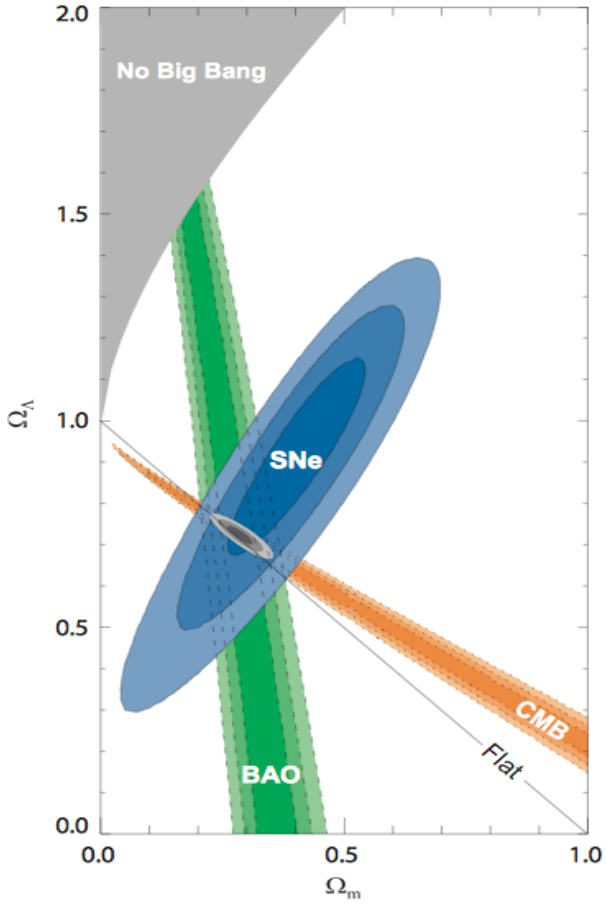

Figure 1.18: Constraints on Ω_Λ & Ω_m from different observational probes. From Reference [120].

1.2.1 Alternative Models of Gravity

It is possible that General Relativity is not the correct theory of gravity. Numerous alternative models of gravity have been explored in the literature (e.g. f(R) gravity [39], Tensor-Vector-Scalar gravity (TeVeS) [27], massive gravity [57] and Scalar-Tensor-Vector Gravity (STVG) [137] among others).

Alternative models of gravity are tightly constrained by the need to reproduce the many successes of GR at solar system scales and observations of binary pulsar systems. For a recent review of experimental tests of GR and alternative models of gravity see Reference [198]. Alternative models of gravity shall be further constrained in the future by observations of gravitational waves [23]. One of the fundamental predictions of GR, gravitational waves were recently discovered by the Advanced Laser Interferometer Gravitational-Wave Observatory (LIGO) [192]. To date there are no observations inconsistent with GR.

1.2.2 Modified Newtonian Dynamics

MOdified Newtonian Mechanics (MOND) was originally proposed by Milgrom in 1983 as an alternative to the Dark Matter hypothesis [136]. The idea behind MOND is to explain observations (e.g. the regularities in galaxy rotation curves) not by invoking Dark Matter, but instead by modifying either Newton's 2nd Law or Newton's Law of Gravity.

MOND has been successful at galactic scales, explaining the rotation curves of spiral galaxies and the Tully-Fisher relation without the need for Dark Matter [135, 180]. However, in order to match the dynamical and gravitational lensing observations at the scales of galaxy clusters, Dark Matter must still be invoked (e.g. Reference [179]). The Bullet Cluster is particularly difficult to explain in the MOND paradigm [48].

1.3 ASTROPHYSICAL DARK MATTER

Given that the majority of mass in the Universe is Dark Matter, the problem becomes identifying the nature of the Dark Matter. There is no *a priori* reason that the Dark Matter

has to be something new and exotic. Any number of astrophysical objects could potentially be the Dark Matter (e.g. brown dwarfs, black holes, cold white dwarfs, neutron stars, and dim red dwarfs). Collectively, these Dark Matter candidates are known as Massive Astrophysical Compact Halo Objects (MACHOs). MACHOs have the advantage that they are known to exist; however, in order to be the Dark Matter they must be present in sufficient number to account for the 'missing' mass in galaxies and clusters.

Observing MACHOs is a difficult but not impossible task. One method is to exploit gravitational microlensing. For a gravitational lens the size of the typical MACHO (ranging from Jupiter to stellar masses) the amount of deflection is small, even compared with weak lensing. The effect of such small deflection angles is that slightly more photon paths lead to the observer, thus a brief brightening of the background source is observed when the MACHO passes in front.

A comprehensive microlensing search for MACHOs in the MW galaxy was undertaken by the MACHO project, which monitored stars in the Large Magellanic Cloud (LMC) and Galactic bulge [17]. This survey found that MACHOs likely account for $\sim 20\%$ of the MW Dark Matter halo, with a halo of 100% MACHOs ruled out at the 95% confidence level [16]. Subsequently, the EROS survey found that MACHOs could only account for 8% of the MW halo [194].

Additional searches for MACHOs have been carried out. An HST search for red dwarfs revealed that they do not contribute significantly to the Galactic mass budget [26]. If these low mass stars were a significant contributor to the Dark Matter, many more would be seen by HST.

A search for microlensing from Primordial Black Holes (PBH) with masses in the range $2 \times 10^9\,\mathrm{M}_\odot$-$10^{-7}\,\mathrm{M}_\odot$ was undertaken with data from the Kepler satellite and found that they could not make up all of the Dark Matter [85]. Subsequently, a novel mechanism for constraining PBHs of even lower mass was proposed in Reference [148]. In a close encounter with a neutron star these low mass PBHs could disrupt the neutron star through rapid accretion. Observations of old neutron stars in Globular Clusters (GC) then constrain the number of primordial black holes in the MW. Combined with existing limits, the results of Reference [148] are generally considered to have effectively ruled out primordial black holes as

the dominant Dark Matter constituent. However, it was recently noted in Reference [46] that black holes could have merged efficiently in the early Universe such that initially substellar PBHs that avoid the CMB constraints could merge and form larger PBHs that avoid the microlensing constraints [47], thereby keeping PBHs viable as a Dark Matter candidate.

Taking all of this evidence into account, MACHOs are not strictly ruled out but are generally disfavored as the dominant Dark Matter constituent. The alternative is then that the Dark Matter represents new physics beyond the SM.

1.4 PARTICLE CANDIDATES

If the Dark Matter is not made up of ordinary astrophysical objects, the explanation may be that Dark Matter is a new exotic form of matter that interacts gravitationally but not electromagnetically. Particles discussed extensively in the literature include Weakly Interacting Massive Particles (WIMP), axions, and sterile neutrinos.

1.4.1 WIMPs

One proposal is that Dark Matter particles interact gravitationally as they have mass, but are otherwise only coupled to the SM particles through the weak force. These so-called WIMPs are currently the most favored particle candidate in cosmology. WIMPs are compelling candidates in part because of the so-called 'WIMP miracle'—a thermally produced Dark Matter particle with weak-scale interactions naturally predicts the correct relic abundance today. Additionally, they appear naturally in Supersymmetric and other extensions to the SM of particle physics. Therefore, they have a natural motivation and are not simply an *ad hoc* solution to the Dark Matter problem. For comprehensive reviews on WIMP Dark Matter see e.g. [114, 62].

1.4.2 Other Candidates

Another well motivated particle candidate is the axion. In particle physics, the axion has been proposed as a possible solution to the strong CP problem (for a full discussion of axions and the strong CP problem see e.g. the review [199]). In cosmology the axion is an appealing Dark Matter candidate as it is coupled to the standard model even more weakly than WIMPs and has a lifetime which is long with respect to the age of the Universe, making it effectively stable. Furthermore, depending on the particular production mechanism, axions can have an energy density today that provides a significant fraction of the observed Dark Matter density [199]. Ultra-light axions ($m_\chi \sim 10^{-22}\,\mathrm{eV}$) may behave as 'Fuzzy' Cold Dark Matter, which could potentially alleviate the small scale problems of ΛCDM discussed in §1.1.6 [107]. Unlike WIMPs, axions are not a thermal relic but are produced in Peccei-Quinn theory by a spontaneously broken symmetry [154].

Another Dark Matter candidate, which has recently been gaining attention, are sterile neutrinos with mass of order $m_\chi \sim \mathrm{keV}/c^2$. Sterile neutrinos are well motivated from a particle physics standpoint as they are a possible solution to the problem of the active neutrino masses through the 'seesaw mechanism' (for a full discussion of sterile neutrinos in particle physics, cosmology, and astrophysics see e.g. the review [12]). Sterile neutrinos are an attractive Dark Matter candidate as they are neutral, massive, and can be effectively stable with respect to the age of the Universe. Moreover, Sterile neutrinos can be Warm Dark Matter, which has been proposed to solve the various problems ΛCDM has at small scales (see §1.1.6) [12]. Sterile neutrinos are different from WIMPs in that they are coupled to the SM only feebly. They have no charged or neutral current weak interactions except those induced by mixing with the active neutrinos [12]. WIMPs on the other hand are expected to couple to the SM through a neutral current-like interaction (e.g. [14]).

1.5 IDENTIFYING THE DARK MATTER PARTICLE

We now turn our attention to the problem of detecting and identifying the Dark Matter particle. There are 3 methods of detecting Dark Matter particles: particle collider searches, direct-detection scattering experiments, and indirect detection of Dark Matter physics *via* its annihilation products.

1.5.1 Collider Experiments

If Dark Matter particles exist, they should be produced in particle colliders, provided the collisions are of sufficiently high energy to produce particles with mass m_χ, and the interaction cross-section is sufficiently large. Dark matter pair production at high energy colliders may leave observable signatures in the energy and momentum spectra of the objects recoiling against the dark matter [71]. The signature of Dark Matter production in a collider is missing energy or momentum from the collision event.

Figure 1.19 shows a schematic of A Toroidal LHC ApparatuS (ATLAS), one of the particle detectors at the Large Hadron Collider (LHC) [25]. Particle detectors at colliders exploit interactions between SM particles in order to reconstruct the collision event. Detectors typically work by surrounding the collider with different layers of material and a magnetic field. Each material is chosen so that a particular type of SM particle will deposit its energy in that layer. Particles can be discriminated based on their energy deposition and their tracks through the detector—charged particles will follow curved tracks through the detector due to the magnetic field. Particles such as neutrinos and WIMPs have extremely long mean free paths in any material, so they will escape the detector. Their production is inferred from the missing momentum or energy in the reconstruction of the collision.

Dark Matter production at colliders relies on the equivalence between mass and energy, and depends on the strength of the interaction between Dark Matter and the SM. Therefore, collider experiments can potentially discover the Dark Matter regardless of its particular particle nature, so long as it has some coupling to the SM beyond gravitational interactions. Collider experiments currently constrain the Dark Matter parameter space m_χ-$\sigma_{\chi \mathrm{p}}$, but have

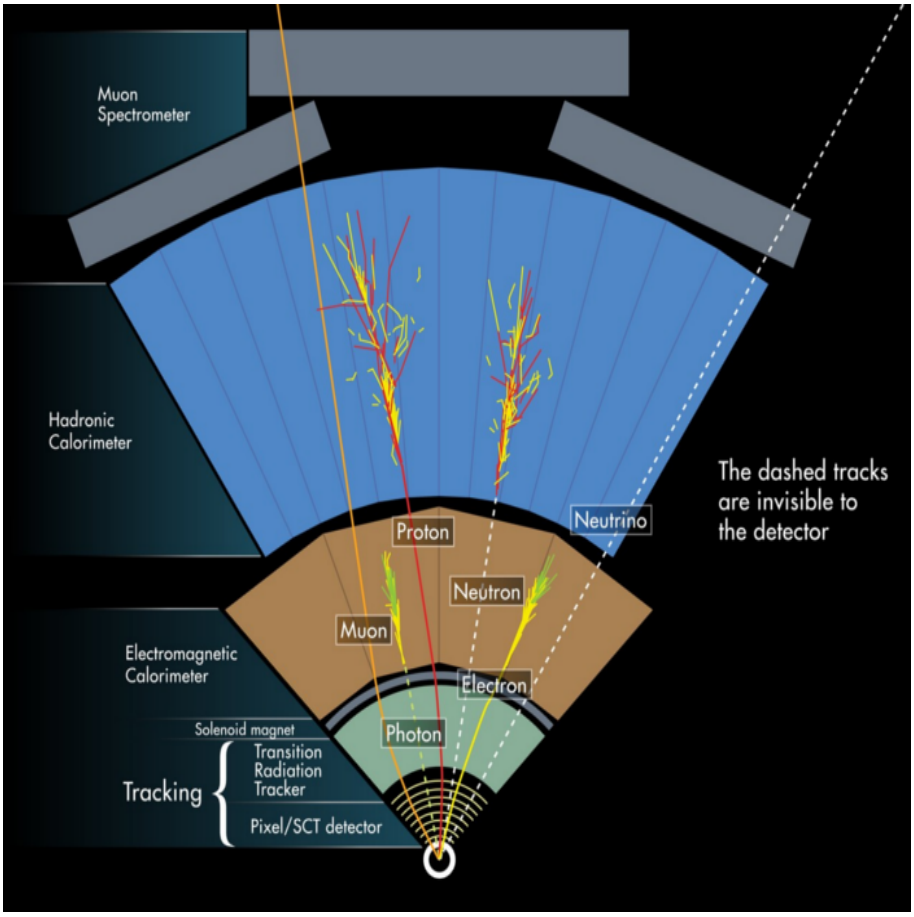

Figure 1.19: Schematic of the ATLAS detector at the LHC. Image credit: ATLAS collaboration © 2016 CERN.

yet to report a positive detection of Dark Matter e.g. [24, 71]. Dark Matter production at colliders is sensitive to the details of the coupling to the SM, so these constraints are model-dependent. Furthermore, a WIMP produced in a collider cannot be unambiguously identified as the Dark Matter particle, because such a WIMP may not be stable on a cosmological time scale [175]. On the other hand, collider experiments have the advantage that they are not affected by astrophysical uncertanties.

1.5.2 Direct Detection

The idea behind a direct-detection experiment is to build a detector on Earth which can observe a scattering event between a Dark Matter particle and a nucleus. Direct detection is a major source of inquiry into the Dark Matter problem with many experiments conducted and ongoing e.g. Coherent Germanium Neutrino Technology (CoGeNT) [3], Cryogenic Dark Matter Search (CDMS) [42], Cryogenic Rare Event Search with Superconducting Thermometers (CRESST) [20], Dark Matter Large sodium Iodide Bulk for RAre processes (DAMA/LIBRA, henceforth just DAMA) [30], the Large Underground Xenon (LUX) experiment [127], and Xenon 1 Ton (Xenon1T) [21]. For a full review of direct-detection experiments see e.g. Reference [132].

As the scattering event rate depends on the details of the coupling to the SM, results from direct-detection experiments are model-dependent. Furthermore, they are not particularly sensitive to Dark Matter candidates such as sterile neutrinos, which are only feebly coupled to the SM. Moreover, they are most sensitive to WIMPs whose event rate is above that of the irreducible (active) neutrino background. Neutrinos are weakly interacting so direct-detection experiments cannot be feasibly shielded from them. Additionally, their spectrum is nearly identical to that expected from Dark Matter [53]. It is therefore difficult, but not impossible to extract a Dark Matter signal which lies below this 'neutrino floor'. Above the neutrino floor, the sensitivity of a given experiment scales in direct proportion to the exposure time. Below the neutrino floor, sensitivity grows as the square root of the exposure time or worse [53].

Thus far Dark Matter has not been conclusively detected in any direct-detection ex-

periment. Several experiments have reported anomalous signals above background, but interpreting these signals as Dark Matter is problematic as they are not consistent with each other or with other searches, which have ruled out the parameter space preferred by a Dark Matter interpretation.

Figure 1.20 shows the confidence regions for a Dark Matter interpretation of the anomalous signals reported by CRESST, CoGeNT, CDMS, and DAMA, as well as the exclusion limits from LUX and SuperCDMS. The viability of a Dark Matter interpretation of any of the anomalous signals is cast into serious doubt by the tension between them and the null results [63]. Note that the null results and signals are not necessarily in conflict as they involve scattering off of different nuclear species; however, reconciling them is difficult. As an example, Reference [84] found that even considering non-standard models of WIMP Dark Matter scattering, such as an Anapole interaction, which can bring the regions of interest for CDMS-Si, CoGeNT, and DAMA into alignment, the parameter space preferred by these experiments is excluded by the LUX limits [109]

In fact, two of the experiments reporting signals in the past have explained the anomalies in terms of known backgrounds. The CRESST experiment treated the clamps holding the detector in place as perfectly smooth when calculating their backgrounds. In fact, the clamps were rough and absorbed some cascade events from decays of ^{206}Pb [53]. For any direct-detection experiment discriminating between surface and bulk events is key, because background events will mostly occur at the surface as they involve SM particles with comparatively high cross-sections. Only weakly interacting particles should be able to penetrate into the bulk of the detector. The CoGeNT experiment misunderstood the bulk fraction of their events and were incorrectly reporting surface events as being possibly due to Dark Matter scattering in the bulk of the detector [53]. These results demonstrate the difficulty of detecting Dark Matter directly and the importance of background discrimination.

1.5.3 Indirect detection

Indirect-detection experiments involve observing the products of Dark Matter annihilation (e.g. photons, neutrinos, positrons) in a given astrophysical environment such as the Sun

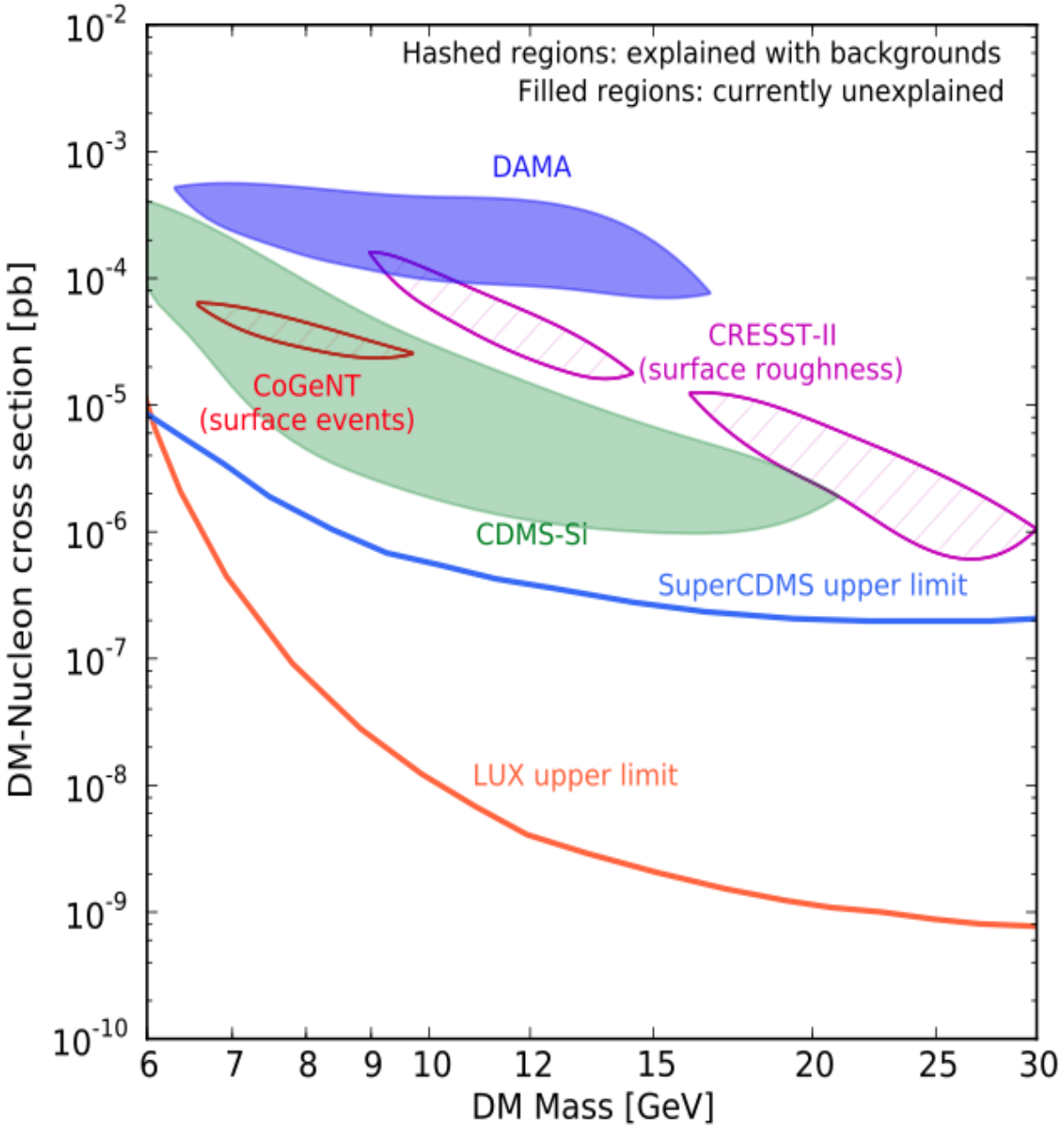

Figure 1.20: Direct-detection confidence regions and exclusion limits. From Reference [53].

[163] or the Galactic halo [9, 5, 19]. Several groups have found evidence that there is an anomalous, extended gamma-ray emission coming from the Galactic Center using data from the Large Area Telescope aboard the *Fermi* Gamma Ray Space Telescope (*Fermi*-LAT). This emission is consistent with the annihilation of a relatively low-mass ($m_\chi \sim$ 5-30 GeV) Dark Matter particle to quarks [7, 77, 104, 8, 78, 128] or leptons [7, 103, 104, 8, 78, 128, 124], but the evidence is not conclusive as the diffuse emission could be due to an unresolved population of pulsars e.g. [33]. *Fermi*-LAT has also observed the dwarf spheroidal satellite galaxies of the Milky Way. The lack of a significant γ-ray signal from these Dark Matter dominated objects places constraints on annihilating Dark Matter in the mass range 2 Gev - 10 TeV [10, 75, 45].

Figure 1.21 shows the exclusion limits from 6 years of *Fermi*-LAT observations of the MW dwarf spheroidals, as well as the exclusion limits from *Fermi*-LAT observations of the MW halo and the results of several other experiments. Closed contours and the point with error bars are the best fit values of several Dark Matter interpretations of the Galactic center excess [10]. Annihilation channels are bottom quarks and tau leptons in the left and right panels respectively. The *Fermi* results begin to constrain a Dark Matter interpretation of the Galactic center excess as they lie just above the 95% confidence limit for the $b\bar{b}$ channel [10].

1.6 THIS THESIS

In this thesis we present several astrophysical probes of the Dark Matter particle and the Dark Matter environments of astrophysical objects. Dark Matter can have significant observable effects on stellar evolution. Examples include altering the mass required for a star to reach the Main Sequence (MS) [202] and possibly an entirely new type of astrophysical object called a Dark Star (DS)—a pre–MS population III star that maintains hydrostatic equilibrium through Dark Matter annihilations alone [187, 143, 111]. The astrophysical effects of Dark Matter generally constrain the parameter space of particle mass m_χ, Dark Matter-nucleon scattering cross-section $\sigma_{\chi \mathrm{p}}$, and the density of the Dark Matter environment ρ_χ.

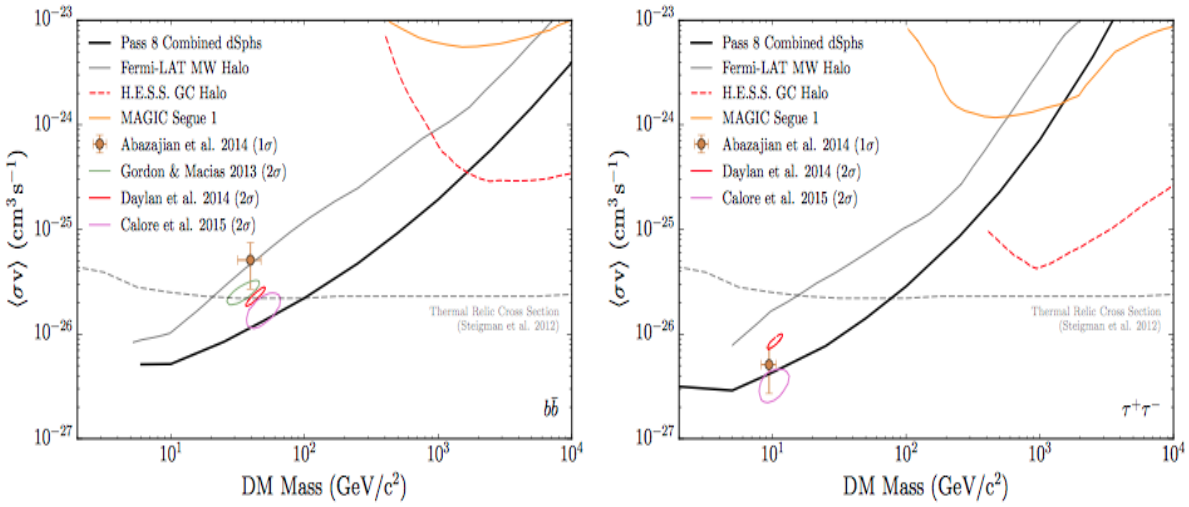

Figure 1.21: Indirect-detection confidence regions and exclusion limits. From Reference [10].

The first astrophysical probe we present involves using observations of cool White Dwarfs (WDs) to constrain the halo environments of Globular Clusters (GCs) and the properties of the Dark Matter particle. It is well known that stars should capture and accumulate Dark Matter in their cores as they orbit their host halos (see e.g. the review [114]). Stars are able to capture Dark Matter particles because occasionally a WIMP should scatter off of a nucleon in the star, potentially losing enough energy to become gravitationally bound to the star. If the Dark Matter is a thermal relic, then we expect that the Dark Matter should be annihilating in the cores of stars. This is intriguing in the case of WDs because these are dead stars that are no longer undergoing nuclear fusion in their cores, meaning that in the absence of Dark Matter they would simply cool indefinitely. If Dark Matter is present and annihilating in the core; however, the cooling will be halted at some finite temperature. Thus, cool WDs are a potential astrophysical probe of their halo environments, as the amount of Dark Matter accumulated depends directly on the density of Dark Matter local to the star.

The Dark Matter environments of GCs are particularly interesting because they are

the largest known structures in the Universe without significant Dark Matter content. For instance, the Dark Matter mass of the GCs NGC 6397, NGC 2419, and MGC1 are all constrained at the order $M_{\rm DM} \lesssim M_*$ where M_* is the stellar mass of the cluster [183, 49]. Furthermore, while the prevailing view is that GCs formed without significant Dark Matter halos, the viability of specific formation and evolution scenarios for the Galactic GCs remains controversial. The controversy is based, in part, around the complex element abundance patterns measured among the stars in several GCs [82, 83, 50] which suggest that the clusters must have had significantly more mass in the past in order to retain significant amounts of heavy elements ejected from supernovae [109]. In this thesis we show that observations of cool WDs have the potential to improve on the existing constraints of the Dark Matter content of NGC 6397 by up to 3 orders of magnitude.

Next, we present additional theoretical work on the Dark Matter content of GCs. As mentioned above, observational evidence suggests that GCs do not have significant Dark Matter halos today, but it is not clear that this was always the case. In this thesis we will investigate whether it is possible that GCs could have lost their Dark Matter through multi-body gravitational interactions. A Dark Matter particle can experience a close encounter with a star in a GC such that it is accelerated to a higher velocity. This is the familiar gravitational slingshot effect used by NASA to accelerate space craft to higher velocities. This mechanism is also the source of hypervelocity stars, and it is known that GCs eject stars in this way [98, 99]. It is then reasonable to ask if GCs could have ejected significant amounts of Dark Matter. Our results show that it is unlikely that GCs could have lost their halos by this mechanism. While many GCs could have had their Dark Matter content tidally stripped, we consider a population of isolated GCs for which this should not be the case. Our results combined with previous work (e.g. Reference [49]) indicate that GCs never possessed significant, extended Dark Matter halos.

The third and final probe we present involves Asymmetric Dark Matter (ADM). Generally the Dark Matter is considered to be its own anti-particle; however, the dark sector need not be so simple. It is possible that there are Dark Matter and anti-Dark Matter particles. Moreover, the Dark Matter need not be a thermal relic. In the case of ADM, the abundance of ADM today is due to an asymmetry in the number of Dark Matter and anti-Dark Mat-

ter particles in the early Universe, similar to baryonic matter. There are several possible mechanisms for producing ADM: an initial asymmetry could exist in the baryon or lepton sector and then be transferred to the dark sector, or the asymmetry could be generated in the dark sector by decays or other mechanisms (for a full discussion of such mechanisms see e.g. Reference [203]). ADM can accumulate in stars, but as it is not annihilating it does not constitute a source of luminosity. Moreover, because it is not annihilating, it can accumulate in much greater number than standard Dark Matter. ADM can have significant effects on the energy transport in stars (e.g. [186, 202]). The mechanism is similar to that which leads to capture: a Dark Matter particle bound to the star can scatter off of a nucleon in the core of the star gaining some energy. Provided the Dark Matter particle is not accelerated above the escape speed of the star, it will orbit the star until it scatters again, depositing its energy at a higher radius than the initial scattering event.

Energy transport by ADM cools the core of a star, decreasing the temperature gradient. This can have significant effects on both MS and post-MS stars. MS stars like the Sun are driven to higher luminosities and effective temperatures as they evolve towards the SubGiant Branch (SGB). The MS lifetime is also extended. ADM can also suppress the development of a convective core in stars slightly more massive than the Sun. During the post-MS evolution, ADM causes thermal pulses in the core. This can have significant effects on the thermal pulses an Asymptotic Giant Branch star ordinarily experiences, as well as their subsequent cooling to WDs.

2.0 PROBING DARK MATTER AND GLOBULAR CLUSTERS WITH COOL WHITE DWARFS

The bulk of the text and the figures in this chapter were previously published as Hurst *et al.* 2015 [109].

2.1 INTRODUCTION

In the current cosmological paradigm, $\approx 26\%$ of the energy of the Universe is in the form of Dark Matter [101, 161]. The nature of this Dark Matter is unknown, but the most popular particle candidates are Weakly-Interacting Massive Particles (WIMPs). Among other reasons, WIMPs are compelling candidates because they can be produced thermally in the early Universe such that their relic abundance yields the correct value for the Dark Matter density ($\Omega_{\rm DM} \approx 0.23$). Moreover, WIMPs arise naturally in various extensions to the Standard Model (SM) of particle physics. As such, detecting, identifying, or excluding broadly WIMP-like Dark Matter is a high priority in cosmology and particle physics. In this chapter, we describe the implications of recent signals in a variety of dark matter search experiments for the structure of globular cluster NGC 6397 and its Dark Matter content.

We also follow up on previous work [31], by demonstrating how observations of cool, dim WDs, in concert with future measurements of dark matter properties, can place unique and powerful constraints on the Dark Matter content of globular clusters.

It is now well known that a star will capture weakly-interacting Dark Matter particles through scattering off of nuclei within the stellar interior as the star orbits within the host Dark Matter halo (see e.g. the review [114] and references therein). Dark Matter particles

captured in this way will accumulate within the star and achieve sufficiently high densities such that annihilation of the Dark Matter particles can come to equilibrium with capture (see §2.2.2). The annihilations will be a source of energy for the stellar interior. Consequently, there should be some heating from Dark Matter annihilation in the cores of stars [140, 141]. The effects of such annihilations have been considered for Main Sequence (MS) stars [64], primordial stars [187, 143, 111], and compact stars [105, 31].

For reasonable models, the luminosity from annihilations is generally not a significant portion of the stellar luminosity; however, it can have significant consequences for WDs. If WDs are heated by Dark Matter annihilations in their cores, they will be prevented from cooling below some minimum temperature set by the equilibration of energy injection from annihilations with energy loss by radiation [105]. Observations of cool, dim WDs lead to constraints on Dark Matter because the energy injected by Dark Matter annihilation cannot exceed the observed WD luminosity.

There are a number of well-developed efforts to identify the dark matter particle. Direct-detection experiments seek to identify Dark Matter by observing scattering events in a detector on Earth. Several direct-detection experiments have reported intriguing results recently including the Coherent Germanium Neutrino Technology (CoGeNT) [3], the silicon detectors of the Cryogenic Dark Matter Search (CDMS-Si) [42], Cryogenic Rare Event Search with Superconducting Thermometers (CRESST) [20] and Dark Matter Large sodium Iodide Bulk for RAre processes (DAMA/LIBRA, henceforth just DAMA) [30]. These experiments all see events that are inconsistent with expected backgrounds. Taking all of these experiments together, there is no consistent interpretation of these events as Dark Matter particle scattering (though there are some models that can alleviate the tension between the experiments, e.g. References [116, 67, 84, 70, 147, 22]). Though CoGeNT and CRESST were able to explain their results in terms of previously misunderstood backgrounds, the CDMS-Si and DAMA anomalies remain unexplained [53].

Broadly speaking these anomalous signals point toward a Dark Matter particle with a mass of $m_\chi \sim$ 5-25 GeV and a cross-section for scattering off of a nucleon of $\sigma_{\chi \mathrm{p}} \sim 10^{-41}\,\mathrm{cm}^2$, though the details of the viable mass ranges and cross-sections depend upon the particular experiment under consideration (the relevant areas of parameter space are shown

in Figure 2.5 below). Recent results from the Large Underground Xenon Dark Matter (LUX) [127] and SuperCDMS [13] experiments exclude nearly all of the parameter space consistent with a Dark Matter interpretation of the anomalous events in the aforementioned experiments, casting serious doubt on the viability of interpreting these events as due to Dark Matter. As an example, Reference [84] found that even considering non-standard models of WIMP Dark Matter scattering, such as an Anapole interaction, which can bring the regions of interest for CDMS-Si, CoGeNT, and DAMA into alignment, the parameter space preferred by these experiments is excluded by the LUX limits.

A second avenue of inquiry into the nature of Dark Matter is indirect detection. Indirect-detection experiments seek to identify the Dark Matter by observing the particles (e.g. photons, neutrinos, positrons) produced by the self-annihilation of Dark Matter in specific astrophysical environments, such as the Sun [163] (for which the relevant annihilation product is the neutrino) or the Galactic Halo (for which the relevant annihilation products may be photons [9], neutrinos [5], or positrons [19]). Several groups have found evidence that there is an anomalous, extended gamma-ray emission coming from the Galactic Center using data from the Large Area Telescope aboard the Fermi Gamma Ray Space Telescope (Fermi-LAT). This emission is consistent with the annihilation of a relatively low-mass ($m_\chi \sim$ 5-30 GeV) Dark Matter particle to quarks [7, 77, 104, 8, 78, 128] or leptons [7, 103, 104, 8, 78, 128, 124], but the evidence is not conclusive (e.g. [33]). Fermi-LAT has also observed the dwarf spheroidal satellite galaxies of the Milky Way. The lack of a significant γ-ray signal from these Dark Matter dominated objects places constraints on annihilating Dark Matter in the mass range 2 Gev - 10 TeV [11, 75, 45]. As an example, new analysis places an upper-limit on the annihilation rate which is below the canonical thermal value for m_χ = 6-35 GeV, depending on the annihilation channel [76].

The anomalous signals mentioned above suggest that it may not be long until some of the basic properties of the Dark Matter particle are determined. Identification of Dark Matter scattering cross-sections opens the door to what some authors have referred to as *WIMP astronomy* (e.g., Reference [158]). The premise of WIMP astronomy is that with the properties of Dark Matter known, observations of astronomical phenomena, such as cosmic ray fluxes or stellar evolution, can yield further information about the structure and

substructure of the Milky Way's Galactic Dark Matter halo. Improved knowledge of the structure of the Galactic Dark Matter halo can, in turn, lead to improved constraints on the processes that lead to the formation of the Galactic halo and the Milky Way Galaxy or Milky Way sub-systems (e.g., dwarf galaxies [105], globular clusters [31]).

Here we follow up on Reference [31] by showing the implications of these recent anomalous signals, interpreted as Dark Matter, for the Dark Matter content of the Milky Way globular cluster NGC 6397. Because the signals coming from direct-detection experiments may not be due to Dark Matter, we also show the reach of WD cooling as a tool for WIMP astronomy as a function of the properties of the Dark Matter particle in a general context.

The data we exploit in order to explore possible constraints on dark matter and/or globular cluster properties are the deep observations of the globular cluster NGC 6397 with the Hubble Space Telescope (HST) [100, 188, 56, 171]. In particular, we use observations of the WD cooling sequence [92]. The WDs observed in NGC 6397 are among the coolest, dimmest WDs that have been observed to date and, importantly, the authors provide compelling evidence that they have observed the limit of the WD cooling sequence in NGC 6397. GCs, such as NGC 6397, are interesting objects in and of themselves in the context of WIMP astronomy.

Globular clusters are the largest structures known that show no evidence of Dark Matter. Moreover, while the prevailing view is that GCs formed without significant Dark Matter halos, the viability of specific formation and evolution scenarios for the Galactic GCs remains controversial. The controversy is based, in part, around the complex element abundance patterns measured among the stars in several GCs [82, 83, 50], which suggest that the clusters must have had significantly more mass in the past in order to retain significant amounts of heavy elements ejected from supernovae. Meanwhile, state-of-the-art constraints on the contemporary amounts of Dark Matter in GCs are not particularly restrictive. Reference [49] found that for NGC 2419 and MGC1 $M_{\rm DM}/M_* \lesssim 1$, where $M_{\rm DM}$ is the mass in Dark Matter of the cluster and M_* is the stellar mass of the cluster. Subsequently, Reference [183] found a similar result for NGC 6397. In the present work we show how WIMP astronomy may be able to improve upon these types of constraints by several orders of magnitude. We will show that if any of the anomalous signals observed in direct search experiments could be

convincingly attributed to Dark Matter, the corresponding constraint on the density of Dark Matter in NGC 6397 would be $M_{\rm DM}/M_* \lesssim 10^{-3}$, at least three orders of magnitude more restrictive than the kinematic constraints.

The remainder of this chapter is organized as follows: In §2.2 we demonstrate how observations of cool WDs can be used to constrain Dark Matter particle and halo model parameters in 4 parts. We first calculate the capture rate of WIMPs in the star in §2.2.1 . We then calculate the annihilation luminosity in §2.2.2. Next, in §2.2.3, we consider the effect of the annihilation luminosity on WD cooling. Finally, in §2.2.4, we use the cooling sequence of NGC 6397 to relate the temperature of the coolest WD observed to the annihilation luminosity. We present our results in §2.3 and summarize our conclusions and discuss possibilities for future applications of our method in §2.4.

2.2 METHODS

In this section, we show how observations of cool WDs in GCs may lead to constraints on the Dark Matter particle and/or the dark matter content of GCs. We first discuss the rates of capture and annihilation of WIMPs in WDs. We then show that if the annihilation luminosity is to be comparable to the luminosity of the WD, an equilibrium may have been reached between Dark Matter capture and annihilation. Equilibration is achieved for a wide range of interesting parameter space, yielding a relationship between the Dark Matter particle properties, the Dark Matter environment of the WD and the observed luminosity of the WD. The annihilation luminosity is particularly relevant in the case of WDs because their cooling will be halted by the injection of energy in the core from Dark Matter annihilations. Therefore, the assumption that the luminosity of the WD is due to Dark Matter annihilations alone yields an upper limit on the local Dark Matter density. In the present work we use observations of the WD cooling sequence in NGC 6397 to derive constraints on the Dark Matter density of the cluster and Dark Matter model parameters m_χ and $\sigma_{\chi \rm p}$.

2.2.1 The Capture Rate of WIMPs

The capture of Dark Matter particles in stars has been studied in numerous papers (e.g [87, 79, 80, 164, 122, 65]). The rate at which a WD will capture Dark Matter is approximately given by Equation (A.16) from Reference [201], namely

$$C_{\rm c} = \sqrt{\frac{3}{2}}\frac{\rho_\chi}{m_\chi}\sigma_i v_{\rm esc}(R)\frac{v_{\rm esc}(R)}{\bar{v}}N_i\langle\hat{\phi}\rangle\frac{{\rm erf}(\eta)}{\eta}, \tag{2.1}$$

where ρ_χ is the local Dark Matter density, R is the radius of the WD, $v_{\rm esc}(R)$ is the escape speed at the surface of the star, $\bar{v}$ is the dispersion of the Dark Matter velocity profile (assumed to be Maxwell-Boltzmann), η is the ratio of the star's velocity through its halo to the local velocity dispersion of the halo (assumed to be of order unity) and

$$\hat{\phi} = \frac{v_{\rm esc}^2(r)}{v_{\rm esc}^2(R)} \tag{2.2}$$

is a dimensionless potential for stellar nucleons. The quantity $\langle\hat{\phi}\rangle$ is the average of $\hat{\phi}$ over all nucleons in the star. The cross-section for scattering off of nuclear species i is σ_i, N_i is the number of nucleons of species i in the star, and the total capture rate is the sum over all species. Note that Equation (2.1) relies upon the assumption that the elemental abundance is not a function of the radius. This is a reasonable approximation as the WD is the remaining core of a dead star, the abundance should not be a strong function of the radius. Moreover, almost all of the interior is carbon and oxygen, which have similar scattering cross-sections and therefore yield virtually identical constraints.

Calculation of $\langle\hat{\phi}\rangle$ requires that we know the density profile of the star. We use the publicly available stellar evolution code `MESA star` [151, 152, 153, 1] to find the density profile and other relevant parameters we require. The specific model we ran of a 0.6 $M_\odot$ WD is provided in the `MESA` test suite in the folder `wd_cool_0.6M`. With this density profile we find $\langle\hat{\phi}\rangle \simeq 2.4$.

Scattering off a given nucleus is coherent at most of the relevant energies that we consider, so the cross-section for scattering off a given nucleus is approximately

$$\sigma_N \approx \sigma_{\chi{\rm p}} A_N^2 \frac{m_\chi^2 M_N^2}{(m_\chi + M_N)^2}\frac{(m_\chi + m_{\rm p})^2}{m_\chi^2 m_{\rm p}^2}, \tag{2.3}$$

where A_N is the atomic mass number of the nucleus of interest, M_N is the mass of the nucleus, and m_p is the proton mass. Capture of WIMPs with $m_\chi \gtrsim 10\,\mathrm{GeV}$ is modestly suppressed compared to Equation (2.3) due to loss of coherence. To account for this, we apply an exponential form-factor suppression as in [79, 114]

$$f(Q) = \exp(-Q/2Q_0) \tag{2.4}$$

where Q is the energy transferred from the WIMP to the nucleus and $Q_0 = \frac{3}{2M_N R_N^2}$ is the 'coherence energy' and $R_N = 10^{-13}\,\mathrm{cm} \times [0.91(M_N/\mathrm{GeV})^{1/3} + 0.3]$ is the nuclear radius.

For simplicity we consider a WD made entirely from carbon and oxygen. This is a reasonable simplification because the progenitors of low mass WDs should not have been hot enough to fuse carbon in their cores and helium is only abundant in the thin stellar atmosphere and thus is unimportant for computing the capture rate. Additionally, the GC we consider below is a metal-poor cluster [95] so we do not expect a significant contribution from metals other than carbon and oxygen. Thus we can write the composition of the WD as

$$N = N_\mathrm{C} + N_\mathrm{O} = f_\mathrm{C}\frac{M_\mathrm{WD}}{M_\mathrm{C}} + (1 - f_\mathrm{C})\frac{M_\mathrm{WD}}{M_\mathrm{O}}, \tag{2.5}$$

where f_C is the fraction of Carbon. Our results are not sensitive to the composition of the WD.

At sufficiently high scattering cross-sections $\sigma_{\chi\mathrm{p}} > \sigma_{\chi\mathrm{p}}^\mathrm{crit}$ (see Figure 2.5 below), the WD will become opaque to the WIMPs it encounters at which point Dark Matter capture will be saturated. The critical cross-section can be evaluated by requiring that $\sigma_N^\mathrm{crit} \sim \Sigma_N^{-1}$, where $\Sigma_N = \frac{M_\mathrm{WD}/M_N}{\pi R_\mathrm{WD}^2}$ is the average projected surface density of the WD seen by infalling WIMPs. This implies that

$$\sigma_{\chi\mathrm{p}}^\mathrm{crit} = \frac{\sigma_N^\mathrm{crit}}{A_N^2}\frac{(m_\chi + M_N)^2}{M_N^2}\frac{m_\mathrm{p}^2}{(m_\chi + m_\mathrm{p})^2}. \tag{2.6}$$

We assume that scattering cross-sections above this threshold all give the same prediction as $\sigma_{\chi\mathrm{p}}^\mathrm{crit}$.

For scattering cross-sections below the saturation threshold, Equation (2.1) will be relevant in the limit that nearly all scattering events lead to capture within the star. The probability for capture in an individual Dark Matter-nucleon encounter is determined by the

kinematics of the scattering and, assuming isotropic scattering, is given by (see the Appendix of Reference [201])

$$P = \frac{v_{\rm esc}^2}{v_{\rm esc}^2 + u^2} \left[1 - \frac{u^2}{v_{\rm esc}^2} \frac{(m_\chi - M_N)^2}{4 m_\chi M_N} \right], \tag{2.7}$$

where $v_{\rm esc}$ is the escape speed at the position of the scattering event, u is the speed at infinity of the incident Dark Matter particle, and M_N is the mass of the nucleon involved in the scattering. Capture is extremely likely in nearly all cases of interest because $u \sim \bar{v} \ll v_{\rm esc}$. In the case of a $0.6\,{\rm M}_\odot$ WD with $R \sim 0.012\,{\rm R}_\odot$, which we consider below, $v_{\rm esc}(R) \approx 4400\,{\rm km/s}$ and the relevant escape speed is $v_{\rm esc}^2 \sim \langle \hat{\phi} \rangle v_{\rm esc}^2(R)$. Typical relative velocities are $u \sim \bar{v} \approx 10\,{\rm km/s}$ within GCs and $u \sim \bar{v} \approx 270\,{\rm km/s}$ in the Milky Way halo. The first factor in Equation (2.7) differs from unity by $\lesssim 1\%$ in both the GC and Milky Way environments.

Consequently, capture will be efficient so long as the mass of the dark matter particle and target nucleon are not too different. Requiring the second term within brackets in Equation (2.7) to be negligible leads to a mass range over which this approximate capture rate is viable,

$$\frac{u^2}{v_{\rm esc}^2} \frac{M_N}{4} \ll m_\chi \ll 4 \frac{v_{\rm esc}^2}{u^2} M_N. \tag{2.8}$$

Assuming that $M_N \simeq 11.2\,{\rm GeV}$, as would be the case for Carbon, this leads to an approximate dark matter particle mass range of $6\ {\rm keV} \ll m_\chi \ll 2 \times 10^4\ {\rm TeV}$ ($4\ {\rm MeV} \ll m_\chi \ll 29\ {\rm TeV}$) in the GC (Milky Way) environment. Outside of this mass range, the capture rate is suppressed significantly compared to Equation (2.1). In nearly all cases, other considerations will limit the mass range over which our calculations are relevant. For example, as we discuss below, dark matter particles with masses $m_\chi \lesssim 100\,{\rm keV}$ evaporate from WDs more rapidly than they are captured, so there is no accumulation of dark matter in WD stars below this mass threshold. Meanwhile, loss of coherence in the scattering event leads to modest form-factor suppression for $m_\chi \gtrsim 10\,{\rm GeV}$, and the upper range of m_χ in the GC environment exceeds the unitarity bound on thermal relic dark matter [86].

In fact, while Equations (2.1) & (2.3) are useful approximations to guide the reader, when calculating the capture rate we actually use the full results of the appendix in Reference [79], which account for the exponential form-factor suppression.

2.2.2 The Annihilation Luminosity

An important aspect of our constraints is that they extend to much lower masses than most other techniques, Cosmic Microwave Background (CMB) constraints being the notable exception [130, 60, 142] (these constraints are discussed at the end of §2.3). We consider stable Dark Matter of mass $m_\chi \gtrsim 100$ keV. WIMPs with $m_\chi \lesssim 100$ keV can escape the WD via evaporation—the ejection of WIMPs by hard elastic scattering from nuclei [114]. We can estimate the evaporation mass by demanding that the typical velocity of a WIMP $v \sim (T_c/m_\chi)^{1/2}$ be less than the local escape speed of the star $v_{esc} \approx 1.1 \times 10^4$ km/s. Here T_c is the temperature in the core of the star [114]. Below we will consider a WD with $M_{WD} \approx 0.6\,M_\odot$ and $T_{eff} \approx 3700$ K. Using `MESA star`, we find that such a WD should have a core temperature $T_c \sim 10^6$ K corresponding to an evaporation mass ~ 100 keV. (For a more careful discussion of the evaporation mass see [87]). Thus, we are justified in neglecting evaporation for $m_\chi \gg 100\,\mathrm{keV}$.

Having computed the capture rate of Dark Matter and justified the neglect of Dark Matter evaporation, the number of WIMPs contained within the star, N_χ, is governed by the differential equation

$$\frac{\mathrm{d}N_\chi}{\mathrm{d}t} = C_c - C_a N_\chi^2, \tag{2.9}$$

where C_a is twice the rate of annihilation events (because each annihilation eliminates 2 particles). The solution to this equation for homogeneous initial conditions is

$$N_\chi = \sqrt{\frac{C_c}{C_a}} \tanh\left(\sqrt{C_c C_a}\, t\right). \tag{2.10}$$

There is a timescale for equilibration between Dark Matter annihilation and capture, $\tau_{eq} = 1/\sqrt{C_c C_a}$, such that for $t \gg \tau_{eq}$, N_χ approaches a steady state solution $N_{\chi,eq} = \sqrt{C_c/C_a}$ [201]. The annihilation rate at equilibrium within a WD will be

$$\Gamma_a = \frac{1}{2} C_a N_{\chi,eq}^2 = \frac{1}{2} C_c, \tag{2.11}$$

because there are $N_{\chi,eq}^2/2$ distinct pairs of Dark Matter particles within the star. To calculate τ_{eq} we first express C_a in terms of effective volumes [87]

$$C_a = \langle \sigma_a v \rangle \frac{V_2}{V_1^2}, \tag{2.12}$$

where $\langle \sigma_{\rm a} v \rangle$ is the thermally averaged annihilation rate, and

$$V_j \simeq 9.1 \times 10^{21} \left(\frac{1 \text{ GeV}}{j m_\chi} \right)^{3/2} \text{cm}^3 \tag{2.13}$$

is the effective volume of captured Dark Matter particles within the star for $j = 1$ [87, 201]. Within the volume of interest the density is approximately $\rho(r) \approx \rho_{\rm c} = 4 \times 10^6$ g/cm^3 and the temperature is approximately $T(r) \approx T_{\rm c} = 10^6$ K, where the subscript c denotes the value in the core and both $\rho_{\rm c}$ and $T_{\rm c}$ were estimated using `MESA star`. Note that when $m_\chi \lesssim 10^{-2}$ GeV the effective volume will be $\sim 20\%$ of the volume of the WD. At this point our approximations will begin to break down as it is not the case that $\rho(r) \approx \rho_{\rm c}$. However, our results are robust to this effect, because we are in the equilibrated regime by many orders of magnitude (see the following paragraph) and the annihilation rate can therefore be determined by the capture rate of WIMPs alone.

For a canonical, thermal WIMP Dark Matter particle with $\langle \sigma_{\rm a} v \rangle = 3 \times 10^{-26}$ cm^3/s, $\sigma_{\chi {\rm p}} = 10^{-41}$ cm^2 and mass $m_\chi = 10$ GeV, captured by a WD like that at the truncation of the cooling sequence in NGC 6397, we find that $\tau_{\rm eq}$ is less than a year for the fiducial constraint with $\rho_\chi = \rho_*$. For our more conservative constraints $\rho_\chi \lesssim \rho_* \times 10^{-3}$ (derived below) we find that $\tau_{\rm eq} \gtrsim 1$ year. In either case, this is many orders of magnitude less than the age of the cluster ~ 10 Gyr. Clearly, the equilibrium relation for the annihilation rate within the star is valid for a large swath of interesting parameter space.

In fact, $\tau_{\rm eq}$ is of order the age of the cluster only for exceptionally small annihilation rates on the order of $\langle \sigma_{\rm a} {\rm v} \rangle \lesssim 10^{-49}$ cm^3/s for the fiducial constraint above and $\langle \sigma_{\rm a} {\rm v} \rangle \lesssim 10^{-46}$ cm^3/s for our more conservative constraints with $\rho_\chi \lesssim \rho_* \times 10^{-3}$. An important consequence of this fact is that this method can be used to probe dark matter with annihilation rates many orders of magnitude smaller than the canonical WIMP rate. Moreover, our results are insensitive to the Dark Matter annihilation rate over many orders of magnitude.

For a specific Dark Matter model, Dark Matter annihilations give rise to an energy source within the WD of luminosity

$$L_\chi \approx \Gamma_{\rm a} m_\chi. \tag{2.14}$$

Interestingly, $\Gamma_{\rm a} \propto m_\chi^{-1}$ and the luminosity is independent of mass in the limit that the kinematics are favorable for Dark Matter capture [see Equation (2.1)]. Note that this is

not merely a coincidence, but is a consequence of the fact that the flow of Dark Matter through the star is independent of the WIMP mass—it is a function of the number density of WIMPs. Since the star is equally effective at capturing mass from this flow over many orders of magnitude, the luminosity is also independent of the Dark Matter particle mass over many orders of magnitude.

If the annihilations proceed to SM particles, nearly all of the energy released at the annihilation will be deposited in the interior of the star, as the only particles capable of escaping the star are low energy neutrinos. To show this, we first note that the projected surface density seen by neutrinos leaving the core is $\Sigma_N = \int_0^R \rho_N(r)\,\mathrm{d}r$. If we assume for the moment that the WD is made entirely of carbon, then $\Sigma_\mathrm{C} = 6.8 \times 10^{37}\,\mathrm{cm}^{-2}$ (using the density profile from `MESA star`). The WD will be opaque so long as the neutrino-nucleus scattering cross-section is greater than $\Sigma_\mathrm{C}^{-1} = 1.4 \times 10^{-38}\,\mathrm{cm}^2$. Therefore, the WD will be opaque to neutrinos with energies $E_\nu \gtrsim 1\,\mathrm{GeV}$ (see e.g. Figure 9 in Reference [69]). Thus, models of low mass Dark Matter annihilating directly to neutrinos are capable of evading our constraints.

2.2.3 Deriving the Constraint from a Cool White Dwarf

WDs cool and dim over time (see Figures 2.1 & 2.2 and Ref [93]). If Dark Matter annihilations occur at a significant rate within a WD, then annihilations constitute a source of energy within the WD that can eventually provide an amount of energy comparable to the luminosity of the WD. If this occurs, the WD cooling will be halted and the WD will come to equilibrium at a minimum luminosity, $L \approx L_\chi$, and corresponding minimum effective surface temperature. (Note that as the annihilation luminosity is small ($\sim 10^{-5}\,\mathrm{L}_\odot$) and WDs are fully conductive, Dark Matter annihilations do not have a significant effect on the internal structure of the WD.) The surface temperature can be related to a bolometric luminosity using a stellar model, which we calculate using `MESA star`. Consequently, the observed luminosities and surface temperatures of WDs can be used to place bounds on Dark Matter properties and the distribution of Dark Matter local to the WDs. (Though we do not discuss them here, another well motivated Dark Matter particle candidate is the axion. It is worth

noting that WDs are also used to constrain the parameters of axions, as they would also have observable effects on WD cooling [166, 113].)

Figure 2.1 shows the cooling curve of a 0.6 $M_\odot$ WD as a function of the cooling time $t_{\rm cool}$ as modeled in `MESA star`. Also shown are the luminosity of the coolest WD in NGC 6397, which we use to derive our constraints, and the annihilation luminosity for a Dark Matter particle with $m_\chi = 5\,\mathrm{GeV}$ and $\sigma_{\chi \mathrm{p}} = 1.0 \times 10^{-41}\,\mathrm{cm}^2$ and an assumed Dark Matter density in NGC 6397 that is 2×10^{-3} times the stellar density. The annihilation luminosity is well above the observed luminosity of the WD; therefore, this model is ruled out by the data.

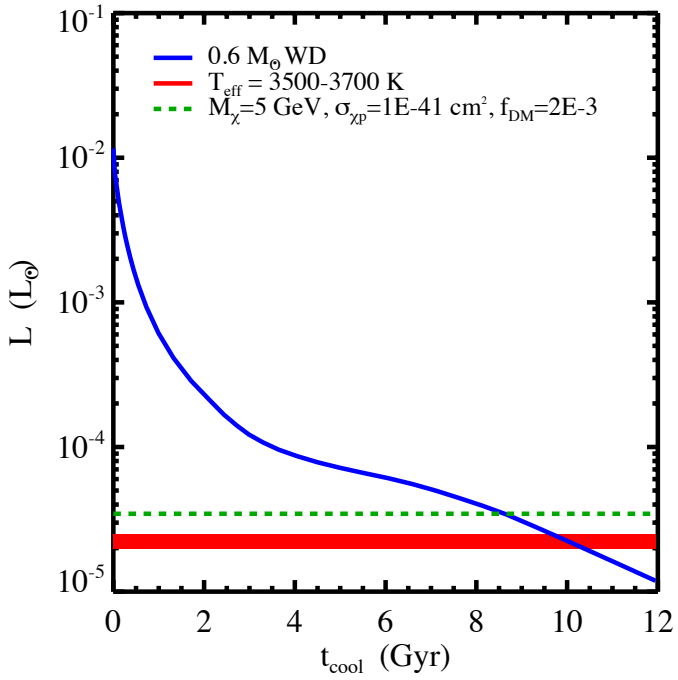

Figure 2.1: The luminosity L in units of $\mathrm{L}_\odot$ vs. cooling time $t_{\rm cool}$ for a WD.

This is the effect that we aim to exploit. In a particular astrophysical environment (we will explore GCs) Dark Matter particles may annihilate within WDs providing a source of annihilation luminosity that is proportional to the Dark Matter-nucleon scattering cross-section $\sigma_{\chi \mathrm{p}}$ and the local Dark Matter density ρ_χ, and inversely proportional to the local Dark Matter velocity dispersion $\bar{v}$. Typical Dark Matter velocities must be similar to the local stellar velocities for an equilibrium structure, so $\bar{v}$ is informed by observational data and has little parametric freedom compared to the Dark Matter density and cross-section. According

to this argument, the minimum luminosity of WDs in a given environment constrains the product $\rho_\chi \sigma_{\chi p}$ such that $L \gtrsim L_\chi$.

WDs are particularly promising probes for WIMP astronomy because they have deeper potential wells, cooler interiors, and significantly lower luminosities than their Main Sequence counterparts. For these reasons, WDs can be used for WIMP astronomy even for dark matter candidates with masses far below those typically considered ($m_\chi \ll 1\,\mathrm{GeV}$) and with annihilation rates orders of magnitude below the standard thermal value. These are important points that appear to have been missed in the discussions of References [105, 31].

In the following section, we will present constraints on the Dark Matter density and scattering cross-section based on high-quality observations of a nearby GC.

2.2.4 The Globular Cluster NGC 6397 and the Milky Way Halo

The WD cooling sequence of NGC 6397 has been measured to unprecedented depth and precision by the Advanced Camera for Surveys (ACS) aboard HST [92, 171], making it an ideal candidate for constraining dark matter and/or GC structure using WD cooling. NGC 6397 is a metal-poor GC located at a distance of 2.6 kpc from the Sun (making it one of the 2 closest GCs along with M4) [95, 168]. This cluster has a mass $M_{6397} = (1.1 \pm 0.1) \times 10^5$ $M_\odot$ [100] determined from kinematics, half-light radius $R_{HL} = 2.2$ pc, velocity dispersion $\bar{v} = 4.5 \pm 0.2$ km/s, and is one of 29 Galactic GCs which has undergone a core-collapse [95]. Core-collapse is a consequence of the Gravothermal Catastrophe and is halted in GCs by the formation of binary stellar systems.

The population of WDs in NGC 6397 has been measured well with deep HST imaging and the color-magnitude diagram of NGC 6397 exhibits a clear WD cooling sequence with a truncation at low luminosity and low temperature, as expected due to the finite age of the cluster [92]. The field in NGC 6397 observed by ACS lies 5' SE of the cluster center [171] well beyond the tidal radius of this core-collapsed cluster ($r_t = .6'$ [95]) and ranges from just inside the half-light radius ($r_{HL} = 174''$ [171]) to several arcminutes beyond r_{HL} such that the WDs mainly probe the outer regions of the cluster. As discussed in Appendix A of Reference [92], the truncation of the WD cooling sequence occurs at an absolute magnitude in the Hubble

F814W filter $M_{814} = 15.15 \pm 0.15$. The best-fit model for the WD is a mass at truncation of roughly $M_{\rm WD} \simeq 0.6$ M$_\odot$ which corresponds to a cooling age of $t_{\rm cool} \simeq 11.0 \pm 0.5$ Gyr. Using the cooling models of Bergeron [102, 121, 29, 66, 28] and applying a correction for WD masses in the range 0.5-0.6 M$_\odot$, we find $T_{\rm eff} \simeq$ 3500-3700 K.

Figure 2.2 shows the color magnitude diagram of WDs in NGC 6397 as imaged in the ACS filters F814W and F606W in the left panel, as well as the luminosity function of WDs in the cluster in the right panel. As mentioned above, the WD cooling sequence is seen quite clearly, as is the truncation at apparent magnitude F814W = 27.6.

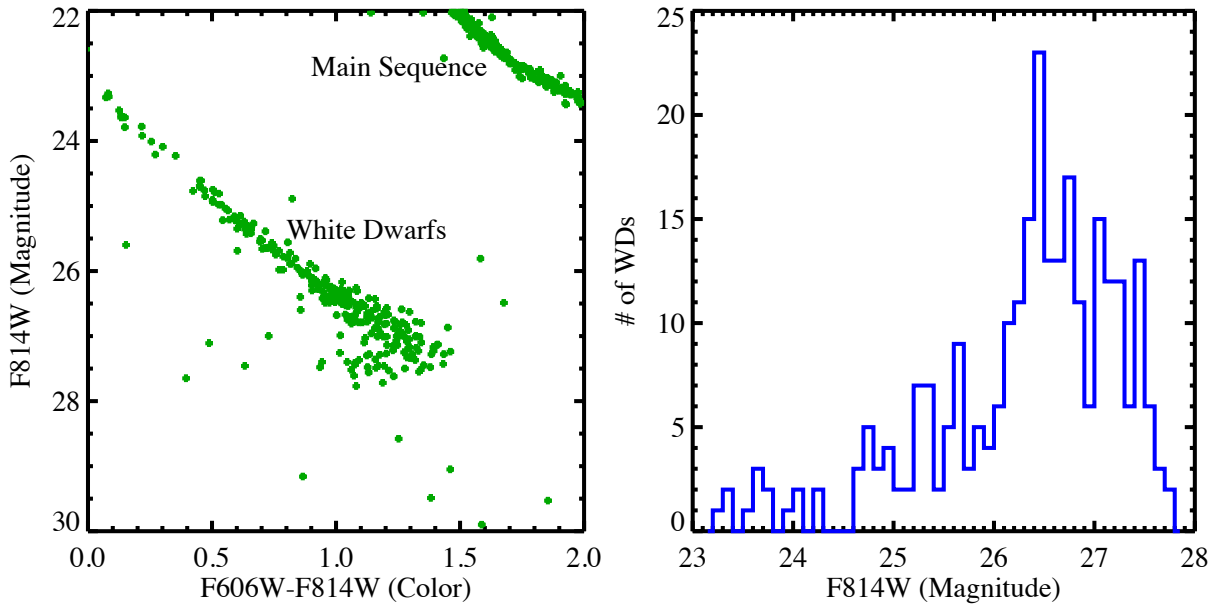

Figure 2.2: *(Left)* The color-magnitude diagram of NGC 6397. *(Right)* The luminosity function of WDs in NGC 6397.

In order to develop constraints on Dark Matter and/or the Dark Matter content of NGC 6397, it is necessary to understand the basic properties of the cluster and to parameterize the density of dark matter within the cluster. We estimate the average density of NGC 6397 as

$$\bar{\rho} \approx \frac{(M_{6397}/2)}{\frac{4}{3}\pi R_{\rm HL}^3} \approx 4.7 \times 10^4 \ {\rm GeV/cm}^3, \tag{2.15}$$

where we have assumed that half of the GC mass is enclosed by the half-light radius. Note that the mass measurement comes from the kinematics of the cluster; therefore, this average

density includes any Dark Matter that may be present. Current bounds on the amount of Dark Matter are roughly at the level of $M_{\rm DM}/M_{6397} \lesssim 1$ [49, 183]. We will demonstrate that if the properties of dark matter become known and reside within a large range of viable parameter space, observations of the WD cooling sequence will provide significantly more restrictive constraints on any Dark Matter component associated with GCs.

There is little guidance on the structures of Dark Matter halos that GCs may have had early in their evolution, therefore we parameterize the amount of Dark Matter in the cluster by the fraction of Dark Matter,

$$f_{\rm DM} = \rho_\chi/\bar{\rho}, \tag{2.16}$$

and take ρ_χ to be a constant function of position within the half-light radius of the cluster. The aforementioned constraints on the dark matter contained within NGC 6397 [183] limit $f_{\rm DM} \lesssim 0.5$. Meanwhile, the ambient Dark Matter contributed by the halo of the MW galaxy places a lower limit on $f_{\rm DM}$. We estimate the lower limit on $f_{\rm DM}$ by scaling the present day local density of Dark Matter $\sim$ 0.4 GeV/cm^3 as $1/r$. Taking the Galactocentric distance of NGC 6397 to be 6.0 kpc [95] the density in the vicinity of the cluster is $\rho_\chi \sim 0.57\,{\rm GeV/cm^3}$.

The density and surface brightness profiles of GCs are typically described by King models which have constant density cores [117, 118] (as a post core-collapse cluster, NGC 6397 has a more centrally-concentrated profile than the typical King model). This is in contrast to the density profiles of galaxy-scale Dark Matter halos, which increase like $1/r$ towards their centers [144]. Thus, our parametrization of the Dark Matter fraction should be conservative in the sense that, if NGC 6397 has a Dark Matter halo with a steep density profile as expected within the context of CDM, then ρ_χ should be much greater near the center of the cluster than at the half-light radius. Note that as GCs are not Dark Matter dominated, the steepness of the Dark Matter density profile is limited by that of the stellar profile.

2.3 RESULTS

By demanding that the annihilation luminosity of Dark Matter within the WDs in NGC 6397 [Equation (2.14)] does not exceed the observed luminosities of the least luminous WDs

in the cluster (Section 2.2.4 above), it is possible to constrain the product $f_{\rm DM}\,\sigma_{\chi {\rm p}}$ as a function of particle mass m_χ, so long as the annihilation rate for the Dark Matter exceeds $\langle \sigma_{\rm a} {\rm v} \rangle \gtrsim 10^{-46}\,{\rm cm}^3/{\rm s}$. (The precise threshold in annihilation rate depends upon $f_{\rm DM}$, $\sigma_{\chi {\rm p}}$, and m_χ, but this is a good rough number to have in mind and is many orders of magnitude smaller than the cross-sections considered for more typical WIMP-like thermal relic Dark Matter.) We show that it is possible to constrain the Dark Matter contents of the GC NGC 6397 (and thus GC evolution) if the Dark Matter properties become well constrained in the future, provided that the scattering cross-section is not too small.

Constraints realized from WD cooling in GCs lie in the three-dimensional parameter space of m_χ, $\sigma_{\chi {\rm p}}$, and $f_{\rm DM}$, which we present in Figures 2.3-2.6. As an example of the astrophysical reach of WD cooling constraints, consider first constraints on $f_{\rm DM}$ as a function of $\sigma_{\chi {\rm p}}$. These are depicted in Figure 2.3 assuming the best-fit values of m_χ from a Dark Matter interpretation of the recent CDMS-Si [42], CoGeNT [3], CRESST [20], and DAMA [181] results (recall that the CRESST and CoGeNT anomalies have been explained as misunderstood backgrounds [53]). The grey shaded band represents the constraints for the best fit values of m_χ from the direct-detection experiments and spans the range 3500-3700 K corresponding to the temperature of the WD at the truncation of the cooling sequence. (The constraints from CoGeNT, CRESST, DAMA and CDMS all lie within this band). The reason for the flattening of the constraint at $\sigma_{\chi {\rm p}} \sim 10^{41}$ cm^2 is that $\sigma_{\chi {\rm p}} > \sigma_{\chi {\rm p}}^{\rm crit}$ and capture is saturated. The pinkish shaded region is the excluded portion of parameter space. The horizontal dotted lines show the fiducial constraints on $f_{\rm DM}$ (see §2.2.4). The solid vertical lines denote the best fit cross-sections for CoGeNT, CRESST, DAMA and CDMS as indicated by the labels on the plot. while the vertical dashed lines indicate the exclusion limits from LUX and SuperCDMS at several different values of m_χ as indicated by the labels.

Figure 2.3 shows that if such an interpretation of any of these results could be taken seriously, then it must be the case that either $f_{\rm DM} \lesssim 10^{-3}$ or that the Dark Matter annihilates with a rate smaller than $\langle \sigma_{\rm a} {\rm v} \rangle \lesssim 10^{-46}\,{\rm cm}^3/{\rm s}$, some *20 orders of magnitude* lower than the canonical thermal relic WIMP value of $\langle \sigma_{\rm a} v \rangle \sim 3 \times 10^{-26} {\rm cm}^3/{\rm s}$. Figure 2.3 also demonstrates that particles consistent with LUX and SuperCDMS can still yield new constraints on $f_{\rm DM}$.

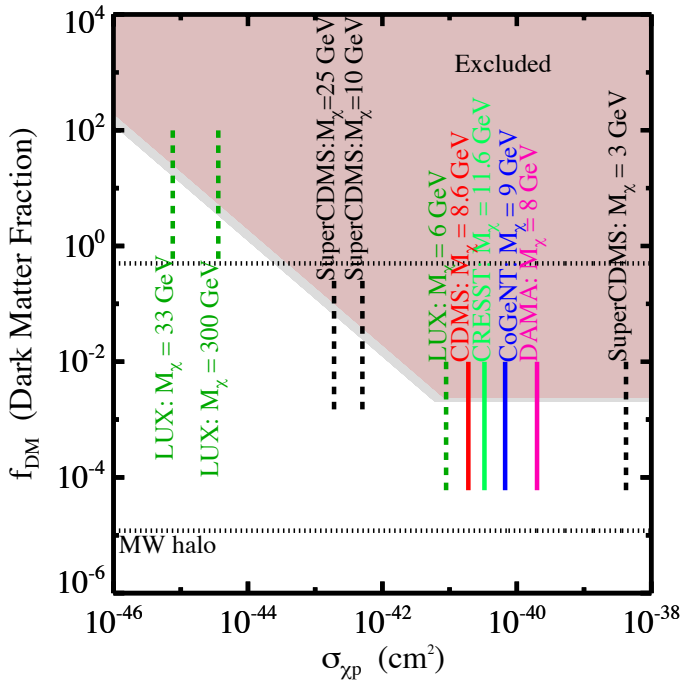

Figure 2.3: The Dark Matter fraction vs. Dark Matter-proton scattering cross-section for NGC 6397.

Figure 2.4 shows the corresponding constraints for $f_{\rm DM}$ as a function of m_χ assuming the best-fit values of $\sigma_{\chi \rm p}$ from a Dark Matter interpretation of the recent CDMS-Si [42], CoGeNT [3], CRESST [20], and DAMA [181] results. The colored bands are the constraints for the best fit values of $\sigma_{\chi \rm p}$ from CDMS-Si, CRESST, CoGeNT, and DAMA (from top to bottom). The widths correspond to the uncertainty in the luminosity of the dimmest WDs used to observe the truncation of the WD cooling sequence in NGC 6397. The horizontal dotted lines are the fiducial constraints on $f_{\rm DM}$. The vertical dashed lines denote the best fit mass for the corresponding experiment. Also shown are the 90% exclusion limits from LUX and SuperCDMS [89]. The constraints all flatten out when $\sigma_{\chi \rm p}$ exceeds $\sigma_{\chi \rm p}^{\rm crit}$ and capture is saturated. It is important to note that our constraints extend to WIMP masses ~ 1 MeV, demonstrating the unique power of this technique to constrain low mass WIMPs.

The consequences for $f_{\rm DM}$ and the annihilation rate are the same as in Figure 2.3. On the other hand, Dark Matter parameter values that are not in conflict with the results of LUX and SuperCDMS can still place strong constraints on $f_{\rm DM}$. Figure 2.4 also shows that if $\sigma_{\chi \rm p} \sim 10^{-41}\,{\rm cm}^2$, then $f_{\rm DM} \lesssim 10^{-2}$ *independent of* m_χ.

Dark matter direct search experiments such as CDMS, CRESST, CoGeNT, DAMA, and LUX typically present their results in the plane of m_χ-$\sigma_{\chi \rm p}$. Figure 2.5 shows the constraints that WD cooling in NGC 6397 place on the Dark Matter scattering cross-section $\sigma_{\chi \rm p}$ as a function of mass m_χ assuming various contributions to the Dark Matter content of the globular cluster NGC 6397. The black dotted curves correspond to the values of $f_{\rm DM}$ indicated by the labels on the figure. The widths of the lines show the uncertainty in the constraints due to uncertainty in the precise luminosities of the dimmest WDs in NGC 6397. The solid black curve shows the critical cross-section $\sigma_{\chi \rm p}^{\rm crit}$ above which capture of Dark Matter particles is saturated, limiting our ability to constrain the Dark Matter WIMP parameters. Shaded regions denote the confidence contours for CDMS-Si (95% purple, 99% blue), CRESST (1-sigma light red, 2-sigma pink), CoGeNT (90% grey, 99% dark red, near the upper left portion of the purple CDMS-Si contour), and DAMA (90% cyan, 3-sigma light green, 5-sigma dark green). The solid curves represent the exclusion limits for LUX (95% light green) and SuperCDMS (90% pink). Confirmation of the anomalous scattering events as due to Dark Matter WIMPs has the potential to limit $f_{\rm DM} \lesssim 10^{-3}$. The limits from the various experiments

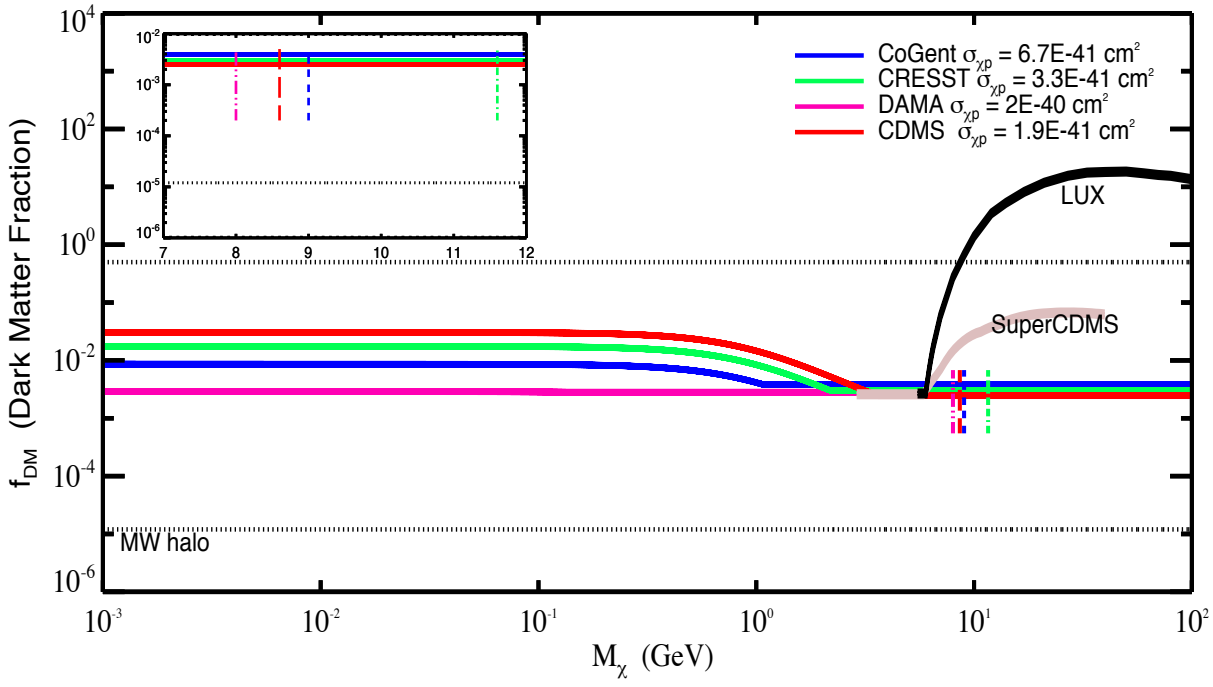

Figure 2.4: The Dark Matter fraction vs. Dark Matter particle mass for NGC 6397.

were obtained from Reference [89].

Figure 2.6 is the same as Figure 2.5, but extending to lower masses m_χ. All curves and contours are the same as Figure 2.5 with the exception of the cyan dot-dashed curve, which shows the constraint from a hypothetical 3500-3700 K WD located in the dwarf galaxy Segue I (discussed below). The pinkish shaded region is the region excluded by observations of the CMB under the assumptions of Reference [142].

In the mass range $m_\chi \gtrsim 3\,\mathrm{GeV}$, the WD cooling constraint is only competitive with direct search constraints from LUX and SuperCDMS if the Dark Matter fraction in NGC 6397 exceeds $f_{\mathrm{DM}} \gtrsim 10^{-1}$. While this value of f_{DM} is not ruled out, there is no compelling reason to believe that NGC 6397 should have such significant Dark Matter content. In any case, the possibility of constraining f_{DM} at this level is intriguing because it exceeds the potential of kinematic constraints.

The results shown in Figures 2.3-2.6 are interesting for several reasons. Interpreting any

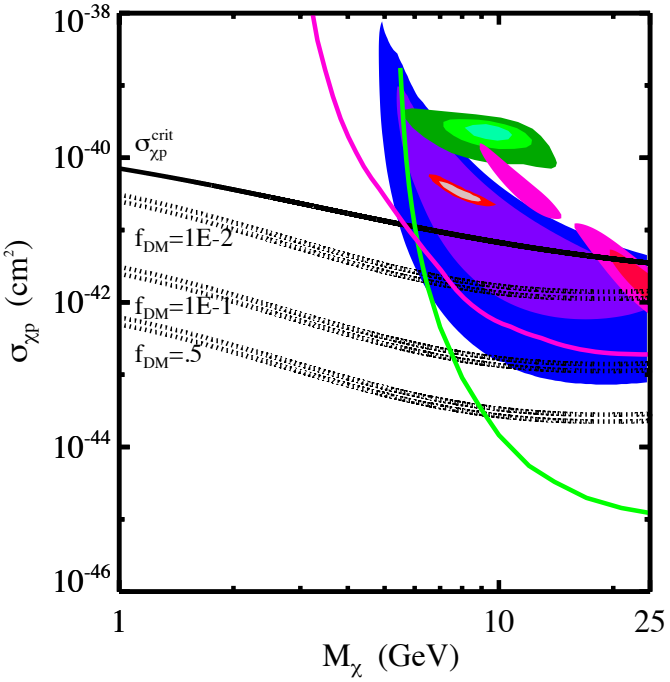

Figure 2.5: Constraints on the Dark Matter scattering cross-section $\sigma_{\chi \mathrm{p}}$ as a function of mass m_χ.

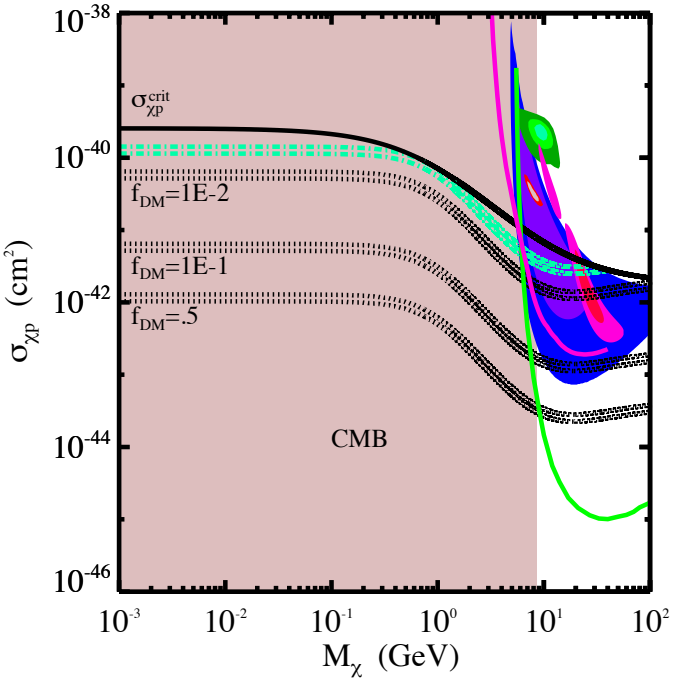

Figure 2.6: Constraints on the Dark Matter scattering cross-section $\sigma_{\chi \mathrm{p}}$ as a function of mass m_χ.

of the anomalous signals in the variety of experiments that have reported events in direct-detection detectors as Dark Matter yields a constraint on the Dark Matter content of GCs that is far more restrictive than any kinematic constraints. Furthermore, even models that exhibit no tension with the recent LUX and SuperCDMS constraints may yield observably large effects on WD cooling so as to either be constrained by WD cooling in GCs or to constrain $f_{\rm DM}$ within these GCs. This is particularly true at low Dark Matter particle masses ($m_\chi \lesssim$ 2-3 GeV), where the WD cooling constraint can be more stringent than direct-detection constraints.

Indeed, we follow-up on the results of Reference [105] by displaying the potential Dark Matter constraints that could be gleaned from the hypothetical observation of a similarly truncated WD cooling sequence in the dwarf galaxy Segue I. These constraints are interesting because unlike NGC 6397, Segue I is known to possess Dark Matter. We take the Dark Matter density and velocity dispersion in Segue I to be 175 GeV/cm^3 and 3.7 km/s respectively [184]. The annihilation rates probed in Segue I will then be $\langle \sigma_{\rm a} {\rm v} \rangle \gtrsim 10^{-46}\,{\rm cm}^3/{\rm s}$ which is similar to those probed in NGC 6397.

Notice that these constraints may be uniquely restrictive in the low-mass regime, as constraints from particle accelerators tend to be strongly model-dependent. A recent example is Reference [24], which explores constraints using an itemization of specific operators. Following the reasoning in this paper, it is clear that collider constraints are more significantly model dependent than our astrophysical bounds. Moreover, collider constraints do not extend to very low mass in general, largely because events are triggered on large missing energy which makes identification of low-mass dark matter difficult. An exception are constraints from LEP which can rule out light Dark Matter matter ($m_\chi \lesssim 10\,{\rm GeV}$) in certain scenarios [71]. However, these constraints are still model-dependent and more generally the constraints from LEP lie roughly 2-3 orders of magnitude above our constrains in the $\sigma_{\chi {\rm p}} - m_\chi$ plane (see the left panel in Figure 3 of Reference [71]). These are important distinctions. Meanwhile, the only competitive astrophysical constraints are those from observations of the CMB. Indeed, we estimate that WD heating can be exploited to constrain Dark Matter with masses as low as 100 keV. Such low Dark Matter masses may be ruled out by the CMB. For instance, Ref [142] found that for s-wave annihilation to bottom quarks $\chi\chi \to b\bar{b}, m_\chi > 8.6\,{\rm GeV}$ at

the 95% confidence level while Reference [130] found that for s-wave annihilation $m_\chi > 5$-26 GeV at the 2σ level depending on the efficiency of energy injection.

However, CMB constraints on particle mass all rely on the assumption of a nearly standard s-wave thermal relic cross section. WD cooling can probe dark matter of both very low mass *and* very low annihilation rates down to $\langle \sigma_{\rm a} {\rm v} \rangle \sim 10^{-46}\,{\rm cm}^3/{\rm s}$ in NGC 6397 and Segue I. Models with such low cross sections are not constrained by the CMB. One way to realize relatively low contemporary annihilation rates in a comprehensive model is through models in which s-wave annihilation is suppressed and p-wave annihilation dominates. CMB constraints on such scenarios are weak. As an example, Reference [60] found that for $m_\chi = 100$ MeV (1 GeV) $\langle \sigma_{\rm a} {\rm v} \rangle \gtrsim 10^{-24} (10^{-23})$ cm^3/s at a reference speed of 100 km/s (typical of Dark Matter speeds in galaxies today). However, if the Dark Matter is a thermal relic and annihilation is p-wave dominated then in order to get the correct relic abundance $\langle \sigma_{\rm a} {\rm v} \rangle \sim 10^{-31} (10^{-32})$ cm^3/s which is many orders of magnitude below the cross section probed by the CMB. On the other hand, the annihilation rate in the WD will be $\langle \sigma_{\rm a} {\rm v} \rangle \sim 10^{-30} (10^{-31})$ cm^3/s. These rates are probed by WD cooling even when the Dark Matter fraction in a GC like NGC 6397 is many orders of magnitude below our constraints and may very well be probed by WDs in a dwarf galaxy such as Segue I if the WD cooling limit could be observed in such objects.

2.4 DISCUSSION & CONCLUSIONS

Stars accumulate weakly-interacting Dark Matter in their cores as they orbit within their host halos. If the dark matter particles annihilate with a cross-section within many orders of magnitude of the canonical thermal relic cross-section of $\langle \sigma_{\rm a} v \rangle \sim 3 \times 10^{-26}\,{\rm cm}^3/{\rm s}$, then the dark matter will contribute energy to the stellar core. In most reasonable cases, this energy contribution is a negligible portion of the energy budget of the star. However, in the case of a WD, the luminosity from annihilations can be significant enough to prevent the star from cooling beyond a minimum temperature that can be probed by contemporary or future astronomical observations. Because the annihilation rate is proportional to the local

Dark Matter density, we can use the coolest WD in a GC to put an upper limit on the Dark Matter density in the environment. We have explored constraints on Dark Matter required by observations of the coolest WDs in the GC NGC 6397.

This WD cooling argument can be used to constrain a combination of GC structure (parameterized as the fraction of the GC mass in Dark Matter, $f_{\rm DM}$) and dark matter particle scattering cross-section. In particular, we have seen that if the events observed in CoGeNT, DAMA, CRESST, and CDMS-Si could be interpreted broadly as WIMP-like Dark Matter, then observations of the WD cooling sequence in NGC 6397 limit $f_{\rm DM} \lesssim 10^{-3}$ for the best-fit values of m_χ and $\sigma_{\chi \rm p}$. This would be a significant improvement over existing, kinematic constraints on the Dark Matter content of GCs ($f_{\rm DM} \sim .5$). Additionally, Dark Matter WIMPs with parameters consistent with the exclusion limits from LUX and SuperCDMS could still potentially place a powerful constraint on $f_{\rm DM}$.

This type of WIMP astronomy may have utility far beyond what we point out here. Note that the capture rate of WIMPs in a star is directly proportional to the local density of Dark Matter and inversely proportional to the velocity dispersion of the Dark Matter distribution. Therefore, the most interesting environments for applying our method have the highest values of the ratio of density to velocity dispersion. Reference [105] has already pointed out that this ratio is almost certainly large in Dwarf Galaxies, so dwarf galaxies can be attractive environments in which to apply such a constraint. Dwarf galaxies have the disadvantage that they are extremely distant from the Solar System, and therefore it is extremely difficult to place a firm lower limit on the luminosities of WDs in these objects. GCs have the advantages that there are a number of relatively dense, nearby clusters, and that GCs are often observed to great depths to further a variety of scientific goals including the study of low-mass stellar evolution, stellar remnants, and cluster structure.

We define the ratio of the density to the velocity dispersion as

$$\alpha = \frac{c}{\bar{v}}, \tag{2.17}$$

where c is the central concentration of the King model for the globular cluster (which can be thought of as a proxy for the central density). In order to constrain $f_{\rm DM}$ in a given environment, our method requires the observation of a cool WD. In particular, the observations

must be sufficiently deep that the coolest, dimmest WDs can be identified with the end of the WD cooling sequence and that no slightly cooler WDs were missed in the observations simply because they are dimmer. Therefore, we should consider nearby GCs such that one could observe the full WD cooling sequence in the cluster.

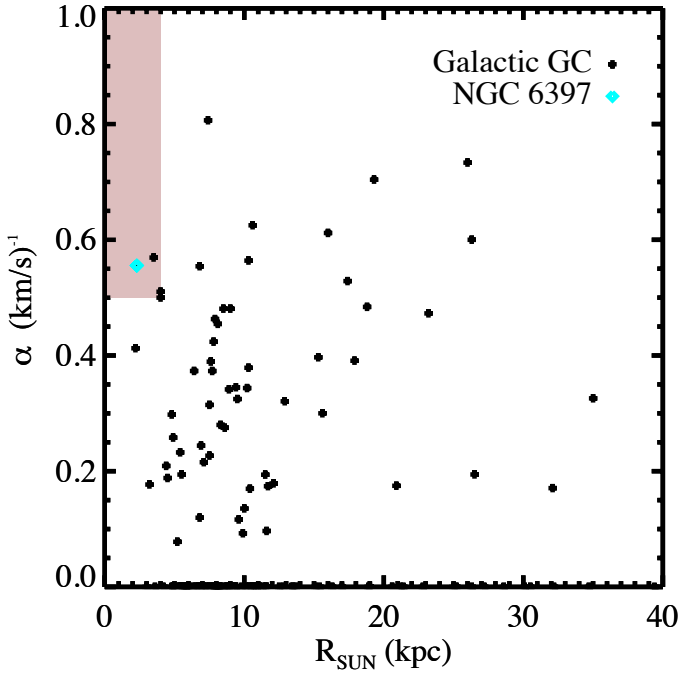

Figure 2.7: The Galactic GC distribution.

Figure 2.7 shows the distribution of Galactic GCs. If we consider GCs with α comparable to or greater than that of NGC 6397 [say $\alpha \gtrsim 0.5\,(\mathrm{km/s})^{-1}$] located not too much further than NGC 6397 (say within 4 kpc of the Sun), then we have 3 candidates for further observation: NGC 6366 ($\alpha = 0.57, R_{\mathrm{sun}} = 3.5\,\mathrm{kpc}$), NGC 6752 ($\alpha = 0.51, R_{\mathrm{sun}} = 4.0\,\mathrm{kpc}$) and NGC 6838 ($\alpha = 0.50, R_{\mathrm{sun}} = 4.0\,\mathrm{kpc}$) [95]. Of these, NGC 6366 and NGC 6838 are quite different than NGC 6397 in that they are neither metal-poor nor post core-collapse clusters, making them all the more intriguing as targets [95]. NGC 6366 is the most different from NGC 6397 in that it appears to have been heavily tidally stripped [149]. Thus, it is not a particularly dense cluster at all (c = 0.74) but is included in our cut because of its correspondingly low velocity dispersion ($\bar{v} = 1.3 \pm 0.5$ km/s) [95]. Meanwhile NGC 6752 is the most similar to NGC 6397, though it is not as metal poor [95]. All 3 of these GCs have been observed

by HST [149, 108, 193]; however, it appears that only NGC 6752 has been imaged deeply enough to potentially identify the truncation of the WD cooling sequence (see Figure 2 in Ref [193] for the color-magnitude diagram).

In addition to GCs, we could potentially apply our method to the dwarf satellite galaxies of the MW. These satellites are known to be Dark Matter dominated objects, with Segue I having the highest central Dark Matter density at $\rho_\chi \sim 100\,\mathrm{GeV/cm^3}$ [184]. The hypothetical observation of a truncated WD cooling sequence in a dwarf galaxy such as Segue I could be uniquely constraining, as pointed out in Reference [105]. In Figure 2.6, we reiterate this point and extend previous results to low-mass Dark Matter candidates in order to show that such observations have the unique ability to probe low-mass Dark Matter, a point which was missed in Reference [105]. The cyan dot-dashed curve in Figure 2.6 shows what the constraint would be if a WD was observed in Segue I with a temperature of 3500-3700 K. Because the Dark Matter density in Segue I is well constrained, observation of a cool WD within the half-light radius of this satellite could potentially rule out a broad range of parameter space extending to low WIMP masses and annihilation rates far below the canonical thermal value.

There is a long history of interplay between particle physics and astrophysics in understanding the fundamental constituents of the universe and the laws that govern their interactions. In this chapter, we explore the possibilities for a unique interplay between the physics of the dark matter and the evolution of star clusters. In particular, we show that possible near-future measurements of the properties of the dark matter may immediately result in profoundly more stringent constraints on models of globular cluster formation. Conversely, if there were ever a strong astrophysical reason to suspect that GCs formed in significant Dark Matter halos, then the evolution of WDs in GCs places strong constraints on dark matter. These constraints are relevant to dark matter masses and annihilation rate far below those that can be probed using any other techniques. Indeed, we have shown that it may be possible in the future to extend the results of Reference [105], such that observations of WDs in nearby dwarf galaxies may constrain dark matter at masses up to three orders of magnitude below what may be attainable with contemporary direct or indirect dark matter searches. This may point the way toward a new frontier for exploration at the interface between particle physics and astrophysics.

3.0 EJECTION OF DARK MATTER FROM GLOBULAR CLUSTERS

3.1 INTRODUCTION

In the ΛCDM paradigm, Dark Matter is the first matter constituent to collapse forming Dark Matter halos which serve as the seeds for galaxy formation. Progressively larger structures are built through the mergers of halos. This hierarchical structure formation is predicted by theory and is seen in N-body simulations as well as observed in the structure of galaxies and galaxy clusters.

One seeming exception to this scenario are Globular Clusters (GC). Reference [155] was the first to propose that GCs form in extended Dark Matter halos. However, observations of many GCs reveal thin tidal tails which N-body simulations predict should not form if they possess halos. Moreover recent studies of several GCs indicate that the ratio of the mass in Dark Matter to stars in several GCs $M_{\rm DM}/M_* \lesssim 1$ [88, 145, 138, 183, 49, 110] and is potentially $\lesssim 10^{-2}$ if the Dark Matter is a low mass ($m_\chi \sim 10\,{\rm GeV}$) weakly interacting particle [109].

It is now generally thought GCs formed in gas compressed by shocks [90, 96]. However, the formation scenarios of GCs remain controversial in part because of the complex abundance patterns measured in stars. These observations indicate that GCs must have been much more massive in the past in order to retain significant amounts of heavy elements that would have been ejected by supernovae [82, 83, 50]. As pointed out in Reference [49] this formation scenario is further complicated by the existence of nuclear star clusters, which demonstrates that at least some GC-like systems form in Dark Matter halos (e.g. [190, 32, 197, 196]).

Though they seemingly do not possess Dark Matter halos today, GCs could have had

them in the past and subsequently lost their Dark Matter. One mechanism invoked for the removal of the halo is tidal stripping by the galaxy [37, 133]. While, the majority of the Galactic Globular Clusters (GGC) orbit within strong tidal fields there does exist a population of isolated GCs with galactocentric distances $r_{gc} > 70\,\mathrm{kpc}$ that should not have lost their halos through tidal interactions. Two such GCs are NGC 2419 ($r_{gc} = 89.9\,\mathrm{kpc}$) and MGC1, which at $\sim 200\,\mathrm{kpc}$ from M31 is the most isolated cluster in the local group [95, 49, 129]. Observations of both these cluster indicate that $M_{\mathrm{DM}}/M_* \lesssim 1$ [49, 110].

In this chapter we investigate an additional mechanism by which GCs could eject Dark Matter halos: through multi-body gravitational interactions. In a close encounter with a star, a Dark Matter particle can be accelerated above the escape speed of the GC and be ejected. In principle, Dark Matter can also evaporate by slowly building up speed through multiple interactions. However, this mechanism is not efficient in GCs because particles with velocities near the escape speed spend most of their time near the outskirts of the GC and therefore, rarely experience an encounter with a star [99].

In this chapter we will investigate the escape rate of Dark Matter particles from a spherically symmetric stellar system in order to ascertain the viability of the ejection scenario. As the interaction is gravitational, we shall not trouble ourselves with the details of the Dark Matter particle. The only assumption we make of the Dark Matter particle is that its mass is significantly less than the mass of a typical star.

The remainder of the chapter is organized as follows: in §3.2 we present the details of the calculation of the escape rate of Dark Matter particles from an isolated, spherical stellar system. In §3.3 we present our results and in §3.4 we discuss our conclusions.

3.2 METHODS

Our calculation will follow the approach of a pair of classic papers by Hénon (Refs [98, 99] henceforth Papers 1 & 2 respectively). As in Paper 2, we begin with the assumption that the Dark Matter and stellar distributions are spherically symmetric and that the particle velocities are isotropic. Then, the number of Dark Matter particles in a phase space volume

element $\mathrm{d}^3r\mathrm{d}^3v$ is

$$(4\pi)^2 r^2 v^2 f(r,v)\mathrm{d}r\mathrm{d}v, \tag{3.1}$$

where $f(r,v)$ is the Dark Matter distribution function. Similarly, if the stellar distribution function is $g(r,v',m')$ then the number of stars in the volume element $\mathrm{d}^3r\mathrm{d}^3v'\mathrm{d}m'$ is

$$(4\pi)^2 r^2 v'^2 g(r,v',m')\mathrm{d}r\mathrm{d}v'\mathrm{d}m'. \tag{3.2}$$

Consider a Dark Matter particle of mass m_χ and coordinates (r,v). According to Paper 1 the probability that a particle will experience an encounter that takes it from a velocity $\vec{v} \to \vec{v} + \vec{e}$ is

$$P = 8\pi \mathrm{G}^2 \mathrm{d}t \frac{\mathrm{d}^3 e}{e^5} \int_0^\infty m'^2 \,\mathrm{d}m' \int_{v_0'}^\infty g(r,v',m') v' \,\mathrm{d}v', \tag{3.3}$$

where $v_0' = \frac{1}{e}|\vec{v}\cdot\vec{e} + \frac{m_\chi + m'}{2m'}e^2|$ and G is Newton's constant. The lower limit v_0' can be thought of as a statement of conservation of momentum. The relative velocity of the Dark Matter particle and star is unchanged in the encounter. It is only the velocity with respect to a thrid body, the GC as a whole in this case, that is changed.

As stated in §3.1, the one assumption of the Dark Matter particle we make is that $m_\chi \ll m'$ so

$$\begin{aligned} v_0' &= \frac{1}{e}|\vec{v}\cdot\vec{e} + \frac{e^2}{2}| \\ &= |v\cos\delta + \frac{e}{2}|. \end{aligned} \tag{3.4}$$

The particle will escape if

$$|\vec{v} + \vec{e}| \geq v_{\mathrm{esc}}(r), \tag{3.5}$$

where $v_{\mathrm{esc}}(r)$ is the local escape velocity. In the remainder of the paper we will denote the local escape velocity simply as v_{esc}. Using the notation of Paper 2, let e, δ, φ be a set of spherical coordinates for the kick velocity $\vec{e}$. Then from Equation (3.5), the condition for escape is

$$v^2 + e^2 + 2ve\cos\delta \geq v_{\mathrm{esc}}^2. \tag{3.6}$$

Then we can write the probability that the Dark Matter particle will escape in a time $\mathrm{d}t$ as:

$$Q = 8\pi \mathrm{G}^2 \mathrm{d}t \int_0^\infty m'^2 \,\mathrm{d}m' \int_{v_0'}^\infty g(r,v',m') v' \,\mathrm{d}v' \int_0^{2\pi} \mathrm{d}\varphi \int \sin\delta \,\mathrm{d}\delta \int e^{-3} \,\mathrm{d}e. \tag{3.7}$$

For a bound Dark Matter particle it must be the case that $v < v_{\text{esc}}$, then from (3.6)

$$v_{\text{esc}}^2 \leq v^2 + e^2 + 2ve\cos\delta \leq v_{\text{esc}}^2 + e^2 + 2ve\cos\delta, \tag{3.8}$$

therefore,

$$v\cos\delta \geq \frac{-e}{2}. \tag{3.9}$$

Hence, we can drop the absolute value in (3.4). Now,

$$Q = 16\pi^2 \mathrm{G}^2 \mathrm{d}t \int_0^\infty m'^2\,\mathrm{d}m' \int_{v_0'}^\infty g(r, v', m')v'\,\mathrm{d}v' \int e^{-3}\,\mathrm{d}e \int \mathrm{d}\cos\delta, \tag{3.10}$$

where integration should satisfy:

$$-1 \leq \cos\delta \leq 1 \tag{3.11}$$

$$0 \leq e \tag{3.12}$$

$$v^2 + e^2 + 2ve\cos\delta \geq v_{\text{esc}}^2 \tag{3.13}$$

$$v\cos\delta + \frac{e}{2} \leq v' < v_{\text{esc}}. \tag{3.14}$$

To find the escape rate, we now integrate over the position and velocity of the Dark Matter particle. Let N_χ be the number of Dark Matter particles in the cluster,

$$N_\chi = \int_0^\infty 4\pi r^2\,\mathrm{d}r \int_0^{v_{\text{esc}}} 4\pi v^2 f(r, v)\,\mathrm{d}v \int_0^\infty N_\chi(m)\,\mathrm{d}m, \tag{3.15}$$

with $f(r, v)$ normalized to 1 and $N_\chi(m) = N_\chi\delta(m - m_\chi)$ assuming the halo is composed of a single Dark Matter constituent. Then the specific escape rate is

$$\begin{aligned}\left|\frac{1}{N_\chi}\frac{\partial N_\chi}{\partial t}\right| &= \int_0^\infty 4\pi r^2\,\mathrm{d}r \int_0^{v_{\text{esc}}} 4\pi v^2 \frac{Q}{\mathrm{d}t} f(r, v)\,\mathrm{d}v \\ &= 256\pi^4 \mathrm{G}^2 \int_0^\infty r^2\,\mathrm{d}r \int_0^{v_{\text{esc}}} v^2 f(r, v)\,\mathrm{d}v \\ &\times \int_0^\infty m'^2\,\mathrm{d}m' \int_{v_0'}^\infty g(r, v', m')v'\,\mathrm{d}v' \int e^{-3}\,\mathrm{d}e \int \mathrm{d}\cos\delta,\end{aligned} \tag{3.16}$$

with the limits in Equations(3.11)-(3.14) satisfied and where we have taken the magnitude since $\frac{\partial N_\chi}{\partial t}$ is negative. If the magnitude of the specific escape rate is greater than τ^{-1} with

τ the age of the Universe, then a typical Dark Matter will have been ejected from the halo. It is therefore likely that the GC would have dissipated its halo by the present time *via* this mechanism. We normalized Equation (3.15) to N_χ rather than 1 to make this point explicit.

As noted in Paper 2, this expression looks quite intractable, but the integrals in e and δ can in fact be calculated analytically. Keeping with the notation of Paper 2 let

$$S = \int e^{-3}\,\mathrm{d}e \int \mathrm{d}\cos\delta, \tag{3.17}$$

and let $C = \cos\delta$. From (3.13)

$$C \geq \frac{v_{\mathrm{esc}}^2 - v^2 - e^2}{2ve} = C_1, \tag{3.18}$$

from (3.14)

$$C \leq \frac{v' - \frac{e}{2}}{v} = C_2, \tag{3.19}$$

and from (3.11)

$$C_3 = -1 \leq C \leq 1 = C_4. \tag{3.20}$$

In order for S to be non-zero we must have that $C_1 < C_4, C_1 < C_2, C_3 < C_4$, and $C_3 < C_2$. Now $C_3 < C_4$ trivially. $C_1 < C_4$ requires that,

$$e > v_{\mathrm{esc}} - v = e_1, \tag{3.21}$$

which is stronger than (3.12). $C_1 < C_2$ requires that,

$$e > \frac{v_{\mathrm{esc}}^2 - v^2}{2v'} = e_2, \tag{3.22}$$

which is again stronger than (3.12). And $C_3 < C_2$ requires that,

$$e < 2(v' + v) = e_3, \tag{3.23}$$

which further restricts (3.12). C_3 will be the lower limit of the $\mathrm{d}C$ integral when $C_1 < C_3$ or when

$$e > v + v_{\mathrm{esc}} = e_4, \tag{3.24}$$

and C_2 will be the upper limit when $C_2 < C_4$ or when

$$e > 2(v' - v) = e_5. \tag{3.25}$$

Thus, in order to determine the limits of the integrals in S, we must consider the order of e_1, e_2, e_3, e_4, and e_5. Elementary calculations show that

$$\begin{aligned} v' \geq \frac{1}{2}(v_{\rm esc} - 3v) = v_1' &\Rightarrow e_1 \leq e_3 \\ v' \geq \frac{1}{2}(v_{\rm esc} - v) = v_2' &\Rightarrow e_2 \leq e_3, e_2 \leq e_4, e_4 \leq e_3 \\ v' \geq \frac{1}{2}(v_{\rm esc} + v) = v_3' &\Rightarrow e_2 \leq e_1, e_1 \leq e_5, e_2 \leq e_5 \\ v' \geq \frac{1}{2}(v_{\rm esc} + 3v) = v_4' &\Rightarrow e_4 \leq e_5 \end{aligned} \tag{3.26}$$

and it is always true that $e_1 \leq e_4$ and $e_5 \leq e_3$. These relations divide the v-v' plane into 5 regions A, B, C, D, and E (see Figure 3.1). In region A,

$$e_5 \leq e_1 \leq e_2 \leq e_4 \leq e_3. \tag{3.27}$$

Thus in region A we have,

$$\begin{aligned} S_{\rm A} &= \int_{e_2}^{e_4} e^{-3}\,{\rm d}e \int_{C_1}^{C_2} {\rm d}C + \int_{e_4}^{e_3} e^{-3}\,{\rm d}e \int_{C_3}^{C_2} {\rm d}C \\ &= \frac{2v'^3}{3v(v_{\rm esc}^2 - v^2)^2} + \frac{1}{8v(v'+v)} - \frac{2v_{\rm esc} + v}{6v(v_{\rm esc}+v)^2}. \end{aligned} \tag{3.28}$$

In region B,

$$e_2 \leq e_1 \leq e_5 \leq e_4 \leq e_3. \tag{3.29}$$

Hence,

$$\begin{aligned} S_{\rm B} &= \int_{e_1}^{e_5} e^{-3}\,{\rm d}e \int_{C_1}^{C_4} {\rm d}C + \int_{e_5}^{e_4} e^{-3}\,{\rm d}e \int_{C_1}^{C_2} {\rm d}C + \int_{e_4}^{e_3} e^{-3}\,{\rm d}e \int_{C_3}^{C_2} {\rm d}C \\ &= \frac{3v_{\rm esc}^2 - v^2}{3(v_{\rm esc}-v)^2(v_{\rm esc}+v)^2} - \frac{1}{4(v'^2 - v^2)}. \end{aligned} \tag{3.30}$$

In region C,

$$e_2 \leq e_1 \leq e_4 \leq e_5 \leq e_3. \tag{3.31}$$

Hence,

$$\begin{aligned} S_{\rm C} &= \int_{e_1}^{e_4} e^{-3}\,{\rm d}e \int_{C_1}^{C_4} {\rm d}C + \int_{e_4}^{e_5} e^{-3}\,{\rm d}e \int_{C_3}^{C_4} {\rm d}C + \int_{e_5}^{e_3} e^{-3}\,{\rm d}e \int_{C_3}^{C_2} {\rm d}C \\ &= \frac{3v_{\rm esc}^2 - v^2}{3(v_{\rm esc}-v)^2(v_{\rm esc}+v)^2} - \frac{1}{4(v'^2 - v^2)} \\ &= S_{\rm B}. \end{aligned} \tag{3.32}$$

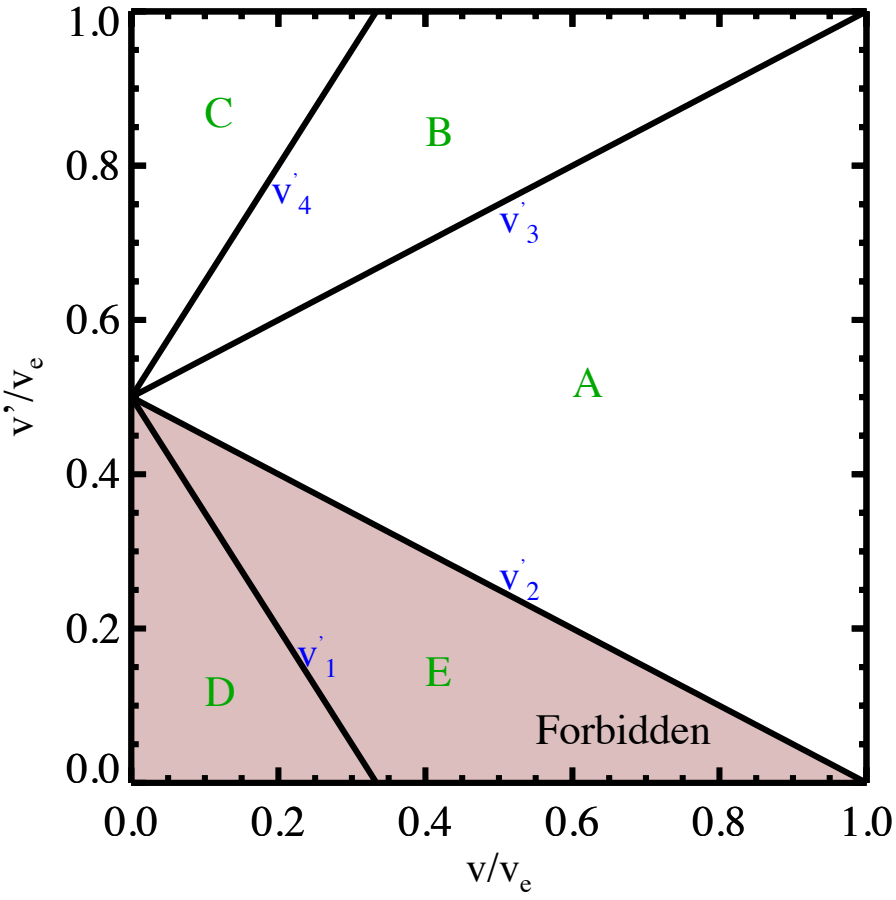

Figure 3.1: The integration regions over the kick velocity $\vec{e}$.

In region D,

$$e_5 \leq e_3 \leq e_1 \leq e_4 \leq e_2. \tag{3.33}$$

Here we can not simultaneously satisfy $e > e_1, e > e_2$, and $e < e_3$, thus region D is forbidden. In region E,

$$e_5 \leq e_1 \leq e_3 \leq e_4 \leq e_2. \tag{3.34}$$

So region E is forbidden for the same reason as D. Then Eq. (3.16) becomes,

$$\begin{aligned}\left|\frac{1}{N_\chi}\frac{\partial N_\chi}{\partial t}\right| = 256\pi^4 \mathrm{G}^2 \int_0^\infty r^2\,\mathrm{d}r \int_0^\infty m'^2\,\mathrm{d}m' \\ \times \Bigg\{ \int_0^{v_{\rm esc}} v^2 f(r,v)\,\mathrm{d}v \int_{v_2'}^{v_3'} v' S_{\rm A} g(r,v',m')\,\mathrm{d}v' \\ + \int_0^{v_{\rm esc}/3} v^2 f(r,v)\,\mathrm{d}v \int_{v_3'}^{v_4'} v' S_{\rm B} g(r,v',m')\,\mathrm{d}v' \\ + \int_{v_{\rm esc}/3}^{v_{\rm esc}} v^2 f(r,v)\,\mathrm{d}v \int_{v_3'}^{v_{\rm esc}} v' S_{\rm B} g(r,v',m')\,\mathrm{d}v' \\ + \int_0^{v_{\rm esc}/3} v^2 f(r,v)\,\mathrm{d}v \int_{v_4'}^{v_{\rm esc}} v' S_{\rm B} g(r,v',m')\,\mathrm{d}v' \Bigg\}.\end{aligned} \tag{3.35}$$

In order to proceed further we must specify the stellar and Dark Matter distribution functions. As in Paper 2, we take for the stellar component a Plummer model

$$\rho_*(r) = \frac{3M_*}{4\pi}\frac{r_0^2}{(r^2+r_0^2)^{5/2}}, \tag{3.36}$$

where r_0 is the half-mass radius of the GC. As there is little guidance on what the distribution function of Dark Matter in a GC might be, we will also use a Plummer model for the Dark Matter

$$\rho_\chi(r) = \frac{3M_{\rm DM}}{4\pi}\frac{r_\chi^2}{(r^2+r_\chi^2)^{5/2}}, \tag{3.37}$$

where r_χ is the half-mass radius of the Dark Matter halo. We choose the Plummer model for the Dark Matter in part because it has some nice mathematical properties that make it a convenient choice. As we shall see below, the Plummer distribution function allows us to separate the radial and velocity integrals. There is also a factor of $\left(\frac{v_{\rm esc}^2 - v^2}{2}\right)^{7/2}$ in the distribution function which cancels out the divergence of $(v_{\rm esc}^2 - v^2)^{-2}$ in $S_{\rm A}$. Moreover, the Plummer model is reasonably realistic for GCs [99] and is similar to the structures of

simulated Dark Matter halos and elliptical galaxies. One shortcoming of the Plummer model is that it lacks mass segregation which is known to occur (e.g. [4]). This in turn implies that velocities are uncorrelated, but the error is small and there is no known analytical cluster model with mass segregation [99].

Now the gravitational potential is

$$\phi(r) = \frac{-GM_*}{\left(r^2 + r_0^2\right)^{1/2}} + \frac{-GM_{\rm DM}}{\left(r^2 + r_\chi^2\right)^{1/2}}. \tag{3.38}$$

In general the half-mass radii of the 2 components need not be the same. If $r_\chi \neq r_0$ the analytic expressions needed to derive the distribution function become cumbersome and we treat this case numerically. Due to the assumption of isotropy, the distribution function depends only on the magnitude of the velocity, or equivalently the kinetic energy. Figure 3.2 shows the distribution function $f(\varepsilon)$ as a function of the magnitude of the specific energy $\left(\varepsilon = \frac{1}{2}[v_{\rm esc}^2 - v^2]\right)$ for a GC with $M_* = 2 \times 10^6\,{\rm M}_\odot$, $r_0 = 10\,{\rm pc}$. The solid line is the standard Plummer model in the case that $r_\chi = r_0$. The dashed green line shows the numerical result for this case, which is in agreement with the analytic case. The dotted line shows the distribution function in the case that $r_\chi = r_0/10$ while the dot-dashed line shows the case where $r_\chi = 10 r_0$. The inset is a zoom in of the latter case, showing the feature at $\varepsilon \approx 150\,({\rm km/s})^2$. Since ε is inversely proportional to r, when $r_\chi = r_0/10$ we expect that most of the Dark Matter should be at large ε (small r). The flat part of the distribution function near $\varepsilon = 2000\,({\rm km/s})^2$ is the transition from mostly stars at large r to stars and Dark Matter at $r \sim r_0/10$. The distribution function is also pushed to higher energies as more mass is concentrated in the center, increasing the orbital velocities in that region. The oppositie is true for the case $r_\chi = 10 r_0$.

In the case that $r_0 = r_\chi$ we will have the standard Plummer distribution,

$$f(r, v) = \frac{24\sqrt{2}}{7\pi^3 r_0^3 \psi_0^5} \left(\frac{v_{\rm esc}^2 - v^2}{2}\right)^{\frac{7}{2}} \tag{3.39}$$

where $\psi_0 = \frac{GM}{r_0}$ with $M = M_* + M_{\rm DM}$ the total mass of the cluster and $E = \frac{-3\pi\psi_0^2 r_0}{64{\rm G}}$ its energy.

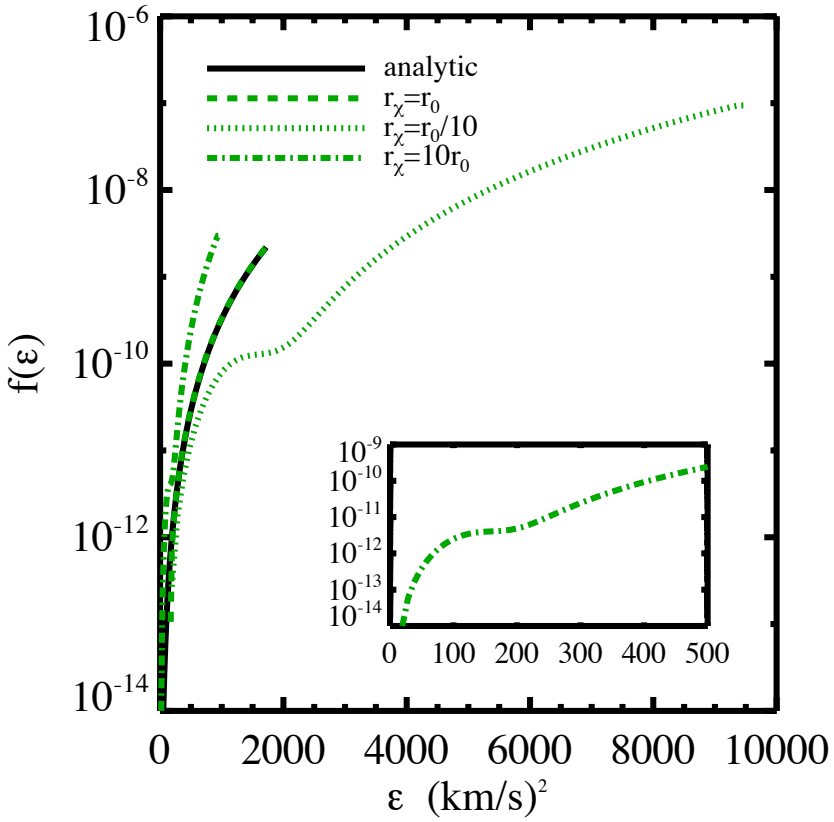

Figure 3.2: The distribution function $f(\varepsilon)$ as a function of the magnitude of the specific energy.

With the choice that $r_\chi = r_0$ we have that

$$\begin{aligned} v_{\rm esc} &= \sqrt{2\psi} \\ &= \frac{(2\psi_0)^{1/2}}{\left(1+\frac{r^2}{r_0^2}\right)^{1/4}}, \end{aligned} \tag{3.40}$$

where we have defined $\psi(r) = -\phi(r)$. Defining the stellar mass spectrum $N_*(m)\mathrm{d}m$ as the number of stars in the mass interval $m \to m+\mathrm{d}m$, we have that $g(r, v', m') = f(r, v')N_*(m')$. Then Equation (3.35) becomes

$$\begin{aligned} \left|\frac{1}{N_\chi}\frac{\partial N_\chi}{\partial t}\right| = \frac{2304\mathrm{G}^2}{49\pi^2 r_0^6 \psi_0^{10}} \int_0^{R_{\rm vir}} r^2\,\mathrm{d}r \int_0^\infty N_*(m') m'^2\,\mathrm{d}m' \\ \times \Bigg\{ \int_0^{v_{\rm esc}} v^2(v_{\rm esc}^2 - v^2)^{\frac{7}{2}}\,\mathrm{d}v \int_{v_2'}^{v_3'} v' S_{\rm A}(v_{\rm esc}^2 - v'^2)^{7/2}\,\mathrm{d}v' \\ + \int_0^{v_{\rm esc}/3} v^2(v_{\rm esc}^2 - v^2)^{\frac{7}{2}}\,\mathrm{d}v \int_{v_3'}^{v_4'} v' S_{\rm B}(v_{\rm esc}^2 - v'^2)^{7/2}\,\mathrm{d}v' \\ + \int_{v_{\rm esc}/3}^{v_{\rm esc}} v^2(v_{\rm esc}^2 - v^2)^{\frac{7}{2}}\,\mathrm{d}v \int_{v_3'}^{v_{\rm esc}} v' S_{\rm B}(v_{\rm esc}^2 - v'^2)^{7/2}\,\mathrm{d}v' \\ + \int_0^{v_{\rm esc}/3} v^2(v_{\rm esc}^2 - v^2)^{\frac{7}{2}}\,\mathrm{d}v \int_{v_4'}^{v_{\rm esc}} v' S_{\rm B}(v_{\rm esc}^2 - v'^2)^{7/2}\,\mathrm{d}v' \Bigg\}. \end{aligned} \tag{3.41}$$

where the virial radius $R_{\rm vir}$ of the Dark Matter halo is chosen to be suitably large ($\sim 10r_0$)such that the integrals in Equation (3.41) are all converged.

Continuing the approach of Paper 2, we now define new variables:

$$x = v/v_{\rm esc}, \qquad x' = v'/v_{\rm esc}. \tag{3.42}$$

Then we can remove $v_{\rm esc}$ from the integrals over v and v' and perform those integrals separately from the radial integral. It is proven in Appendix II of Paper 2 that the Plummer

model is the only steady state distribution for which this separation is possible. Then Equation (3.41) becomes

$$\begin{aligned}\left|\frac{1}{N_\chi}\frac{\partial N_\chi}{\partial t}\right| = \frac{2304\mathrm{G}^2}{49 r_0^6 \psi_0^{10}} \int_0^{R_{\mathrm{vir}}} v_{\mathrm{esc}}^{17} r^2 \,\mathrm{d}r \int_0^\infty N_*(m') m'^2 \,\mathrm{d}m' \\ \times \Bigg\{ \int_0^1 x^2(1-x^2)^{\frac{7}{2}} \,\mathrm{d}x \int_{x_2'}^{x_3'} x' S_{\mathrm{A}}'(1-x'^2)^{7/2} \,\mathrm{d}x' \\ + \int_0^{1/3} x^2(1-x^2)^{\frac{7}{2}} \,\mathrm{d}x \int_{x_3'}^{x_4'} x' S_{\mathrm{B}}'(1-x'^2)^{7/2} \,\mathrm{d}x' \\ + \int_{1/3}^1 x^2(1-x^2)^{\frac{7}{2}} \,\mathrm{d}x \int_{x_3'}^1 x' S_{\mathrm{B}}'(1-x'^2)^{7/2} \,\mathrm{d}x' \\ + \int_0^{1/3} x^2(1-x^2)^{\frac{7}{2}} \,\mathrm{d}x \int_{x_4'}^1 x' S_{\mathrm{B}}'(1-x'^2)^{7/2} \,\mathrm{d}x' \Bigg\},\end{aligned} \tag{3.43}$$

where

$$\begin{aligned} x_2' &= \frac{1}{2}(1-x) \\ x_3' &= \frac{1}{2}(1+x) \\ x_4' &= \frac{1}{2}(1+3x), \end{aligned} \tag{3.44}$$

and the $'$ in S_i' denotes the fact that it is now a function of x and x' with v_{esc} factored out.

Let us now choose a particular stellar mass spectrum. We begin with the Initial Mass Function (IMF) from Reference [123]. All of the GGCs should have ages of order ~ 10 Gyr, meaning that their Main Sequence (MS) turnoffs should be at approximately $1\,\mathrm{M}_\odot$. Therefore, in order to obtain a crude approximation of the present day stellar mass spectrum, we simply cut off the IMF at $1\,\mathrm{M}_\odot$ (see Figure 3.3). Note that this is highly conservative as stellar remnants such as Neutron Stars, White Dwarfs, and Black Holes as well as any stars still on the Giant and Horizontal Branches should contribute to the escape rate. Furthermore, higher mass stars are given more weight in the integral over mass in Equation (3.43).

With this choice of stellar mass spectrum we have that

$$\int_0^\infty N_*(m') m'^2 \,\mathrm{d}m' = 0.18M. \tag{3.45}$$

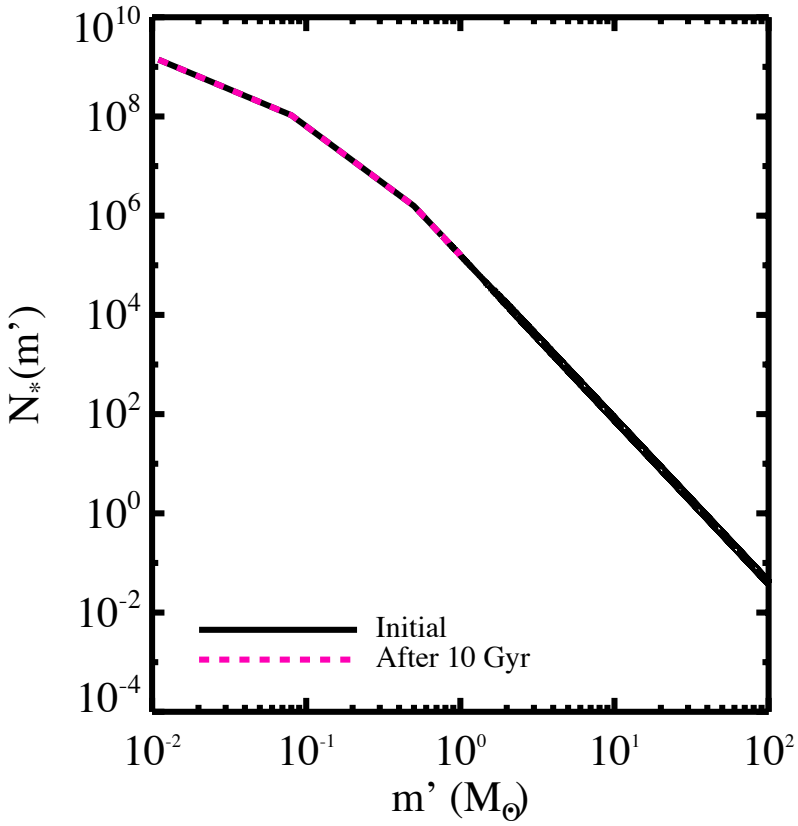

Figure 3.3: Initial and current stellar mass spectra.

3.3 RESULTS

In Figure 3.4 we consider the result of integrating Equation (3.43) numerically for different values of the ratio $M_{\rm DM}/M_*$ and compare these results to the GGCs (as well as the cluster MGC1 located in M31). Contours of the specific escape rate for GCs with $r_0 = r_\chi$ are shown with solid black lines. The red star represents MGC1, an isolated cluster orbiting M31, while the blue diamonds represent the isolated population of GGCs ($r_{gc} > 70$ kpc). As noted in §3.1, most of the GGCs could have lost their Dark Matter halos through tidal interactions with the Galaxy. We shall therefore pay particular attention to the most isolated GCs. GGCs that have been selected for further investigation in Figure 3.5 are marked with pink squares while the green triangles denote the remaining GGCs. The solid blue line is the location where the specific escape rate is $1/\tau$ with $\tau = 13.8$ Gyr the approximate age of the Universe [161]. GCs with escape rates comparable to or exceeding this limit should have ejected a significant portion of their Dark Matter halos. However, none of the clusters reach this limit regardless of the value of $M_{\rm DM}/M_*$. Note that the escape rate is no longer sensitive to the value of $M_{\rm DM}/M_*$ once this ratio has dropped below $\sim 10^{-2}$. We also note that more massive GCs have lower escape rates due to their higher escape speeds, while GCs which are larger in size have lower escape rates due to the decreased probability of experiencing an encounter at higher radii (see Figure 3.2).

In Figures 3.5 & 3.6 we consider the effect of varying r_χ with respect to r_0 while holding $M_{\rm DM}/M_* = 1$. We consider $r_\chi = 10 r_0$ which might correspond to an extended primordial halo as well as $r_\chi = 10^{-1} r_0$ which might correspond to a cluster which has had the outer part of its Dark Matter halo stripped by tidal interactions. The results are obtained by integrating Equation (3.35) with the appropriate numerically derived distribution functions (see Figure 3.2). Note that for $r_\chi = 10 r_0$, much of the Dark Matter exists beyond the stellar content of the GC and therefore never experiences a close encounter with a star. Thus we might normalize Equation (3.35) by the number of Dark Matter particles within the stellar content, rather than the total number of particles. Since we have taken the virial radius of the cluster to be $R_{\rm vir} = 10 r_0$, exactly half the Dark Matter particles should be within $R_{\rm vir}$ in the case of an extended halo. Therefore we could multiply the results for $r_\chi = 10 r_0$ by a

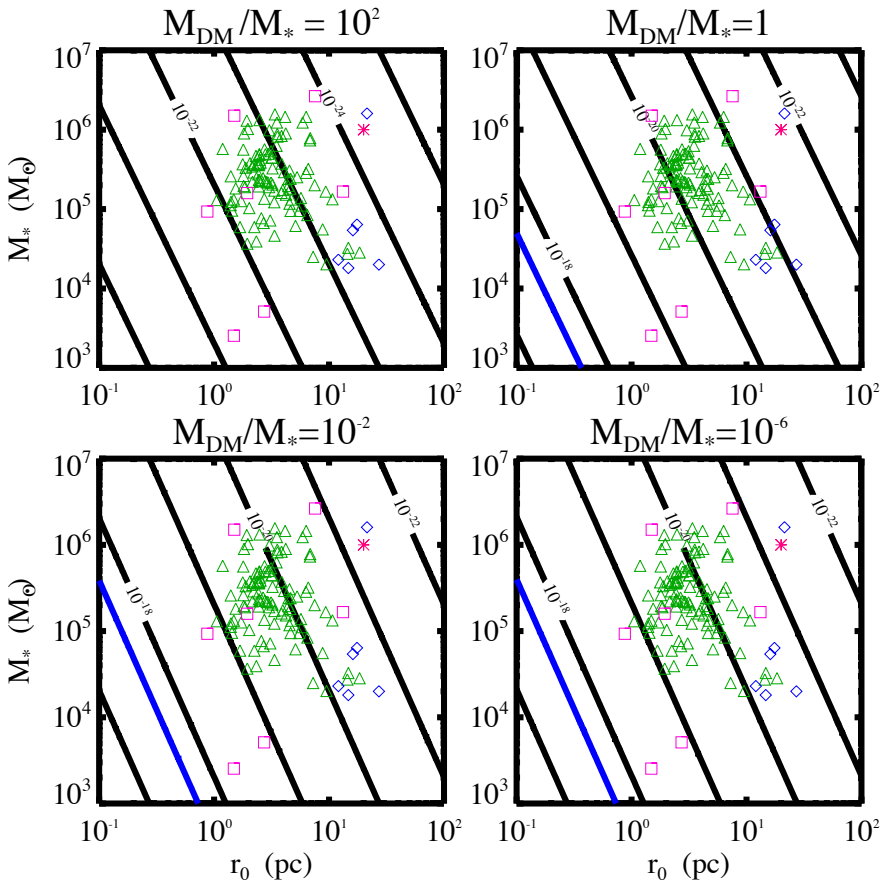

Figure 3.4: Contours of the specific escape rate for GCs with $r_0 = r_\chi$.

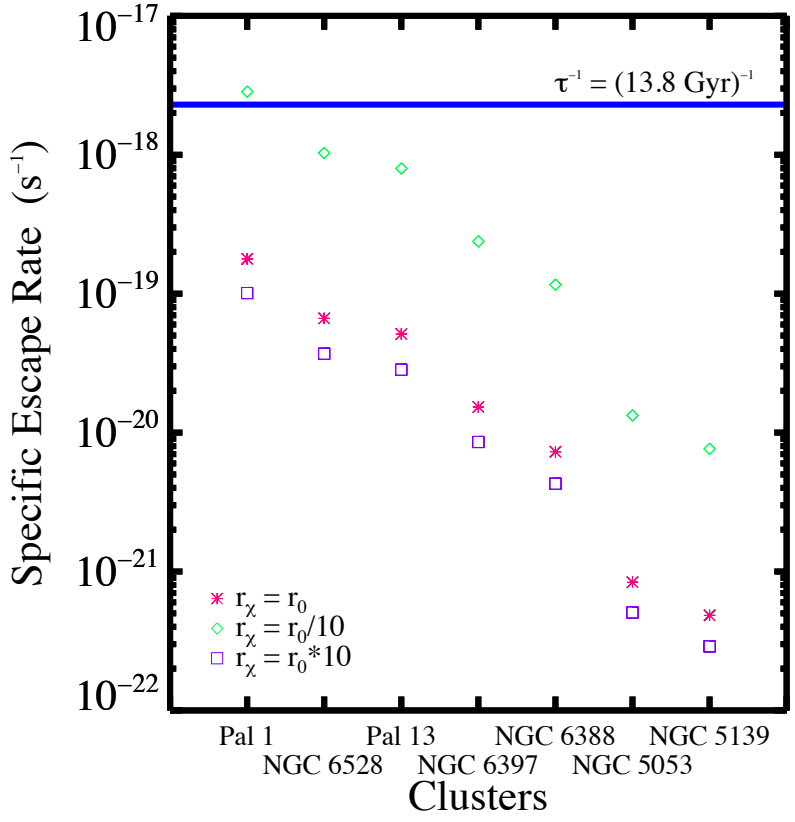

Figure 3.5: Escape rates for several GGCs for different values of r_χ/r_0.

factor of 2 in Figures 3.5 & 3.6.

We first consider, in Figure 3.5, the GCs that are marked with pink squares in Figure 3.4. The parameters for these clusters are summarized in Table 3.1 and span the full range of GGCs. Note that decreasing r_χ increases the escape rate. This result is perhaps counter intuitive as a smaller halo should have a deeper potential well which is correspondingly more difficult to escape from. However, in a smaller halo, the probability of experiencing an encounter is much higher, which explains the results. Of course, the opposite is true for larger halos. Though they are easier to escape from, the probability of encounter is decreased. Note, that for $M_{\rm DM}/M_* = 1$ the only halo which exceeds $1/\tau$ is that of Pal 1 in the case that $r_\chi = 10^{-1} r_0$. However, the escape rate can be increased by an additional half dex for smaller values of the ratio $M_{\rm DM}/M_*$. Fig 3.5 then indicates that clusters with $M_{\rm DM}/M_* \lesssim 10^{-2}$ and r_0 not more than a few parsecs, could have ejected a small remnant halo after the initial halo was tidally stripped. This also suggests that such clusters could have significantly dispersed the inner regions of their halos, even if their halos were larger.

In Figure 3.6 we consider the escape rates for the most isolated clusters in the Milky Way (and M31) which are marked with blue diamonds in Fig 3.4. The parameters for these clusters are summarized in Table 3.2. Due to their large sizes ($r_0 > 10\,{\rm pc}$), these clusters all have escape rates far below $1/\tau$. This is further evidence against the formation of GCs in Dark Matter halos.

3.4 CONCLUSIONS

GCs are peculiar systems in that they are the largest structures in the Universe not dominated by Dark Matter. Though they do not possess halos today, it is possible that they did in the past. One viable mechanism by which GCs can lose Dark Matter halos is through tidal interactions with the Galaxy. However, there exists a population of isolated GCs which should not have had their halos tidally stripped if they ever possessed them. Observations of 2 of these GCs (NGC 2419 & MGC1) indicate that they do not possess significant halos today ($M_{\rm DM} \lesssim M_*$ see Table 3.2).

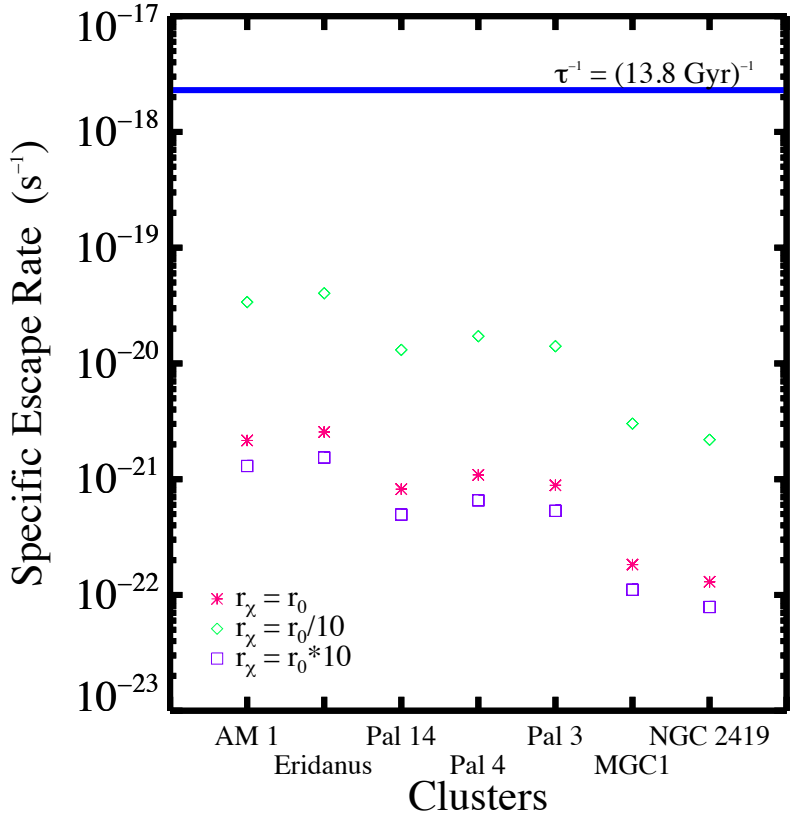

Figure 3.6: Escape rates for the isolated GCs for different values of r_χ/r_0.

GC	$M_*(\mathrm{M}_\odot)$	r_0 (pc)	M_{DM}/M_*
Pal 1	2.54×10^3	1.49	—
Pal 13	5.12×10^3	2.72	—
NGC 5053	1.66×10^5	13.2	—
NGC 5139	2.64×10^6	7.56	—
NGC 6388	1.50×10^6	1.50	—
NGC 6397	1.59×10^5	1.94	$\lesssim 1$ [183]
NGC 6528	9.31×10^4	0.87	—

Table 3.1: Parameters for the GCs in Figure 3.5 [95].

GC	$M_*(\mathrm{M}_\odot)$	r_0 (pc)	r_{gc} (kpc)	M_{DM}/M_*
AM 1	1.81×10^4	14.7	124.6	—
Eridanus	2.30×10^4	12.1	95.0	—
Pal 3	6.38×10^4	17.5	95.7	—
Pal 4	5.41×10^4	16.1	111.2	—
NGC 2419	1.60×10^6	21.4	89.9	$\lesssim 1$ [49, 110]
Pal 14	2.00×10^4	27.1	71.6	—
MGC 1	1×10^6	20	200	$\lesssim 1$ [49]

Table 3.2: Parameters for the isolated GCs in Figure 3.6 [95].

In this chapter we have investigated an additional mechanism for the removal of Dark Matter from a GC: the ejection of Dark Matter by multi-body gravitational interactions. We have found that GCs could not have ejected a significant Dark Matter halo with one exception. GCs that are sufficiently small could have ejected a small remnant halo after the majority of the halo was tidally stripped. Our results cast further doubt on the formation of GCs in extended, massive Dark Matter halos.

In the context of WIMP astronomy, GCs remain interesting targets. As the stellar density of a GC is extremely high ($10^4 - 10^6\,\mathrm{stars/pc}^3$), even a subdominant Dark Matter halo could have a density several orders of magnitude greater than that of the Solar neighborhood $\rho_\chi \sim 0.4\,\mathrm{GeV/cm}^3$. Current limits on the mass of any hypothetical Dark Matter halo are of order the stellar mass of the cluster. Our results indicate that such a halo should persist to the present day. This would make the isolated GCs viable targets for the methods of §2.

4.0 ASYMMETRIC DARK MATTER AND STARS

4.1 INTRODUCTION

In the current concordance model of cosmology ΛCDM, $\approx 26\%$ of the matter-energy content of the Universe is composed of Dark Matter [101, 161]. While the nature of this Dark Matter is currently unknown, the most popular particle candidates are Weakly Interacting Massive Particles (WIMPs). WIMPs are compelling candidates in part because they arise naturally in extensions to the Standard Model of particle physics such as supersymmetry and because Weak scale interactions generically yield the correct relic abundance today—the so-called WIMP miracle. However, the WIMP need not be a thermal relic. An alternative is that the presence of Dark Matter today is the result of an asymmetry between WIMPs and anti-WIMPs in the early Universe, just as the existence of baryons today is the result of an asymmetry between matter and anti-matter.

Asymmetric Dark Matter (ADM) can potentially explain the apparent coincidence that the densities of Dark Matter and baryons in the Universe are the same order of magnitude ($\Omega_{\rm dm} \approx 5\Omega_{\rm b}$) [161, 203]. If the baryons are the result of an asymmetry and Dark Matter is a thermal relic, then they have completely different production mechanisms. It is then curious that they are the same order of magnitude. However, if both types of matter are asymmetric, this could hint at a natural explanation: either the asymmetry could be generated in both the baryonic and dark sector at the same time (e.g. from the decay of a heavy parent particle) or the asymmetry could be generated in one sector and then transferred to the other (e.g. by Dark Matter annihilations) [203].

ADM could also explain the null results of indirect-detection experiments. Indirect-detection experiments seek to identify the Dark Matter particle by observing its annihilation

or decay products in a given astrophysical environment. Examples include the detection of neutrinos from annihilations in the Solar interior [5] and photons [9], positrons [19], or neutrinos [5] from annihilations in the galactic halo. The dwarf satellite galaxies of the MW are highly Dark Matter dominated objects with mass-to-light ratios as large as $3400\,\mathrm{M}_\odot/\mathrm{L}_\odot$ [184], making them particularly promising targets for indirect detection. The lack of a signal in 6 years of data from the *Fermi* γ-ray satellite places strong constraints on Dark Matter in the parameter space of particle mass and annihilation rate [10]. The *Fermi* constraints lie above the canonical thermal relic cross-section for Dark Matter mass $m_\chi \lesssim 100\,\mathrm{GeV}$ for the quark and τ lepton annihilation channels. The Sun is also a promising target for indirect detection. The null results of the IceCube neutrino telescope have now reached the level that they can exclude several models in the weak-scale Minimal Supersymmetric Standard Model (MSSM) [6].

In the simplest models of ADM no annihilation signal is expected as the WIMP is not its own anti-particle and the relic density of anti-WIMPs is negligible [94]. Furthermore, if the WIMP is stable with respect to the age of the Universe, then there will be no significant decay signal. Thus ADM can naturally explain the null results of indirect-detection experiments. It should be noted that in more complicated models of ADM, the relic density of anti-WIMPs can be non-negligible or anti-WIMPs can be replenished by decays of WIMPs leading to indirect-detection signals [94, 203].

ADM was originally proposed as a potential solution to the Solar Neutrino Problem [203]. WIMPs will accumulate in stars over time by scattering off of nuclei into bound orbits. Once bound, a WIMP will eventually settle into the core of the star through further scattering events (see e.g. the review [114] and references therein). If the WIMP is a thermal relic, then the capture of WIMPs will eventually equillibrate with annihilations, preventing the star from accumulating a large amount of Dark Matter. Conversely, if the Dark Matter is asymmetric, then there is no such limit and WIMPs will continue to accumulate with time, potentially reaching a large fractional abundance within the star.

ADM in the core of the star will occasionally be scattered to a higher energy. For scattering cross-sections above (below) $\sigma_{\chi\mathrm{p}} \sim 10^{-36}\,\mathrm{cm}^2$ energy is transported conductively (diffusively) [58], decreasing the effective opacity and temperature gradient of the core [186].

This transport mechanism can potentially be extremely efficient, because the orbits of Dark Matter particles are of order minutes, while the thermal timescale of the Solar core is of the order of millions of years [186]. For $\sigma_{\chi \mathrm{p}} \sim 4 \times 10^{-36}\,\mathrm{cm}^2$ the number density of WIMPs need only be 1 part in 10^{12} of the number density of protons in the Sun in order to have order unity effects on the effective opacity [186]. This value scales linearly with cross-section, in the sense that an order of magnitude change in the cross-section in either direction can be compensated by an order of magnitude increase in the number density of WIMPs. Reference [186] showed that ADM could potentially cool the innermost neutrino producing portion of the core without disturbing the larger luminosity producing region, thereby solving the Solar Neutrino Problem.

The solution to the Solar Neutrino Problem is in fact neutrino oscillations [15]; however, energy transport by ADM in stars can still be interesting in its own right (e.g. [169]). Reference [58] found that conductive energy transport by WIMPs can induce thermal pulses during the Horizontal Branch (HB) phase of stellar evolution. Such high cross-sections are ruled out today by collider and direct-detection constraints (e.g. Refs. [127, 71]), but diffusive WIMP energy transport can also have significant effects on stars.

Reference [112] found that Main Sequence (MS) stars in Dark Matter densities $\rho_\chi \geq 10^2\,\mathrm{GeV/cm}^3$ can be significantly affected by WIMPs with Spin-Dependent scattering cross-sections $\sigma_{\mathrm{SD}} \geq 10^{-37}\,\mathrm{cm}^2$. Inside a very central region of a Sun-like star, WIMPs can transport all of the energy created by nuclear reactions. This is the region where the WIMP temperature is less than the baryonic temperature, termed the inversion core in Reference [112]. WIMPs then cool this region and decrease the efficiency of nuclear energy generation. In order to maintain hydrostatic equilibrium, nuclear energy production must increase outside the inversion core. This heats the outer layers of the star leading to higher luminosity and effective temperature. At even higher Dark Matter densities WIMPs can cool the entire core, lowering the energy generation and forcing the star to contract, decreasing the luminosity [112]. As ADM decreases the core temperature and increases the core density, it can have significant effects on the central structure of a star. For instance, ADM can cool the cores of MS stars slightly more massive than the Sun ($1.1 - 1.3\ \mathrm{M}_\odot$) such that they do not develop convective cores [41, 40, 36]. Such effects in the cores of stars can be observed via

asteroseismology.

Asteroseismology is the study of stars by observation of natural, resonant oscillations [44]. Oscillations can be either radial, resulting in pulsation of the star as a whole; or non-radial, resulting in deviations from spherical symmetry. Non-radial oscillations separate the stellar surface into expanding and receding, and heating or cooling regions [91]. The oscillations have their origin in two stypes of standing waves: acoustic modes, where pressure gradients act as the restoring force (p-modes), or internal gravity waves (g modes), where buoyancy is important [44]. Radial modes must be p-modes, as the graviational force increases during compression. Modes that are predominantly transverse are g-modes, as gravity restores the motion through buoyancy [91]. Modes of mixed character also exist [44]. Asteroseismology can reveal details about the structure of the stellar interior, because the frequency of the oscillations depends on the speed of sound of the material through which they propagate.

Finally, the effects of ADM on White Dwarfs (WD) have been considered. In Reference [125] it was found that a significant accumulation ($\sim 10^{-3}\,\mathrm{M}_\odot$ at $m_\chi = 10\,\mathrm{GeV}$) of ADM can alter the evolution of WDs making them more compact. Accumulation of this much ADM requires extremely large scattering cross-sections and/or Dark Matter densities [203].

In the present work, we follow up on the results of References [58, 112, 41, 40, 36, 125]. We focus on Spin-Independent (SI) cross-sections that are consistent with current constraints from direct-detection experiments and Spin-Dependent (SD) cross-sections that are consistent with indirect-detection experiments from neutrino telescopes. In either case, the energy transport is in the diffusive regime. Though no exact analytic solution exists, an approximate treatment of this energy transport was worked out in Reference [186]. In the present work, we implement this diffusive approximation in the publicly available stellar evolution code Modules for Experiments in Stellar Astrophysics (`MESA`) [151, 152, 153, 1]. Previously, in Reference [202] this code was used to study the effect of ADM on Brown Dwarfs (BD). It was found that WIMPs could cool the core sufficiently enough to stave off nuclear fusion at the canonical BD limit $0.08\,\mathrm{M}_\odot$, increasing the mass required for a MS star. In this work we update this ADM `MESA` module to be appropriate for Main Sequence (MS) and post-MS stars.

We confirm the findings of [112, 41, 40, 36], which used different stellar evolution and asteroseismology codes. We then study the effect of ADM on post-MS stars, which have yet to be considered. We find that ADM can have significant effects on Red Giant Branch (RGB) and Asymptotic Giant Branch (AGB) stars. During these phases thermal oscillations are induced in the core, which has a significant effect on asteroseismology, the thermal pulses of AGB stars, and their subsequenct cooling to WDs.

The remainder of this chapter is organized as follows: in §4.2 we outline our methodology. In §4.3 we demonstrate our results, while in §4.4 we discuss our conclusions.

4.2 METHODS

For $m_\chi \lesssim 15\,\mathrm{GeV}$ Dark Matter is captured by stars at the rate [202]

$$C_c \approx C_\odot \left(\frac{\rho_\chi}{0.4\,\mathrm{GeV/cm^3}}\right)\left(\frac{\sigma_{\chi p}}{10^{-43}\,\mathrm{cm^2}}\right)\left(\frac{v_{esc}}{618\,\mathrm{km/s}}\right) \times \left(\frac{270\,\mathrm{km/s}}{\bar{v}}\right)\left(\frac{M_*}{M_\odot}\right), \tag{4.1}$$

where $C_\odot \approx 7 \times 10^{22}\mathrm{s}^{-1}$ ($5 \times 10^{21}(\frac{5\,\mathrm{GeV}}{m_\chi})\mathrm{s}^{-1}$) is the SI (SD) capture rate for the Sun, ρ_χ is the Dark Matter density local to the star, $\sigma_{\chi p}$ is either the SI or SD cross-section, v_{esc} is the escape velocity, $\bar{v}$ is the velocity dispersion of the Dark Matter halo, and M_* is the mass of the star. While Equation (4.1) is useful in guiding the reader, we use the full formula from Reference [80] as described in Reference [201]. We do not quote the full relation here, because it is quite lengthy.

As the capture rate depends on the Dark Matter environment of the star, we define the boost factor

$$\Gamma_B = \left(\frac{\rho_\chi}{0.4\,\mathrm{GeV/cm^3}}\right)\left(\frac{270\,\mathrm{km/s}}{\bar{v}}\right), \tag{4.2}$$

which parametrizes the ratio of the capture rate to that in the Solar neighborhood. Environments with $\Gamma_B \gg 1$ are known to exist. As discussed in Reference [202] models of the MW with a co-rotating dark disk could provide a boost $\Gamma_B \sim 10$ [38, 165], while models of Dark Matter with self-interactions have enhanced capture rates equivalent to $\Gamma_B \sim 10^2$

[72, 201]. Other promising environments include Globular Clusters (GC) and the dwarf satellite galaxies of the Milky Way. Though limits on the Dark Matter content of GCs are of the order $M_{\rm DM}/M_*$, they're high stellar densities and comparatively low velocity dispersions mean that potentially $\Gamma_{\rm B} \gg 1$. The dwarf satellite galaxies on the other hand are known to be Dark Matter dominated objects. Segue I is the most Dark Matter dominated with Dark Matter density $10 - 10^2$ times the local value [184] and typical velocities $\sim 10^2$ times lower. Therefore, the dwarf satellites likely have $\Gamma_{\rm B} \sim 10^3 - 10^4$.

For our purposes, the Dark Matter need not be strictly asymmetric, we only require that the annihilation rate is sufficiently low such that the accumulation of WIMPs is not hindered. Dark Matter annihilations equilibrate with capture on a timescale $\tau_{\rm eq} = (C_{\rm c}C_{\rm a})^{-1/2}$ where $C_{\rm a}$ is twice the annihilation rate (because each annihilation removes 2 particles). We then require that $\tau_{\rm eq}$ be larger than the MS lifetime of the star. This is achieved for the Sun for $\langle \sigma_{\rm a} {\rm v} \rangle \lesssim 10^{-33}\,{\rm cm}^3/{\rm s}$ [189].

Dark Matter particles can also be lost to evaporation. This occurs when the typical thermal velocity $(T/m_\chi)^{1/2}$ is comparable to the escape speed. For the Sun this occurs when $m_\chi \lesssim 3.7\,{\rm GeV}$ [202].

As in Reference [186], we use the approximation that the Dark Matter has an effective temperature T_χ. Baryons at radius r are in local thermal equilibrium at some temperature $T(r)$. Scattering events between baryons and Dark Matter then try to bring the Dark Matter distribution function into a Maxwellian form $\propto e^{-E/kT_\chi}$. However, Dark Matter orbits between different radii between interactions, so scattering events try to bring the Dark Matter into equilibrium at different temperatures. Thus T_χ is not a precisely defined quantity. Thus there is no value of T_χ which yields an exact solution to the collisional Boltzmann equation. Our approach is then to assume an effective temperature, and to require that the distribution function satisfy the first moment of the Boltzmann equation. This is equivalent to the assumption that there is no net energy flow into the WIMP distribution, so that the WIMPs transport energy in a steady state [186].

For SD scattering off hydrogen, the energy per unit mass transmitted to the Dark Matter is [202]

$$\epsilon = 8\sqrt{\frac{2}{\pi}}\frac{n_\chi \sigma_{\chi {\rm p}} m_\chi}{(m_\chi + m_{\rm p})^2}\frac{f_{\rm H}}{m_{\rm p}}\left(\frac{m_{\rm p}T_\chi + m_\chi T}{m_\chi m_{\rm p}}\right)(T - T_\chi), \tag{4.3}$$

where n_χ is the local Dark Matter number density, m_p is the proton mass, f_H is the fraction of hydrogen, T is the temperature of the baryons and T_χ is fixed by requiring that there be no net energy transfer. For SI scattering, Equation (4.3) should be summed over all nuclear species. While Equation (4.3) is only an approximation, corrections are of order unity and there is no general treatment that can be feasibly incorporated into a stellar evolution code [81, 202]. In order to perform a self-consistent calculation we compute the capture rates as in Reference [80] and implement the Dark Matter energy transport of Equation (4.3) in the stellar evolution code `MESA star`. We base our stellar models off similar models in the `MESA` test suite and include Dark Matter energy transport *via* the `other_energy` module.

4.3 RESULTS

In this section we demonstrate the effects of ADM on Sunlike Main Sequence (MS) and post-MS stars, and stars slightly more massive than the Sun. In order to interpret our results, a basic discussion of stellar evolution without ADM is necessary (for more details see any undergraduate astronomy text). Stars begin their lives as giant clouds of collapsing gas. As the cloud collapses, gravitational energy is converted to thermal energy. This is known as the protostar phase of stellar evolution (this phase is not affected by ADM as there is insufficient time for Dark Matter accumulation). If the mass of the cloud is greater than $0.08\,\mathrm{M}_\odot$, then the core will eventually become hot and dense enough for nuclear fusion of hydrogen to begin. The star will then settle into hydrostatic equilibrium, becoming a MS star. The MS is where stars spend the majority of their lifetimes.

When core Hydrogen becomes significantly depleted, the star will begin to evolve off the MS on what is known as the SubGiant Branch (SGB). When core hydrogen is completely exhausted, the core of the star will begin to collapse. In a Sunlike star this collapse will be halted by electron degeneracy. Without radiative support from nuclear reactions in the core, layers just outside the core will also collapse. These layers are hydrogen rich, and they reach temperature sufficient to ignite fusion in a shell around the core. The pressure from the hydrogen burning shell causes the outer layers of the star to expand driving the star to

higher luminositiy and lower surface temperature. During this phase of evolution the star ascends the Red Giant Branch (RGB).

During the RGB, the core continues to heat up and eventually reaches a high enough temperature to ignite helium burning. In a Sunlike star this happens under degenerate conditions in a process known as the helium flash. Because the equation of state is decoupled from the temperature, the ignition of helium does not cause the core to expand until the degeneracy is lifted. The helium flash only lasts a few minutes but for a few seconds the energy generated rivals that of the entire Galaxy [59]. After the helium flash, the star continues burning helium in the core and moves on to the Horizontal Branch (HB). When helium is exhausted in the core, a helium burning shell develops around the core just as the hydrogen burning shell did. At this point the star ascends the Asymptotic Giant Branch (AGB). A star like the Sun will not become hot enough to burn carbon in its core. At the end of the AGB the star undergoes several thermal pulses and loses a significant fraction of its mass. The outer layers are lost exposing the core, which is supported by electron degeneracy. At this point the star is known as a White Dwarf (WD) and will spend the remainder of its lifetime simply cooling. The left panel of Figure 4.1 shows the color-magnitude diagram of the Glovular Cluster NGC 6397. Labelled are the MS, Giant Branches, and WDs. Color is a proxy for temperature, increasing from right-to-left and magnitude is a proxy for luminosity, increasing from bottom to top. Figure 4.1 shows the evolution of an individual Sunlike star from the onset of hydrogen burning through the giant branches and onto the WD cooling sequence. Triangles denote the passage of 1 Gyr.

4.3.1 Sunlike MS Stars

We first consider the effect of ADM on Sun-like ($M_* = 1\,\mathrm{M}_\odot, Z_* = 0.02$) MS stars and compare our results to those of Reference [112]. To facillitate the comparison we use the same Dark Matter parameters: SD scattering cross-section $\sigma_{\chi \mathrm{p}} = 10^{-37}\,\mathrm{cm}^2$ and mass $m_\chi = 10\,\mathrm{GeV}$. These parameters are consistent with current constraints, e.g. [6]. We evolved the stars from the Zero Age Main Sequence (ZAMS) until the core ^{1}H fraction reached 0.1. In Figure 4.2 we see that as the stars evolve, their paths towards the sub-giant branch are

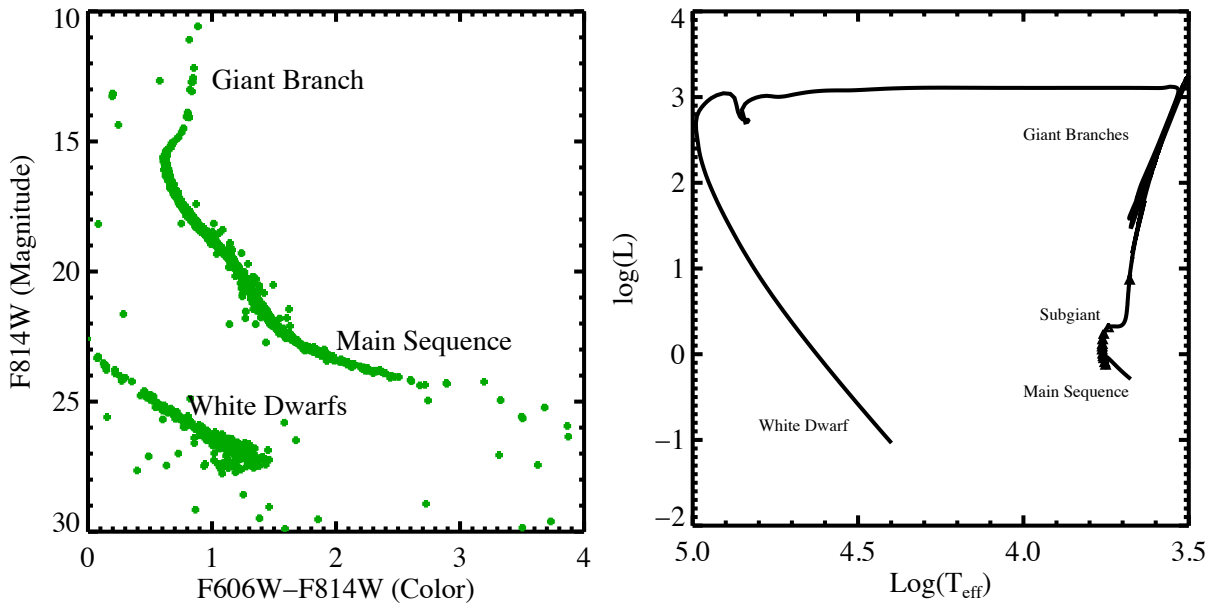

Figure 4.1: *(Left)* The color-magnitude diagram of NGC 6397. *(Right)* The evolution of a Sunlike star.

significantly affected, with the luminosity increased by as much as $\approx 30\%$ when $\Gamma_B = 10^4$. This behavior is in qualitative agreement with Reference [112] (see Figure 3 therein); however, those authors observed significant oscillations in the HR diagram, which they noted were possibly a numerical artifact of their stellar evolution code. Since `MESA` is a state of the art stellar evolution code capable of resolving such oscillations, our results indicate that this is indeed the case. As Γ_B increases, MS stars are pushed to higher surface temperatures and luminosities. As noted in §4.1 this is because ADM cools the central region of the core decreasing the efficiency of energy generation from nuclear reactions. In order to maintain hydrostatic equilibrium, the rate of nuclear reactions outside the inversion core must increase, which heats the outer layers of the star. This behavior can be seen in Figure 4.3, which shows the luminosity profile of the star as a function of radius. The time of the figure is the end of the MS. In the main panel we see that near the core the luminosity is decreased as Γ_B increases from $10^0 - 10^4$, and the luminosity of the outer regions is increased. The inset

shows the overall luminosity producing region.

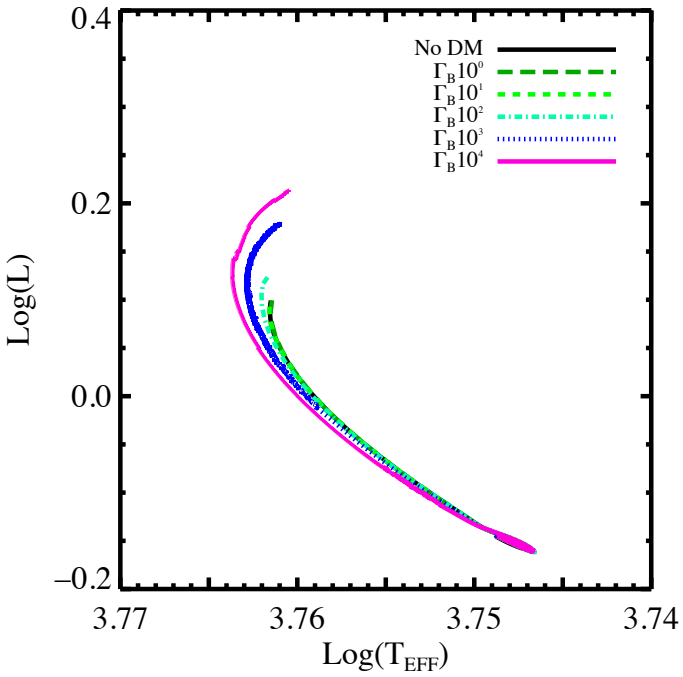

Figure 4.2: MS evolution of a Sun-like star for different values of Γ_B.

ADM also prolongs the MS lifetime of a Sun-like star. As the central temperature and nuclear reaction rate are lowered, it takes a greater amount of time to deplete the central ^{1}H. This behavior is observed in Figure 4.4, which is again in agreement with the results of Reference [112]. Figure 4.4 shows the central hydrogen fraction as a function of time. The diamonds denote the point at which the ^{1}H fraction is 10%, which we defined to be the end of the MS in Figure 4.2. For clarity we omitted the case of no ADM because the standard evolution lies on top of the curve for $\Gamma_B = 1$.

4.3.2 MS Stars More Massive Than The Sun

We next compare our results with those of References [41, 40, 36]. As discussed in §4.1 those authors noted that ADM increases the density of the stellar core and can therefore have significant effects on asteroseismology. Notably, for a wide range of acceptable WIMP parameters, stars in the mass range $1.1 - 1.3\,M_\odot$ do not develop convective cores. To check

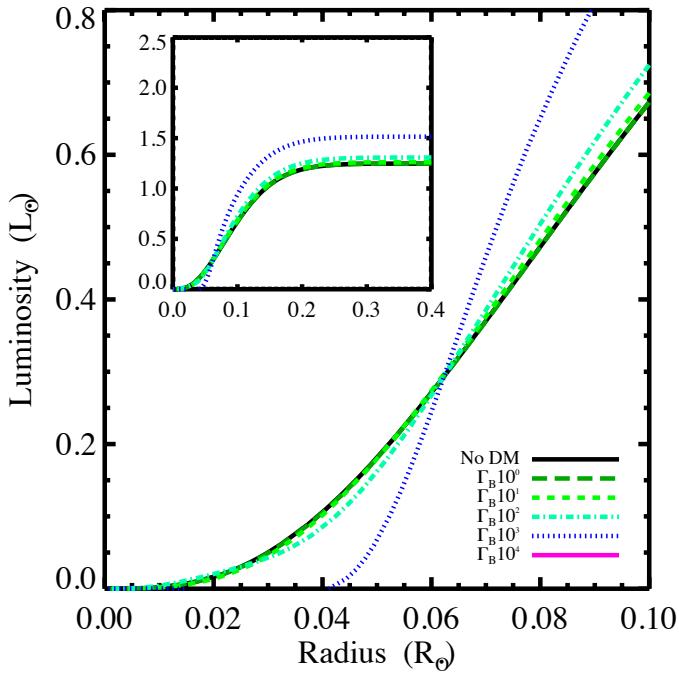

Figure 4.3: Luminosity of a Sunlike star at the end of the Main Sequence for varying values of $\Gamma_{\rm B}$.

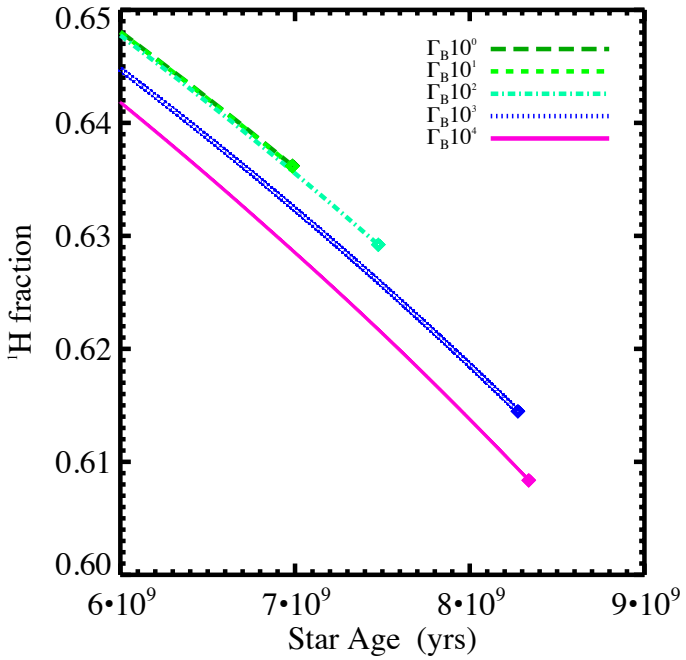

Figure 4.4: The timescale for depletion of the central hydrogen.

this behavior we evolved a series of stars with $1.2\,M_\odot$ in the presence of ADM with $m_\chi = 5\,\mathrm{GeV}$ and SI scattering cross-section $\sigma_{\chi p} = 10^{-40}\,\mathrm{cm}^2$ and varying values of Γ_B. Convection in stars occurs where the temperature gradient is *superadiabatic*. When the temperature gradient is adiabatic, gas which rises or falls will have the same temperature and pressure as its surroundings. When, the temperature gradient is steeper than the adiabatic temperature gradient, the gas is convectively unstable. When this is the case energy will be transported *via* convection. Figure 4.5 shows the convective velocity required to transport the core luminosity versus the stellar radius. For moderate values of Γ_B convection is modestly suppressed, whereas for $\Gamma_B \gtrsim 10^3$ convection is completely suppressed (this is not visible on the plot because the convective velocity is identically zero). This is because the temperature gradient is less steep than the adiabatic temperature gradient. The time of the Figure is the point at which the central ^{1}H fraction is 0.1, but convection is suppressed beginning at $\sim$ 1 Gyr after the star reaches the MS—some time is required for the accumulation of Dark

Matter.

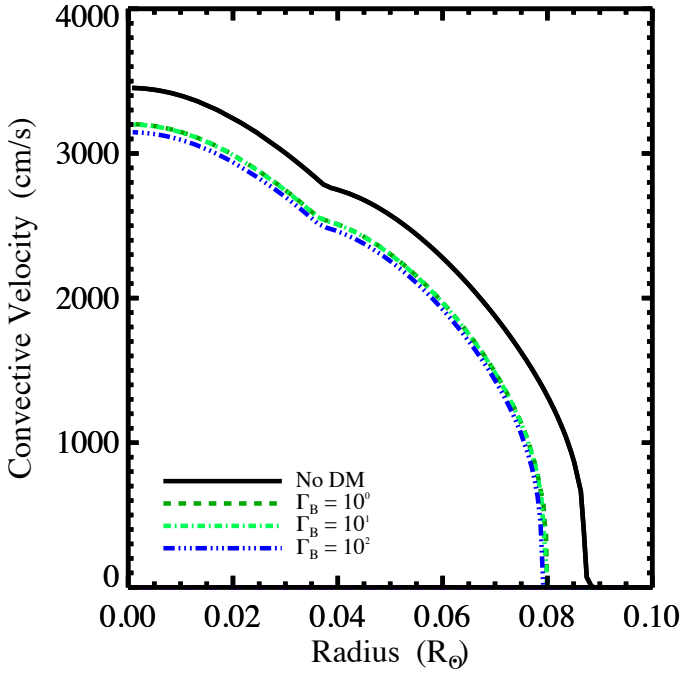

Figure 4.5: Effect of ADM on the convective velocity for different vaules of $\Gamma_{\rm B}$.

We parametrize the effect of ADM on asteroseismology by the large and small frequency separations $\Delta\nu$ and $\delta\nu_{ll+2}$. These are both commonly used parameters in asteroseismology. A given oscillation mode has radial order n and non-radial modes are spherical harmonics with order l, m. n, l with $m = 0$ quantify standing waves while $m \neq 0$ is associated with travelling waves. The large frequency separation is the separation in frequency of p-modes with the same l, $\Delta\nu_{nl} = \nu_{nl} - \nu_{n-1l} = \Delta\nu$, and is sensitive to the mean density of the star $\Delta\nu \propto <\ \rho\ >^{1/2}$ [41, 44]. The small frequency separation $\delta\nu_{ll+2} = \nu_{nl} - \nu_{n-1l+2}$ on the other hand, depends on the sound speed gradient in the central regions of the star [44]. In particular, the average value $<\ \delta_{02}\ >$ has been shown to be an effective diagnostic for the effects of ADM on the cores of stars [41, 40, 36]. Figure 4.6 shows the smoothed frequency-power spectrum of a G type MS star observed by the *Kepler* satellite. In the main plot peaks are labeled with the value of l. Several important frequency separations have been labelled, making their physical meaning clear. The top left inset is a wider range in frequency showing the Gaussian-like oscillation modulation of the powers of the modes. The top right inset is

a zoom in showing rotational frequency splitting of the non-radial $l = 1, n = 20$ mode. The raw spectrum is shown in light blue, and the smoothed spectrum in black [44]. For more information on asteroseismology see e.g. Reference [44].

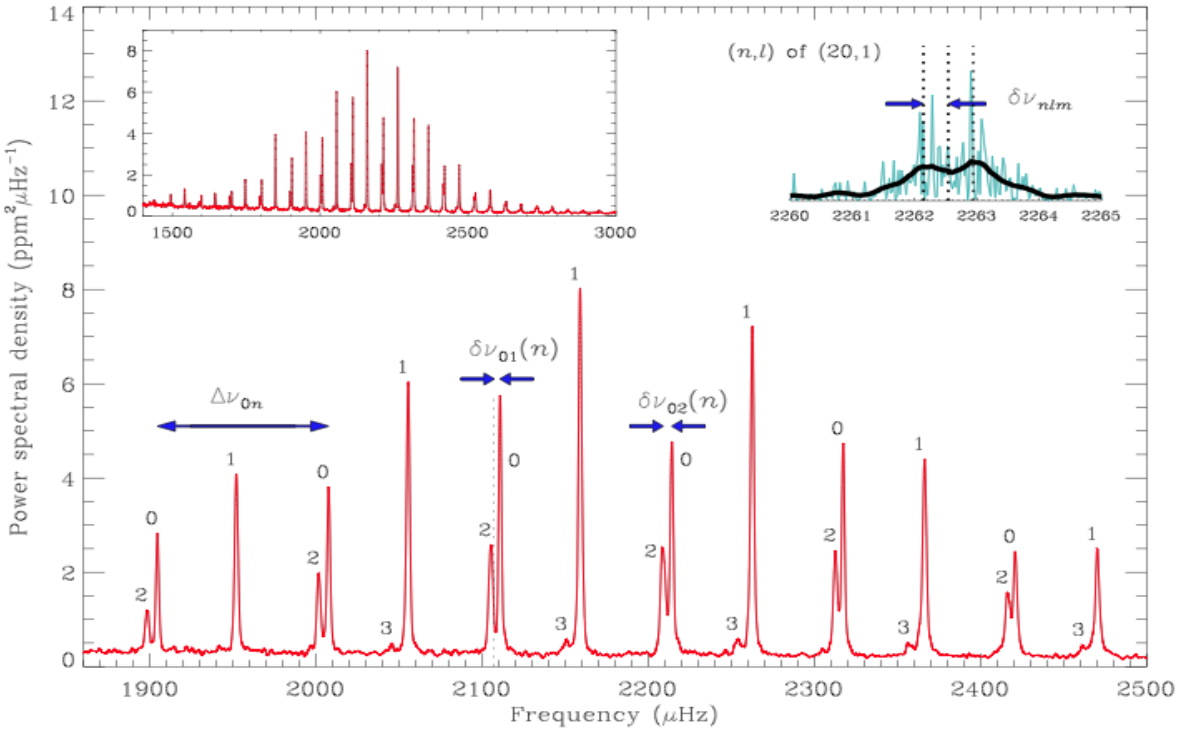

Figure 4.6: Oscillation spectrum of a G type MS star, as observed by *Kepler*. From Reference [44].

Figure 4.7 shows the large frequency separation as a function of time for the same models as in Figure 4.5 as well as $\Gamma_B = 10^3$. Unsurprisingly, $\Delta\nu$ is only mildly affected as ADM has only a small effect on the stellar radius ($\approx 15\%$ for $\Gamma_B = 10^4$). Note that the MS lifetime is shortened for $\Gamma_B \gtrsim 10^3$, whereas it was lengthened for Sunlike stars. This is because of the complete suppression of convection in the core. Without convective mixing it takes less time to deplete the central hydrogen.

Figure 4.8 shows the average value of $\delta\nu_{02}$ for the same models as in Figure 4.7. The time of the plot is when the core hydrogen fraction is 10%. Here we see that the small frequency separation is significantly affected, as expected, when $\Gamma_B = 10^3$ and convection is completely suppressed.

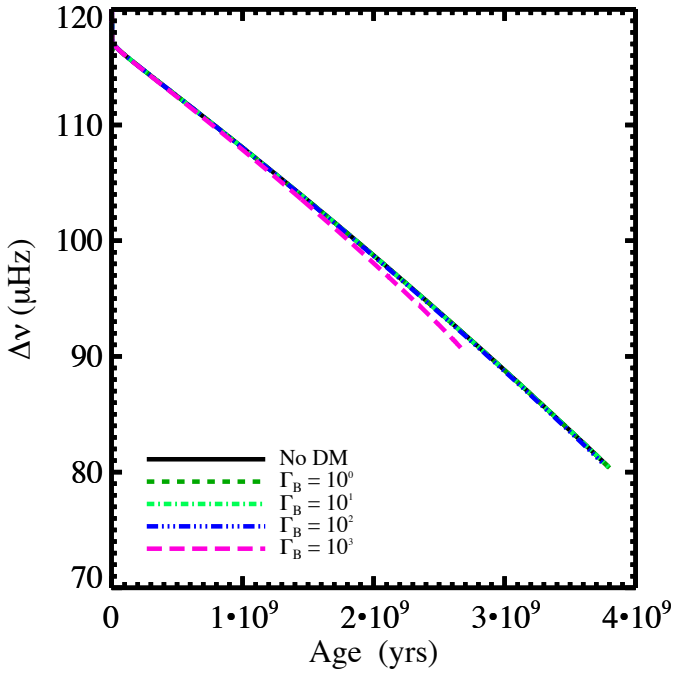

Figure 4.7: The effect of ADM on the large frequency separation.

4.3.3 Sunlike post-MS stars

Finally, we consider the effect of ADM on post-MS stars, which has yet to be considered in the literature. In the diffusive energy transport regime ADM can have effects on the Red Giant Branch (RGB) and Asymptotic Giant Branch (AGB) phases of stellar evolution. The morphology of the RGB and early-AGB is unaffected, but during these phases the core experiences thermal pulses associated with the development of a small convective core. During the RGB and AGB phases there is a temperature inversion such that the center of the star is not the hottest region. Hence, energy transport by ADM makes the temperature gradient steeper, rather than shallower as it does during the MS. This induces convection in a very small central region of the star.

Figure 4.9 shows the central temperature as a function of time for a model without Dark Matter and for a model with $\Gamma_{\rm B} = 1, m_\chi = 4\,{\rm GeV}$ and SI scattering cross-section $\sigma_{\chi{\rm p}} = 10^{-42}$. In addition to the oscillations it experiences, the core is slightly cooled. This

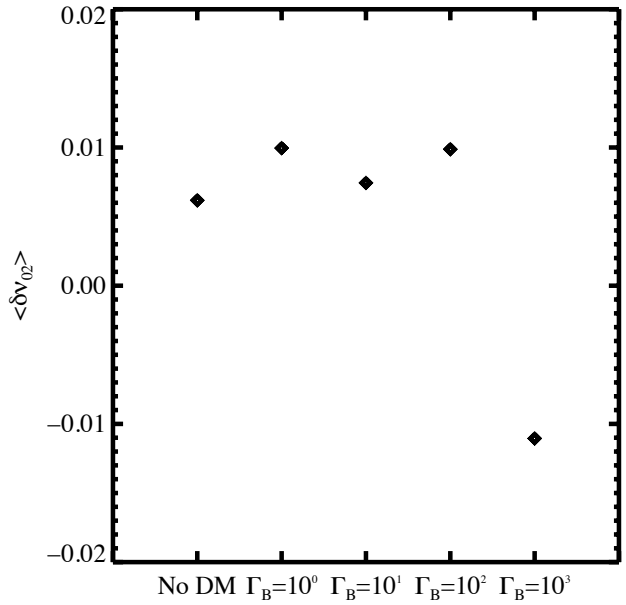

Figure 4.8: The effect of ADM on the small frequency separation.

can be seen in the inset, which shows that the envelope of the oscillations lies just below the standard model. When the central temperature is at its minimum, the convective core appears, and when the temperature is at maximum the convection is suppressed.

Figure 4.10 shows the effect of ADM with $m_\chi = 4\,\mathrm{GeV}$, SI cross-section $\sigma_{\chi\mathrm{p}} = 10^{-42}$, and $\Gamma_\mathrm{B} = 1$ on the AGB phase of a Sunlike star. The morphology of the AGB is unaffected until the end of the AGB phase, when Sun-like stars under go several thermal pulses. We find that ADM changes the effective temperature and luminosity of the star during the pulsations (see the inset). Moreover, the additional heat transferred from the core is able to trigger a *late thermal pulse*. In the standard case, just before the final cool down, the star nearly experiences a thermal pulse, which fizzles out. This is the cause of the feature at $\log(T_\mathrm{eff}) \approx 5.0$. With the additional energy transport from ADM, the star is able to undergo a full thermal pulse, seen as the large loop before the final cool down of the star. We find that after the late thermal pulse, the cooling track is not significantly affected by ADM.

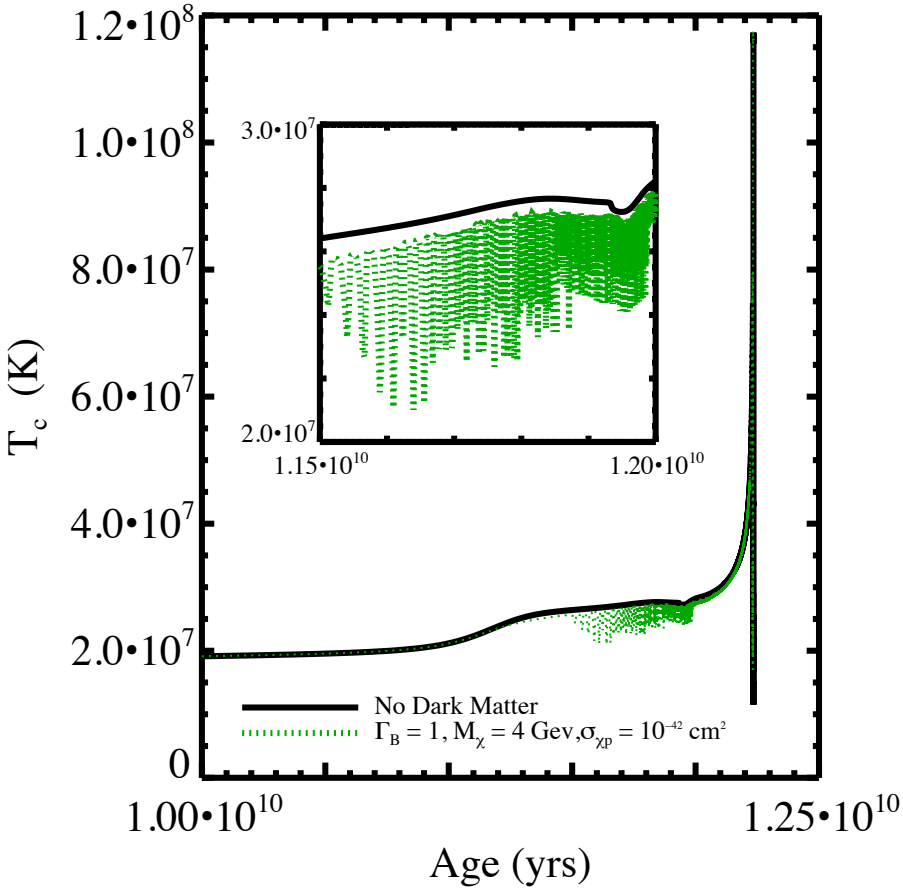

Figure 4.9: Thermal pulses on the RGB.

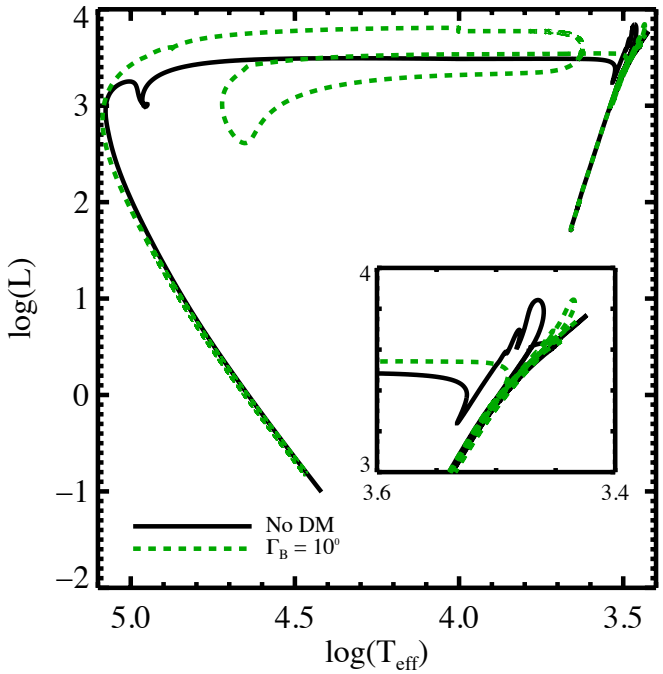

Figure 4.10: Thermal pulses on the AGB.

4.4 CONCLUSIONS

Energy transport by ADM can have significant effects on stellar evolution for a wide range of viable parameters. In regions where Dark Matter capture is significantly enhanced compared to the solar neighborhood (high Dark Matter density, low velocity dispersion), ADM could significantly affect e.g. the morphology of the SubGiant Branch. This could be potentially observable in the HR diagrams of star clusters. ADM can also have observable effects on asteroseismology. We have confirmed the work of previous authors on the MS evolution of Sun-like and slightly more massive stars. This confirmation is relevant as we used different stellar evolution and asteroseismology codes from previous work.

We have also shown that post-MS stars are affected by ADM. RGB and AGB stars undergo thermal pulses in the center of the star which can induce a small convective region. Though the morphology of the RGB and early-AGB are unchanged, this effect could poten-

tially be observed *via* asteroseismology. We find that the morphology of the late-AGB when Sun-like stars undergo thermal pulsation and mass loss before cooling to become WDs is significantly affected by ADM.

5.0 CONCLUSIONS

Approximately 26% of the matter-energy content of the Universe is in the form of a hitherto unidentified Dark Matter. Identifying the nature of this Dark Matter is one of the most pressing problems in cosmology and astrophysics. Observations indicate that the Dark Matter is a new exotic particle representing physics beyond the Standard Model. As such, Dark Matter is also one of the most important problems in particle physics. The most popular particle candidates are Weakly Interacting Massive Particles (WIMPs). Should the Dark Matter be identified as a WIMP and its properties (mass, scattering cross-section, and annihilation rate) become known, then WIMP astronomy will become possible. As Dark Matter can have observable effects on astrophysical systems, Dark Matter must be accounted for when evaluating observations. In this thesis we have explored 3 different astrophysical effects of Dark Matter.

We have shown that the annihilation of Dark Matter particles could provide an important energy source in White Dwarfs (WD) (§2.2.2). If Dark Matter annihilations provide a significant source of luminosity, then the cooling of WDs will be halted at some finite temperature (§2.2.3 and Figure 2.1). Observations of cool WDs then have the potential to constrain the density of their Dark Matter environments. This effect could be particularly interesting in the case of Globular Clusters (GC). GCs are thought not to possess significant Dark Matter halos. However, given the extraordinarily high stellar density of GCs, even a sub-dominant Dark Matter halo could be far denser than the Solar neighborhood and other Dark Matter environments. We have shown that observations of the coolest WDs in GCs constrain the 3 parameter family of Dark Matter particle mass m_χ, scattering cross-section $\sigma_{\chi \mathrm{p}}$, and the fraction of Dark Matter in the cluster f_{DM} (Figures 2.3-2.6). We find that WIMP astronomy has the potential to improve the bounds on f_{DM} by up to 3 orders of magnitude. Another

interesting enviornment for WIMP astronomy are the dwarf satellite galaxies of the Milky Way, which are known to be Dark Matter dominated. We considered them only briefly for the case of Segue I, because at those distances WDs are difficult to observe. However, with the next generation of space and ground based telescopes it may be possible to observe the WD cooling sequences of the dwarf satellites in the near future.

We next investigated the possibility of a GC ejecting its Dark Matter halo through multi-body gravitational interactions(§3). Though they are thought not to possess Dark Matter halos today, GCs could have possessed halos in the past and subsequently lost them. One mechanism invoked for the removal of the halo is tidal stripping by the Galaxy. Most of the Galactic GCs orbit in strong tidal fields and could have lost their halos due to tidal forces. However, there exists a population of very isolated Galactic GCs which could not have lost their halos this way (Table 3.1). Scattering events between stars and Dark Matter particles can potentially eject Dark Matter particles from the halo. We found that the ejection rate is too low for the halo to be lost within a Hubble time (Figures 3.4-3.6). We therefore conclude that GCs likely never possessed extended, massive Dark Matter halos; however, this does not necessarily mean that GCs are unintereresting environments for WIMP astronomy and/or indirect detection experiments. The stellar density of GCs is several orders of magnitude greater than that of the Solar neighborhood. Therefore, the density of even a subdominant Dark Matter halo could be orders of magnitude greater than that of the Solar neighborhood. Our results indicate that a hypothetical subdominant halo should have survived to the present day in the case of the isolated GCs.

Finally, we investigated the effect of Asymmetric Dark Matter (ADM) particles on Sun-like and slightly more massive stars (§4). Energy transport by ADM can have significant effects on stellar evolution. We found that the Main Sequence lifetimes of Sun-like stars are extended (Figure 4.4), and that as they evolve such stars are forced to higher effective temperatures and luminosities in the presence of ADM (Figure 4.2). We also found that stars slightly more massive than the Sun do not form convective cores in the presence of ADM (Figure 4.5). This can have observable effects on asteroseismology Figures 4.7 & 4.8. Finally we showed that Red Giant Branch (RGB) (Figure 4.9) and Asymptotic Giant Branch (AGB) (Figure 4.10) stars experience thermal oscillations associated with the development of small

convective cores and that the thermal pulses at the end of the AGB, and the subsequent cooling to WDs are significantly affected by ADM.

Our results show that if the Dark Matter particle is identified, that this will not be the end of the story, but rather only the beginning of a new era of WIMP astronomy. With the properties of the Dark Matter particle known (mass, scattering cross-section, annihilation rate), astrophysical observations can place limits on specific Dark Matter environments such, as the center of the galaxy, the dwarf satellites, and GCs (§2). Improved knowledge of the structure and substructure of the Galactic halo can potentially improve constraints on the processes that lead to the formation of the Milky Way and similar systems and subsystems.

BIBLIOGRAPHY

[1] Mesa: Modules for experiments in stellar astrophysics http://mesa.sourceforge.net/index.html.

[2] Millennium simulation project http://wwwmpa.mpa-garching.mpg.de/galform/virgo/millennium/.

[3] C. E. Aalseth, P. S. Barbeau, J. Colaresi, J. I. Collar, J. Diaz Leon, J. E. Fast, N. E. Fields, and *et al.* *Phys Rev D*, 88(1):012002, July 2013.

[4] S. J. Aarseth. Dynamical evolution of clusters of galaxies, II. *MNRAS*, 132:35, 1966.

[5] M. G. Aartsen, R. Abbasi, Y. Abdou, M. Ackermann, J. Adams, J. A. Aguilar, M. Ahlers, D. Altmann, J. Auffenberg, X. Bai, and et al. *Phys Rev D*, 88(12):122001, December 2013.

[6] M. G. Aartsen, K. Abraham, M. Ackermann, J. Adams, J. A. Aguilar, M. Ahlers, M. Ahrens, D. Altmann, T. Anderson, I. Ansseau, and et al. Improved limits on dark matter annihilation in the Sun with the 79-string IceCube detector and implications for supersymmetry. *JCAP*, 4:022, April 2016.

[7] K. N. Abazajian, N. Canac, S. Horiuchi, and M. Kaplinghat. Astrophysical and dark matter interpretations of extended gamma-ray emission from the Galactic Center. *Phys Rev D*, 90(2):023526, July 2014.

[8] K. N. Abazajian and M. Kaplinghat. *Phys Rev D*, 86(8):083511, October 2012.

[9] M. Ackermann, M. Ajello, W. B. Atwood, L. Baldini, and *et al.* *ApJ*, 761:91, December 2012.

[10] M. Ackermann, A. Albert, B. Anderson, W. B. Atwood, L. Baldini, G. Barbiellini, D. Bastieri, K. Bechtol, Fermi-LAT Collaboration, and *et al.* Searching for Dark Matter Annihilation from Milky Way Dwarf Spheroidal Galaxies with Six Years of Fermi Large Area Telescope Data. *Physical Review Letters*, 115(23):231301, December 2015.

[11] M. Ackermann, A. Albert, B. Anderson, L. Baldini, J. Ballet, G. Barbiellini, D. Bastieri, K. Bechtol, Fermi-LAT Collaboration, and *et al.* Dark matter constraints

from observations of 25 MilkyÂ Way satellite galaxies with the Fermi Large Area Telescope. *Phys Rev D*, 89(4):042001, February 2014.

[12] R. Adhikari, M. Agostini, N. A. Ky, T. Araki, M. Archidiacono, M. Bahr, J. Behrens, F. Bezrukov, and *et al.* A White Paper on keV Sterile Neutrino Dark Matter. *ArXiv e-prints*, February 2016.

[13] R. Agnese, A. J. Anderson, M. Asai, D. Balakishiyeva, R. Basu Thakur, D. A. Bauer, J. Beaty, J. Billard, SuperCDMS Collaboration, and *et al.* Search for Low-Mass Weakly Interacting Massive Particles with SuperCDMS. *Physical Review Letters*, 112(24):241302, June 2014.

[14] A. A. Aguilar-Arevalo, B. Batell, R. Cooper, P. deNiverville, R. Dharmapalan, Z. Djurcic, R. Ford, F. G. Garcia, and *et al.* Low Mass WIMP Searches with a Neutrino Experiment: A Proposal for Further MiniBooNE Running. *ArXiv e-prints:1211.2258*, November 2012.

[15] Q. R. Ahmad, R. C. Allen, T. C. Andersen, J. D. Anglin, G. Bühler, J. C. Barton, E. W. Beier, M. Bercovitch, and *et al. Physical Review Letters*, 87(7):071301, August 2001.

[16] C. Alcock, R. A. Allsman, D. R. Alves, T. S. Axelrod, A. C. Becker, D. P. Bennett, K. H. Cook, N. Dalal, and *et al.* The MACHO Project: Microlensing Results from 5.7 Years of Large Magellanic Cloud Observations. *ApJ*, 542:281–307, October 2000.

[17] C. Alcock, R. A. Allsman, T. S. Axelrod, D. P. Bennett, K. H. Cook, H. S. Park, S. L. Marshall, C. W. Stubbs, and *et al.* The MACHO Project - a Search for the Dark Matter in the Milky-Way. In B. T. Soifer, editor, *Sky Surveys. Protostars to Protogalaxies*, volume 43 of *Astronomical Society of the Pacific Conference Series*, page 291, January 1993.

[18] R. A. Alpher and R. C. Herman. On the Relative Abundance of the Elements. *Physical Review*, 74:1737–1742, December 1948.

[19] AMS Collaboration, M. Aguilar, J. Alcaraz, J. Allaby, B. Alpat, G. Ambrosi, H. Anderhub, L. Ao, A. Arefiev, P. Azzarello, and et al. The Alpha Magnetic Spectrometer (AMS) on the International Space Station: Part I - results from the test flight on the space shuttle. *Physics Reports*, 366:331–405, August 2002.

[20] G. Angloher, M. Bauer, I. Bavykina, and *et al. European Physical Journal C*, 72:1971, April 2012.

[21] E. Aprile and XENON1T collaboration. The XENON1T Dark Matter Search Experiment. *ArXiv e-prints:1206.6288*, June 2012.

[22] C. Arina, E. Del Nobile, and P. Panci. Dark Matter with Pseudoscalar-Mediated Interactions Explains the DAMA Signal and the Galactic Center Excess. *Physical Review Letters*, 114(1):011301, January 2015.

[23] K. G. Arun and A. Pai. Tests of General Relativity and Alternative Theories of Gravity Using Gravitational Wave Observations. *International Journal of Modern Physics D*, 22:1341012, January 2013.

[24] A. Askew, S. Chauhan, B. Penning, W. Shepherd, and M. Tripathi. *International Journal of Modern Physics A*, 29:30041, September 2014.

[25] ATLAS Collaboration, G. Aad, E. Abat, J. Abdallah, A. A. Abdelalim, A. Abdesselam, O. Abdinov, B. A. Abi, M. Abolins, H. Abramowicz, and *et al.* The ATLAS Experiment at the CERN Large Hadron Collider. *Journal of Instrumentation*, 3:S08003, August 2008.

[26] J. N. Bahcall, C. Flynn, A. Gould, and S. Kirhakos. M dwarfs, microlensing, and the mass budget of the Galaxy. *ApJL*, 435:L51–L54, November 1994.

[27] J. D. Bekenstein. Relativistic gravitation theory for the modified Newtonian dynamics paradigm. *Phys Rev D*, 70(8):083509, October 2004.

[28] P. Bergeron, G. Fontaine, P. E. Tremblay, and P. M. Kowalski. Synthetic colors and evolutionary sequences of hydrogen- and helium-atmosphere white dwarfs http://www.astro.umontreal.ca/ bergeron/coolingmodels.

[29] P. Bergeron, F. Wesemael, P. Dufour, and *et al. ApJ*, 737:28, August 2011.

[30] R. Bernabei, P. Belli, F. Cappella, and *et al. European Physical Journal C*, 56:333, August 2008.

[31] G. Bertone and M. Fairbairn. *Phys Rev D*, 77(4):043515, February 2008.

[32] T. Böker, M. Sarzi, D. E. McLaughlin, R. P. van der Marel, H.-W. Rix, L. C. Ho, and J. C. Shields. A Hubble Space Telescope Census of Nuclear Star Clusters in Late-Type Spiral Galaxies. II. Cluster Sizes and Structural Parameter Correlations. *AJ*, 127:105–118, January 2004.

[33] A. Boyarsky, D. Malyshev, and O. Ruchayskiy. *Physics Letters B*, 705:165–169, November 2011.

[34] M. Boylan-Kolchin, J. S. Bullock, and M. Kaplinghat. Too big to fail? The puzzling darkness of massive Milky Way subhaloes. *MNRAS*, 415:L40–L44, July 2011.

[35] M. Boylan-Kolchin, V. Springel, S. D. M. White, A. Jenkins, and G. Lemson. Resolving cosmic structure formation with the Millennium-II Simulation. *MNRAS*, 398:1150–1164, September 2009.

[36] I. M. Brandão and J. Casanellas. Constraints to dark-matter properties from asteroseismic analysis of KIC 2009504. *ArXiv e-prints*, May 2015.

[37] V. Bromm and C. J. Clarke. The Formation of the First Globular Clusters in Dwarf Galaxies before the Epoch of Reionization. *ApJL*, 566:L1–L4, February 2002.

[38] T. Bruch, J. Read, L. Baudis, and G. Lake. Detecting the Milky Way's Dark Disk. *Ap J*, 696:920–923, May 2009.

[39] H. A. Buchdahl. Non-linear Lagrangians and cosmological theory. *MNRAS*, 150:1, 1970.

[40] J. Casanellas and I. Lopes. Constraints on asymmetric dark matter from asteroseismology. *ArXiv e-prints*, July 2013.

[41] J. Casanellas and I. Lopes. First Asteroseismic Limits on the Nature of Dark Matter. *ApJL*, 765:L21, March 2013.

[42] CDMS Collaboration, R. Agnese, Z. Ahmed, A. J. Anderson, S. Arrenberg, D. Balakishiyeva, R. Basu Thakur, D. A. Bauer, J. Billard, and *et al.* Silicon Detector Dark Matter Results from the Final Exposure of CDMS II. *ArXiv e-prints:1304.4279*, April 2013.

[43] S. Chandrasekhar. The highly collapsed configurations of a stellar mass. *MNRAS*, 91:456–466, March 1931.

[44] W. J. Chaplin and A. Miglio. Asteroseismology of Solar-Type and Red-Giant Stars. *ARAA*, 51:353–392, August 2013.

[45] I. Cholis and P. Salucci. *Phys Rev D*, 86(2):023528, July 2012.

[46] S. Clesse and J. García-Bellido. Massive primordial black holes from hybrid inflation as dark matter and the seeds of galaxies. *Phys Rev D*, 92(2):023524, July 2015.

[47] S. Clesse and J. García-Bellido. The clustering of massive Primordial Black Holes as Dark Matter: measuring their mass distribution with Advanced LIGO. *ArXiv e-prints:1603.05234*, March 2016.

[48] D. Clowe, M. Bradač, A. H. Gonzalez, M. Markevitch, S. W. Randall, C. Jones, and D. Zaritsky. *ApJ Letters*, 648:L109–L113, September 2006.

[49] C. Conroy, A. Loeb, and D. N. Spergel. *ApJ*, 741:72, November 2011.

[50] C. Conroy and D. N. Spergel. *ApJ*, 726:36, January 2011.

[51] G. Cupani, M. Mezzetti, and F. Mardirossian. Cluster mass estimation through fair galaxies. *MNRAS*, 403:838–847, April 2010.

[52] S. Das, T. Louis, M. R. Nolta, G. E. Addison, E. S. Battistelli, J. R. Bond, E. Calabrese, D. Crichton, and *et al.* The Atacama Cosmology Telescope: temperature and gravitational lensing power spectrum measurements from three seasons of data. *JCAP*, 4:014, April 2014.

[53] J. H. Davis. The past and future of light dark matter direct detection. *International Journal of Modern Physics A*, 30:1530038, May 2015.

[54] W. J. G. de Blok. The Core-Cusp Problem. *Advances in Astronomy*, 2010:789293, 2010.

[55] C. De Boni and G. Bertin. The relative concentration of visible and dark matter in clusters of galaxies. *Nuovo Cimento B Serie*, 123:31–41, 2008.

[56] G. De Marchi, F. Paresce, and L. Pulone. *ApJ*, 530:342–351, February 2000.

[57] C. de Rham, G. Gabadadze, and A. J. Tolley. Resummation of Massive Gravity. *Physical Review Letters*, 106(23):231101, June 2011.

[58] D. Dearborn, G. Raffelt, P. Salati, J. Silk, and A. Bouquet. Dark matter and thermal pulses in horizontal-branch stars. *ApJ*, 354:568–582, May 1990.

[59] R. G. Deupree and R. K. Wallace. The core helium flash and surface abundance anomalies. *ApJ*, 317:724–732, June 1987.

[60] R. Diamanti, L. Lopez-Honorez, O. Mena, and *et al.* *JCAP*, 2:17, February 2014.

[61] R. H. Dicke, P. J. E. Peebles, P. G. Roll, and D. T. Wilkinson. *ApJ*, 142:414–419, July 1965.

[62] M. Drees and G. Gerbier. Mini–Review of Dark Matter: 2012. *ArXiv e-prints:1204.2373*, April 2012.

[63] C. Faham and for the LUX Collaboration. First Dark Matter Search Results from the Large Underground Xenon (LUX) Experiment. *ArXiv e-prints:1405.5906*, May 2014.

[64] M. Fairbairn, P. Scott, and J. Edsjö. *Phys Rev D*, 77(4):047301, February 2008.

[65] J. Faulkner and R. L. Gilliland. *ApJ*, 299:994–1000, December 1985.

[66] G. Fontaine, P. Brassard, and P. Bergeron. *PASP*, 113:409–435, April 2001.

[67] R. Foot. *Phys Rev D*, 88(2):025032, July 2013.

[68] R. Foot and S. Vagnozzi. Solving the small-scale structure puzzles with dissipative dark matter. *ArXiv e-prints:1602.02467*, February 2016.

[69] J. A. Formaggio and G. P. Zeller. *Reviews of Modern Physics*, 84:1307–1341, July 2012.

[70] N. Fornengo, P. Panci, and M. Regis. *Phys Rev D*, 84(11):115002, December 2011.

[71] P. J. Fox, R. Harnik, J. Kopp, and Y. Tsai. *Phys Rev D*, 84(1):014028, July 2011.

[72] M. T. Frandsen and S. Sarkar. Asymmetric Dark Matter and the Sun. *Physical Review Letters*, 105(1):011301, July 2010.

[73] J. A. Frieman, M. S. Turner, and D. Huterer. Dark Energy and the Accelerating Universe. *ARAA*, 46:385–432, September 2008.

[74] L. Fu, M. Kilbinger, T. Erben, C. Heymans, H. Hildebrandt, H. Hoekstra, T. D. Kitching, Y. Mellier, and *et al.* CFHTLenS: cosmological constraints from a combination of cosmic shear two-point and three-point correlations. *MNRAS*, 441:2725–2743, July 2014.

[75] A. Geringer-Sameth and S. M. Koushiappas. *Physical Review Letters*, 107(24):241303, December 2011.

[76] A. Geringer-Sameth, S. M. Koushiappas, and M. G. Walker. Comprehensive search for dark matter annihilation in dwarf galaxies. *Phys Rev D*, 91(8):083535, April 2015.

[77] L. Goodenough and D. Hooper. Possible Evidence For Dark Matter Annihilation In The Inner Milky Way From The Fermi Gamma Ray Space Telescope. *ArXiv e-prints:0910.2998*, October 2009.

[78] C. Gordon and O. Macías. *Phys Rev D*, 88(8):083521, October 2013.

[79] A. Gould. *ApJ*, 321:571–585, October 1987.

[80] A. Gould. *ApJ*, 388:338–344, April 1992.

[81] A. Gould and G. Raffelt. Cosmion energy transfer in stars - The Knudsen limit. *Ap J*, 352:669–680, April 1990.

[82] R. Gratton, C. Sneden, and E. Carretta. *ARAA*, 42:385–440, September 2004.

[83] R. G. Gratton, E. Carretta, and A. Bragaglia. *AAPR*, 20:50, February 2012.

[84] M. I. Gresham and K. M. Zurek. Light dark matter anomalies after LUX. *Phys Rev D*, 89(1):016017, January 2014.

[85] K. Griest, A. M. Cieplak, and M. J. Lehner. New Limits on Primordial Black Hole Dark Matter from an Analysis of Kepler Source Microlensing Data. *Physical Review Letters*, 111(18):181302, November 2013.

[86] K. Griest and M. Kamionkowski. *Physical Review Letters*, 64:615–618, February 1990.

[87] K. Griest and D. Seckel. *Nuclear Physics B*, 283:681–705, 1987.

[88] C. J. Grillmair, K. C. Freeman, M. Irwin, and P. J. Quinn. Globular Clusters with Tidal Tails: Deep Two-Color Star Counts. *AJ*, 109:2553, June 1995.

[89] Brown University Particle Physics Group. Dmtools: Dark matter limit plot generator http://dmtools.brown.edu:8080/plots, 2014.

[90] J. E. Gunn. Some thoughts concerning the origin of globular clusters. In D. Hanes and B. Madore, editors, *Globular Clusters*, page 301, 1980.

[91] G. Handler. *Asteroseismology*, page 207. 2013.

[92] B. M. S. Hansen, J. Anderson, J. Brewer, and *et al. ApJ*, 671:380–401, December 2007.

[93] B. M. S. Hansen and J. Liebert. *ARAA*, 41:465–515, 2003.

[94] E. Hardy, R. Lasenby, and J. Unwin. Annihilation signals from asymmetric dark matter. *Journal of High Energy Physics*, 7:49, July 2014.

[95] W. E. Harris. *The Astronomical Journal*, 112:1487, October 1996.

[96] W. E. Harris and R. E. Pudritz. Supergiant molecular clouds and the formation of globular cluster systems. *ApJ*, 429:177–191, July 1994.

[97] D. Harvey, R. Massey, T. Kitching, A. Taylor, and E. Tittley. The nongravitational interactions of dark matter in colliding galaxy clusters. *Science*, 347:1462–1465, March 2015.

[98] M. Hénon. *Annales d'Astrophysique*, 23:467, February 1960.

[99] M. Henon. *Astronomy and Astrophysics*, 2:151, June 1969.

[100] J. S. Heyl, H. Richer, J. Anderson, and *et al. ApJ*, 761:51, December 2012.

[101] G. Hinshaw, D. Larson, E. Komatsu, and *et al. APJS*, 208:19, October 2013.

[102] J. B. Holberg and P. Bergeron. *The Astronomical Journal*, 132:1221–1233, September 2006.

[103] D. Hooper and L. Goodenough. *Physics Letters B*, 697:412–428, March 2011.

[104] D. Hooper and T. Linden. *Phys Rev D*, 84(12):123005, December 2011.

[105] D. Hooper, D. Spolyar, A. Vallinotto, and N. Y. Gnedin. *Phys Rev D*, 81(10):103531, May 2010.

[106] W. Hu. Lecture Notes on CMB Theory: From Nucleosynthesis to Recombination. *ArXiv e-prints*, February 2008.

[107] W. Hu, R. Barkana, and A. Gruzinov. Fuzzy Cold Dark Matter: The Wave Properties of Ultralight Particles. *Physical Review Letters*, 85:1158–1161, August 2000.

[108] R. H. H. Huang, W. Becker, P. D. Edmonds, R. F. Elsner, and *et al. Astronomy and Astrophysics*, 513:A16, April 2010.

[109] T. J. Hurst, A. R. Zentner, A. Natarajan, and C. Badenes. *Phys Rev D*, 91(10):103514, May 2015.

[110] R. Ibata, C. Nipoti, A. Sollima, M. Bellazzini, S. C. Chapman, and E. Dalessandro. Do globular clusters possess dark matter haloes? A case study in NGC 2419. *MNRAS*, 428:3648–3659, February 2013.

[111] F. Iocco, A. Bressan, E. Ripamonti, R. Schneider, A. Ferrara, and P. Marigo. *MNRAS*, 390:1655–1669, November 2008.

[112] F. Iocco, M. Taoso, F. Leclercq, and G. Meynet. Main Sequence Stars with Asymmetric Dark Matter. *Physical Review Letters*, 108(6):061301, February 2012.

[113] J. Isern, E. García-Berro, S. Torres, and S. Catalán. *Ap. J. Letters*, 682:L109–L112, August 2008.

[114] G. Jungman, M. Kamionkowski, and K. Griest. *Physics Reports*, 267:195–373, March 1996.

[115] V. Kalinova and G. Gyulchev. In I. Zhelyazkov and T. Mishonov, editors, *American Institute of Physics Conference Series*, volume 1356 of *American Institute of Physics Conference Series*, pages 60–66, July 2011.

[116] C. Kelso, D. Hooper, and M. R. Buckley. *Phys Rev D*, 85(4):043515, February 2012.

[117] I. King. *The Astronomical Journal*, 67:471, October 1962.

[118] I. R. King. *The Astronomical Journal*, 71:64, February 1966.

[119] A. Klypin, A. V. Kravtsov, O. Valenzuela, and F. Prada. Where Are the Missing Galactic Satellites? *ApJ*, 522:82–92, September 1999.

[120] M. Kowalski, D. Rubin, G. Aldering, R. J. Agostinho, A. Amadon, R. Amanullah, C. Balland, K. Barbary, and *et al.* Improved Cosmological Constraints from New, Old, and Combined Supernova Data Sets. *ApJ*, 686:749–778, October 2008.

[121] P. M. Kowalski and D. Saumon. *APJ Letters*, 651:L137–L140, November 2006.

[122] L. M. Krauss, K. Freese, D. N. Spergel, and W. H. Press. *ApJ*, 299:1001–1006, December 1985.

[123] P. Kroupa. *MNRAS*, 322:231–246, April 2001.

[124] B. Kyae and J.-C. Park. Light dark matter for Fermi-LAT and CDMS observations. *Physics Letters B*, 732:373–379, May 2014.

[125] S.-C. Leung, M.-C. Chu, L.-M. Lin, and K.-W. Wong. Dark-matter admixed white dwarfs. *Phys Rev D*, 87(12):123506, June 2013.

[126] E. L. Łokas and G. A. Mamon. Dark matter distribution in the Coma cluster from galaxy kinematics: breaking the mass-anisotropy degeneracy. *MNRAS*, 343:401–412, August 2003.

[127] LUX Collaboration, D. S. Akerib, H. M. Araujo, X. Bai, A. J. Bailey, J. Balajthy, S. Bedikian, E. Bernard, A. Bernstein, and *et al.* First results from the LUX dark matter experiment at the Sanford Underground Research Facility. *ArXiv e-prints:1310.8214*, October 2013.

[128] O. Macias and C. Gordon. Contribution of cosmic rays interacting with molecular clouds to the Galactic Center gamma-ray excess. *Phys Rev D*, 89(6):063515, March 2014.

[129] A. D. Mackey, A. M. N. Ferguson, M. J. Irwin, N. F. Martin, A. P. Huxor, N. R. Tanvir, S. C. Chapman, R. A. Ibata, G. F. Lewis, and A. W. McConnachie. Deep Gemini/GMOS imaging of an extremely isolated globular cluster in the Local Group. *MNRAS*, 401:533–546, January 2010.

[130] M. S. Madhavacheril, N. Sehgal, and T. R. Slatyer. *Phys Rev D*, 89(10):103508, May 2014.

[131] M. Markevitch, A. Vikhlinin, W. R. Forman, and C. L. Sarazin. Mass Profiles of the Typical Relaxed Galaxy Clusters A2199 and A496. *ApJ*, 527:545–553, December 1999.

[132] T. Marrodán Undagoitia and L. Rauch. Dark matter direct-detection experiments. *Journal of Physics G Nuclear Physics*, 43(1):013001, January 2016.

[133] S. Mashchenko and A. Sills. Globular Clusters with Dark Matter Halos. II. Evolution in a Tidal Field. *ApJ*, 619:258–269, January 2005.

[134] M. L. Mateo. Dwarf Galaxies of the Local Group. *AARA*, 36:435–506, 1998.

[135] M. Milgrom. A modification of the Newtonian dynamics - Implications for galaxies. *ApJ*, 270:371–389, July 1983.

[136] M. Milgrom. A modification of the Newtonian dynamics as a possible alternative to the hidden mass hypothesis. *ApJ*, 270:365–370, July 1983.

[137] J. W. Moffat. Scalar tensor vector gravity theory. *JCAP*, 3:004, March 2006.

[138] B. Moore. Constraints on the Global Mass-to-Light Ratios and on the Extent of Dark Matter Halos in Globular Clusters and Dwarf Spheroidals. *ApJL*, 461:L13, April 1996.

[139] B. Moore, S. Ghigna, F. Governato, G. Lake, T. Quinn, J. Stadel, and P. Tozzi. Dark Matter Substructure within Galactic Halos. *ApJL*, 524:L19–L22, October 1999.

[140] I. V. Moskalenko and L. L. Wai. *ApJ Letters*, 659:L29–L32, April 2007.

[141] I. V. Moskalenko and L. L. Wai. In S. Ritz, P. Michelson, and C. A. Meegan, editors, *The First GLAST Symposium*, volume 921 of *American Institute of Physics Conference Series*, pages 508–509, July 2007.

[142] A. Natarajan. *Phys Rev D*, 85(8):083517, April 2012.

[143] A. Natarajan, J. C. Tan, and B. W. O'Shea. *ApJ*, 692:574–583, February 2009.

[144] J. F. Navarro, C. S. Frenk, and S. D. M. White. *ApJ*, 490:493, December 1997.

[145] M. Odenkirchen, E. K. Grebel, W. Dehnen, H.-W. Rix, B. Yanny, H. J. Newberg, C. M. Rockosi, D. Martínez-Delgado, J. Brinkmann, and J. R. Pier. *AJ*, 126:2385–2407, November 2003.

[146] N. Okabe, T. Futamase, M. Kajisawa, and R. Kuroshima. *ApJ*, 784:90, April 2014.

[147] P. Panci. New Directions in Direct Dark Matter Searches. *ArXiv e-prints:1402.1507*, February 2014.

[148] P. Pani and A. Loeb. Tidal capture of a primordial black hole by a neutron star: implications for constraints on dark matter. *JCAP*, 6:026, June 2014.

[149] N. E. Q. Paust, A. Aparicio, G. Piotto, I. N. Reid, and *et al. The Astronomical Journal*, 137:246–256, January 2009.

[150] M. S. Pawlowski, J. Pflamm-Altenburg, and P. Kroupa. The VPOS: a vast polar structure of satellite galaxies, globular clusters and streams around the Milky Way. *MNRAS*, 423:1109–1126, June 2012.

[151] B. Paxton, L. Bildsten, A. Dotter, and *et al. ApJ Supplement Series*, 192:3, January 2011.

[152] B. Paxton, M. Cantiello, P. Arras, and *et al. ApJ Supplement Series*, 2013.

[153] B. Paxton, P. Marchant, J. Schwab, E. B. Bauer, L. Bildsten, M. Cantiello, L. Dessart, and *et al.* Modules for Experiments in Stellar Astrophysics (MESA): Binaries, Pulsations, and Explosions. *ApJS*, 220:15, September 2015.

[154] R. D. Peccei and H. R. Quinn. CP conservation in the presence of pseudoparticles. *Physical Review Letters*, 38:1440–1443, June 1977.

[155] P. J. E. Peebles. Dark matter and the origin of galaxies and globular star clusters. *ApJ*, 277:470–477, February 1984.

[156] A. A. Penzias and R. W. Wilson. *ApJ*, 142:419–421, July 1965.

[157] S. Perlmutter, G. Aldering, S. Deustua, S. Fabbro, G. Goldhaber, D. E. Groom, A. G. Kim, M. Y. Kim, Supernova Cosmology Project, and *et al.* Cosmology From Type IA Supernovae: Measurements, Calibration Techniques, and Implications. In *American Astronomical Society Meeting Abstracts*, volume 29 of *Bulletin of the American Astronomical Society*, page 1351, December 1997.

[158] A. H. G. Peter. *Phys Rev D*, 83(12):125029, June 2011.

[159] M. M. Phillips. The absolute magnitudes of Type IA supernovae. *ApJL*, 413:L105–L108, August 1993.

[160] Planck Collaboration, P. A. R. Ade, N. Aghanim, C. Armitage-Caplan, M. Arnaud, M. Ashdown, F. Atrio-Barandela, J. Aumont, C. Baccigalupi, A. J. Banday, and *et al.* Planck 2013 results. XVII. Gravitational lensing by large-scale structure. *AAP*, 571:A17, November 2014.

[161] Planck Collaboration, P. A. R. Ade, N. Aghanim, M. Arnaud, M. Ashdown, J. Aumont, C. Baccigalupi, A. J. Banday, R. B. Barreiro, J. G. Bartlett, and et al. Planck 2015 results. XIII. Cosmological parameters. *ArXiv e-prints*, February 2015.

[162] Planck Collaboration, P. A. R. Ade, N. Aghanim, M. Arnaud, M. Ashdown, J. Aumont, C. Baccigalupi, A. J. Banday, R. B. Barreiro, J. G. Bartlett, and *et al.* Planck 2015 results. XV. Gravitational lensing. *ArXiv e-prints:1502.01591*, February 2015.

[163] K. Prasad Modak, D. Majumdar, and S. Rakshit. A possible explanation of low energy γ-ray excess from galactic centre and Fermi bubble by a Dark Matter model with two real scalars. *JCAP*, 3:011, March 2015.

[164] W. H. Press and D. N. Spergel. *ApJ*, 296:679–684, September 1985.

[165] C. W. Purcell, J. S. Bullock, and M. Kaplinghat. The Dark Disk of the Milky Way. *Ap J*, 703:2275–2284, October 2009.

[166] G. G. Raffelt. *Physics Letters B*, 166:402–406, January 1986.

[167] S. W. Randall, M. Markevitch, D. Clowe, A. H. Gonzalez, and M. Bradač. Constraints on the Self-Interaction Cross Section of Dark Matter from Numerical Simulations of the Merging Galaxy Cluster 1E 0657-56. *ApJ*, 679:1173–1180, June 2008.

[168] I. N. Reid and J. E. Gizis. *The Astronomical Journal*, 116:2929–2935, December 1998.

[169] A. Renzini. Effects of cosmions in the sun and in globular cluster stars. *Astronomy and Astrophysics*, 171:121, January 1987.

[170] J. Richard, J.-P. Kneib, M. Limousin, A. Edge, and E. Jullo. Abell 370 revisited: refurbished Hubble imaging of the first strong lensing cluster. *MNRAS*, 402:L44–L48, February 2010.

[171] H. B. Richer, A. Dotter, J. Hurley, and *et al. The Astronomical Journal*, 135:2141–2154, June 2008.

[172] A. G. Riess, A. V. Filippenko, P. Challis, A. Clocchiatti, A. Diercks, P. M. Garnavich, R. L. Gilliland, C. J. Hogan, and *et al.* Observational Evidence from Supernovae for an Accelerating Universe and a Cosmological Constant. *AJ*, 116:1009–1038, September 1998.

[173] A. G. Riess, W. H. Press, and R. P. Kirshner. Using Type IA supernova light curve shapes to measure the Hubble constant. *ApJL*, 438:L17–L20, January 1995.

[174] M. Roos. Dark Matter: The evidence from astronomy, astrophysics and cosmology. *ArXiv e-prints:1001.0316*, January 2010.

[175] L. Roszkowski, E. M. Sessolo, S. Trojanowski, and A. J. Williams. Reconstructing WIMP properties through an interplay of signal measurements in direct detection, Fermi-LAT, and CTA searches for dark matter. *ArXiv e-prints*, March 2016.

[176] V. C. Rubin and W. K. Ford, Jr. *ApJ*, 159:379, February 1970.

[177] V. C. Rubin, W. K. Ford, Jr., N. Thonnard, and D. Burstein. *ApJ*, 261:439–456, October 1982.

[178] V. C. Rubin, N. Thonnard, and W. K. Ford, Jr. *ApJ Letters*, 225:L107–L111, November 1978.

[179] R. H. Sanders. The Virial Discrepancy in Clusters of Galaxies in the Context of Modified Newtonian Dynamics. *ApJL*, 512:L23–L26, February 1999.

[180] R. H. Sanders and S. S. McGaugh. Modified Newtonian Dynamics as an Alternative to Dark Matter. *ARAA*, 40:263–317, 2002.

[181] C. Savage, K. Freese, P. Gondolo, and D. Spolyar. *JCAP*, 9:36, September 2009.

[182] M. Sereno, M. Lubini, and P. Jetzer. A multiwavelength strong lensing analysis of baryons and dark matter in the dynamically active cluster AC 114. *AAP*, 518:A55, July 2010.

[183] J. Shin, S. S. Kim, and Y.-W. Lee. *Journal of Korean Astronomical Society*, 46:173–181, August 2013.

[184] J. D. Simon, M. Geha, Q. E. Minor, G. D. Martinez, and *et al. ApJ*, 733:46, May 2011.

[185] Y. Sofue and V. Rubin. Rotation Curves of Spiral Galaxies. *ARAA*, 39:137–174, 2001.

[186] D. N. Spergel and W. H. Press. Effect of hypothetical, weakly interacting, massive particles on energy transport in the solar interior. *ApJ*, 294:663–673, July 1985.

[187] D. Spolyar, K. Freese, and P. Gondolo. *Physical Review Letters*, 100(5):051101, February 2008.

[188] D. Stello and R. L. Gilliland. *ApJ*, 700:949–955, August 2009.

[189] M. Taoso, F. Iocco, G. Meynet, G. Bertone, and P. Eggenberger. Effect of low mass dark matter particles on the Sun. *Phys Rev D*, 82(8):083509, October 2010.

[190] M. A. Taylor, T. H. Puzia, M. Gomez, and K. A. Woodley. Observational Evidence for a Dark Side to NGC 5128's Globular Cluster System. *Ap J*, 805:65, May 2015.

[191] The Dark Energy Survey Collaboration, T. Abbott, F. B. Abdalla, S. Allam, A. Amara, J. Annis, R. Armstrong, D. Bacon, M. Banerji, and *et al.* Cosmology from Cosmic Shear with DES Science Verification Data. *ArXiv e-prints:1507.05552*, July 2015.

[192] The LIGO Scientific Collaboration, the Virgo Collaboration, B. P. Abbott, R. Abbott, T. D. Abbott, M. R. Abernathy, F. Acernese, K. Ackley, C. Adams, T. Adams, and *et al.* GW150914: First results from the search for binary black hole coalescence with Advanced LIGO. *ArXiv e-prints:1602.03839*, February 2016.

[193] G. S. Thomson, C. Knigge, A. Dieball, T. J. Maccarone, and *et al. MNRAS*, 423:2901–2916, July 2012.

[194] P. Tisserand, L. Le Guillou, C. Afonso, J. N. Albert, J. Andersen, R. Ansari, É. Aubourg, P. Bareyre, and EROS-2 Collaboration *et al.* Limits on the Macho content of the Galactic Halo from the EROS-2 Survey of the Magellanic Clouds. *AAP*, 469:387–404, July 2007.

[195] A. van Engelen, R. Keisler, O. Zahn, K. A. Aird, B. A. Benson, L. E. Bleem, J. E. Carlstrom, C. L. Chang, and *et al.* A Measurement of Gravitational Lensing of the Microwave Background Using South Pole Telescope Data. *ApJ*, 756:142, September 2012.

[196] C. J. Walcher, T. Böker, S. Charlot, L. C. Ho, H.-W. Rix, J. Rossa, J. C. Shields, and R. P. van der Marel. Stellar Populations in the Nuclei of Late-Type Spiral Galaxies. *Ap J*, 649:692–708, October 2006.

[197] C. J. Walcher, R. P. van der Marel, D. McLaughlin, H.-W. Rix, T. Böker, N. Häring, L. C. Ho, M. Sarzi, and J. C. Shields. Masses of Star Clusters in the Nuclei of Bulgeless Spiral Galaxies. *Ap J*, 618:237–246, January 2005.

[198] C. M. Will. The Confrontation between General Relativity and Experiment. *Living Reviews in Relativity*, 17, June 2014.

[199] Q. Yang. Axions and Dark Matter. *ArXiv e-prints:1509.00673*, September 2015.

[200] D. G. York, J. Adelman, J. E. Anderson, Jr., S. F. Anderson, J. Annis, N. A. Bahcall, J. A. Bakken, R. Barkhouser, SDSS Collaboration, and *et al.* The Sloan Digital Sky Survey: Technical Summary. *AJ*, 120:1579–1587, September 2000.

[201] A. R. Zentner. *Phys Rev D*, 80(6):063501, September 2009.

[202] A. R. Zentner and A. P. Hearin. *Phys Rev D*, 84(10):101302, November 2011.

[203] K. M. Zurek. Asymmetric Dark Matter: Theories, signatures, and constraints. *Physics Reports*, 537:91–121, April 2014.

[204] F. Zwicky. *ApJ*, 86:217, October 1937.